A SINGLE CRYSTAL ESR AND QUANTUM CHEMICAL STUDY OF

PHOSPHORUS CENTRED RADICALS

A SINGLE CRYSTAL ESR AND QUANTUM CHEMICAL STUDY OF PHOSPHORUS CENTRED RADICALS

door

RENÉ ALBERT JOHAN JANSSEN

geboren te Roermond

DIT PROEFSCHRIFT IS GOEDGEKEURD DOOR

DE PROMOTOREN

PROF. DR. H.M. BUCK

EN

PROF. DR. J.B.F.N. ENGBERTS

Aan mijn Ouders,

Aan Ria

CONTENTS

CHAPTER 1

Introduction

1. SCOPE OF THE THESIS

Since phosphoranyl radicals were first detected as intermediates by electron spin resonance (ESR), spectroscopy in the late 1960s a large number of different electronic configurations and geometrical structures have been suggested.[1] Initially a trigonal bipyramid structure with missing equatorial ligand (TBP-e) was proposed as energetically favoured (Fig. 1). The assignments were based on the values of phosphorus hyperfine couplings obtained from liquid phase ESR studies. The recent development of anisotropic ESR, coupled with x-ray diffraction analysis of the radical precursor, has generated results causing the prior findings to be partially reconsidered. Besides the confirmation of the existence of TBP-e structures, configurations different from TBP-e have been envisioned (Fig. 1). The different structures are in general interconvertible and show an interesting dynamical behaviour and reactivity.
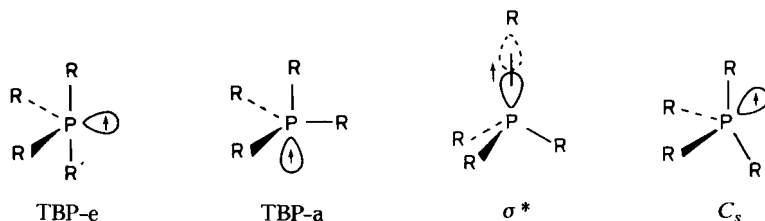
Figure 1. Schematic representation of phosphoranyl radical structures.

The aim of this thesis is to study the various possible structures of phosphoranyl radicals via single–crystal ESR and quantum chemical methods, and to determine the conditions that rule the specific formation of each configuration.

Another interesting aspect of the study of phosphoranyl radicals is based on their possible relevance to radiation induced deactivation of DNA. ESR studies have provided valuable information concerning the nature, structure and reactivity of various free radicals generated in irradiated nucleic acids and their constituents. It appears that predominantly base centred radicals or carbon and oxygen centred sugar radicals are formed. The detection of phosphoranyl radicals for a range of mono-, di- and trialkylphosphates, in combination with the observation of subsequent dissociation reactions, indicates that these radicals can be the precursors of DNA strand breaks.[2-3]

To determine the role of the phosphate moiety in the complex temporal development of reactions involved in the radiation chemistry of nucleic acids, a fundamental approach on the effects of ionizing radiation on organophosphorus compounds and the structure of phosphorus centred radicals, and more particularly of phosphoranyl radicals, is required. With this knowledge it will be possible to elucidate the involvement of transient phosphorus centred radicals via fast-response ESR. This technique enables the detection of radicals shortly after (1 μs) they are generated.[4]

2. STRUCTURE OF PHOSPHORANYL RADICALS

Phosphoranyl radicals are formed in a variety of ways. In solution they can be generated by the addition of radicals to three-coordinated phosphorus or by a homolytic abstraction of weakly bound substituents from five-coordinated phosphoranes. In solid state the most convenient way is the use of ionizing radiation (e.g. γ rays, x rays or UV laser radiation). The initial chemical effect of high-energy radiation can be considered as an indiscriminate ionization, the ejected electron being considerably delocalized. The ejected electrons may return to their cations (Fig. 2). This generally leads to electronically and vibrationally excited parent molecules which may undergo homolysis. The overall process resembles then a normal photolysis. On the other hand, the delocalized electron may be stabilized by physical trapping or they may react with available electron acceptors leading to electron capture. The electron capture process is longlived provided the relaxation of the acceptor is fast, and leads to sufficiently deep traps. The relaxation may take the form of bond streching or bending, or bond breaking (dissociative electron capture) or even bond making. It is important to note that only if electron-loss and electron-gain centres are trapped they will be detected by ESR spectroscopy.

$$AB \xrightarrow{\text{irradiation}} AB^+ + e^- \xrightarrow{\text{return}} AB^* \longrightarrow AB$$

$$\downarrow \text{homolysis}$$

$$A\cdot \ \cdot B$$

$$AB + e^- \xrightarrow{\text{electron capture}} A\dot{B}^- \xrightarrow{\text{dissociation}} A\cdot + B^-$$

$$\downarrow \text{relaxation}$$

$$\dot{A}'B'^-$$

Figure 2. Ionization by high-energy radiation.

In the first report of a single-crystal ESR study of a phosphoranyl radical, Gillbro and Williams presented anisotropic information on oriented $O\dot{P}Cl_3^-$ generated by γ

irradiation induced electron capture of phosphorus oxychloride.[5] The results were interpreted in terms of a TBP structure, with missing equatorial ligand, two apical chlorines, and an equatorial location of the third chlorine nucleus and oxygen. They established that the unpaired electron is largely confined to a three-centre molecular orbital, and emphasized the applicability of Rundle's molecular orbital (MO) theory.

Shortly after, Hasegawa at al. succeeded in generating $\dot{P}F_4$ radicals by γ irradiation of a single crystal of PF_3 and obtained a detailed description of the unpaired electron distribution.[6] The electronic and geometric structure was assigned to a TBP-e configuration (Fig. 1). The phosphorus atom and the two apical fluorines bear a large amount of spin density, whereas the delocalization onto the two equatorial fluorines is small. The experimental data reveal furthermore that the two axial fluorine $2p_\sigma$ orbitals are aligned and perpendicular to the phosphorus $3p_\sigma$ orbital.

The first phosphoranyl radical structure which is totally different from the TBP-e configuration was found by Berclaz et al. for the $Ph_3\dot{P}Cl$ radical.[7] Their single-crystal analysis revealed a high spin density on phosphorus and chlorine and an alignment of their atomic $3p_\sigma$ orbitals. The structure was assigned to a C_{3v} $\sigma*$ configuration in which the unpaired electron occupies an antibonding orbital between phosphorus and chlorine, resulting in a three-electron bond (Fig. 1).

Finally, Hamerlinck et al. reported the formation of the $\cdot\overline{P(OCH_2CH_2)_3N^+}BF_4^-$ radical in which the unpaired electron acts as a ligand in the apical position of a TBP (TBP-a, Fig. 1).[8] This TBP-a structure is stabilized by the presence of small rings, spanning the apical nitrogen nucleus with each of the three equatorial oxygens.

The limiting structures TBP-e, TBP-a and $\sigma*$ are interconvertible, and an intermediate configuration between TBP-e and $\sigma*$ has been established (C_s, Fig. 1).[9]

The fact that phosphoranyl radicals contain more than eight electrons in the valence shell results in some antibonding character of the singly occupied molecular orbital (SOMO) of these hypervalent species. The antibonding nature is most pronounced for the $\sigma*$ radicals because the SOMO extends over only two nuclei. TBP-e and TBP-a structures can be considered as multi-centre $\sigma*$ configurations.

The SOMO of a phosphoranyl radical invariably contains a large contribution from the valence $3s$ and $3p$ orbitals of the central phosphorus atom. The $3s$ character is very sensitive to the nature and electronegativity of the ligands with $\dot{P}H_4$ and $\dot{P}F_4$ at the opposite ends of the range.[6,10] Surprisingly, the phosphorus $3s$ contribution increases with increasing ligand electronegativity. This, at least in part, reflects the antibonding nature of the orbital involved.

Quantum chemical calculations using the unrestricted Hartree–Fock method within a 4-31G basis set for $\dot{P}H_4$ and $\dot{P}F_4$ revealed a C_{2v} form, closely resembling a TBP-e configuration, as the the structure of minimum energy.[11] The calculated spin densities were in reasonable agreement with the experimental values. TBP-a, tetrahedral (T_d) and square pyramidal (SP) configurations were found to be higher in energy, both for $\dot{P}H_4$ and $\dot{P}F_4$. It is interesting to note that these calculations reveal that for TBP-e phosphoranyl radicals the apical bonds are longer than the equatorial bonds, in accordance with five-coordinated phosphoranes. For TBP-a structures, however, the bond lengths are reversed and the equatorial bonds are now substantially longer than the apical bond.

3. ESR OF TRAPPED RADICALS

3.1. The spin Hamiltonian

The general spin Hamiltonian for $S = \frac{1}{2}$ radicals trapped in a solid matrix, is expressed by[12]

$$H = \beta\, S{\cdot}g{\cdot}H - \sum_n g_n\, \beta_N\, H{\cdot}I_n + \sum_n S{\cdot}A_n{\cdot}I_n \qquad 1.1$$

where the summation extends over the interacting nuclei. This Hamiltonian describes successively the electron Zeeman interaction, the nuclear Zeeman energy and the electron–nuclear hyperfine interaction.

In this equation S is the electron spin, H is the applied magnetic field, β is the Bohr magneton and g is a tensor. The elements of g can be written as

$$g_{ij} = g_e\, \delta_{ij} + \Delta g_{ij} \qquad 1.2$$

where the indices i and j represent the spatial coordinates x, y and z, δ_{ij} is the Kronecker delta and g_e is the g value of the free electron ($g_e = 2.00232$). The g tensor is anisotropic when the electron possesses both spin and orbital angular momentum. Since the ground state of most radicals has zero orbital momentum, the only way the odd electron can acquire orbital momentum is through the effect of spin orbit coupling, which is represented by the Hamiltonian

$$H_{LS} = \xi\, L{\cdot}S \qquad 1.3$$

where ξ is an effective spin–orbit coupling constant of the molecule and L is the orbital angular momentum. In general, the spin–orbit coupling constant ξ is dependent on the location of the unpaired electron with respect to each atomic nucleus and reflects the atomic spin–orbit coupling constants ζ of the constituting atoms. In general ζ increases rapidly with increasing atom number. The H_{LS} operator has the effect of mixing the ground state $|\,0>$ with excited states $|\,n>$, giving rise to $\Delta g_{ij} \neq 0$. The sign of Δg_{ij} will depend on wether the coupling to an empty level or to a filled level is more important. If the induced mixing involves a transfer of one of the paired electrons into the SOMO, Δg_{ij} will be positive. If, on the other hand, the unpaired electron is removed from the SOMO the value of Δg_{ij} will be negative. In general the values of Δg_{ij} are relatively small for organic radicals (<0.01), and their analysis in terms of molecular structure is hampered by the large number of unknown molecular parameters involved.

Thus the g tensor provides information about magnetically coupled excited states and this supplements that gained from the electron–nuclear coupling discussed below.

The hyperfine coupling tensor **A**, which couples the electron spin **S** with the nuclear spin **I**, consists of an isotropic part and an anisotropic part, resulting from two different types of magnetic electron–nuclear hyperfine interaction.

The energy of the isotropic hyperfine coupling, or Fermi contact interaction, between an electron and a nucleus is expressed by the following Hamiltonian

$$H_c = (8\pi/3)\, g\, \beta\, g_N\, \beta_N\, \delta(r_N)\, \mathbf{S\cdot I} \; = \; A^{iso}\, \mathbf{S\cdot I} \qquad\qquad 1.4$$

where $\delta(r_N)$ is the δ-function. The isotropic hyperfine coupling constant (A^{iso}) is found by applying the Hamiltonian to the ground state wave function Ψ_0 of the radical.

$$A^{iso} = (8\pi/3)\, g\, \beta\, g_N\, \beta_N < \Psi_0 \mid \delta(r_N) \mid \Psi_0> \qquad\qquad 1.5$$

Since only s orbitals have a nonvanishing electron density at the nucleus, only s orbital spin density contributes to A^{iso}.

The anisotropic hyperfine coupling results from a direct dipolar interaction between the magnetic moments of electron spin and nuclear spin. The interaction Hamiltonian is given by

$$H_{dip} = -g\, \beta\, g_N\, \beta_N \left[\frac{\mathbf{S\cdot I}}{r^3} - \frac{3(\mathbf{S\cdot r})(\mathbf{I\cdot r})}{r^5} \right] \qquad\qquad 1.6$$

usually expressed in matrix notation as

$$H_{dip} = \mathbf{S\cdot B\cdot I} \qquad\qquad 1.5$$

where **B** is the dipolar hyperfine tensor. The elements of **B** are given by

$$B_{ij} = -g\, \beta\, g_N\, \beta_N < \Psi_0 \mid \frac{r^2 \delta_{ij} - 3ij}{r^5} \mid \Psi_0> \qquad\qquad 1.8$$

B is a traceless and symmetric tensor which can be diagonalized giving three principal values B_{xx}, B_{yy} and B_{zz} together with their directions. If the molecular orbital in which the unpaired electron resides is axially symmetric, as in a p_z orbital, diagonalization results in $B_{xx} = B_{yy} = -B$ and $B_{zz} = 2B$. Only spin density in $l \neq 0$ orbitals (p, d and so on) can contribute to the anisotropic coupling. The anisotropic coupling vanishes to zero in motionally averaged systems and can only be determined for radicals in a rigid matrix.

The total hyperfine coupling tensor **A** is the sum of the isotropic and anisotropic contributions

$$A = A^{iso} \mathbf{1} + B \qquad \qquad 1.9$$

and possesses the same principal directions as the tensor **B**. The experimental determination of the hyperfine couplings of several nuclei for a radical in different orientations with respect to the external magnetic field **H**, results in a discription of the **A** tensors and their relative orientations. The isotropic hyperfine coupling, $A^{iso} = 1/3(\text{trace } A)$, gives a measure of the valence s orbital spin density (ρ_s) in the atom having the coupling nucleus.

$$\rho_s = \frac{A^{iso}}{A_0^{iso}} \qquad \qquad 1.10$$

where A_0^{iso} is an atomic parameter representing the expected isotropic coupling for unit electron density in the valence s orbital. Similarly, the largest principal value of the dipolar tensor $(B_{zz} = A_{zz} - A^{iso})$ can be related to the valence p orbital spin density (ρ_p), via the atomic parameter B_0, by

$$\rho_p = \frac{B_{zz}}{2B_0} \qquad \qquad 1.11$$

The relations 1.10 and 1.11 are approximate, since they are based on an elementary LCAO-MO description of the wave function of the molecular state. They are nevertheless very convenient and almost universally applied to interpret ESR data. The atomic hyperfine parameters A_0^{iso} and B_0 can sometimes be determined from gas-phase studies, but are generally abstracted from a quantum chemical calculation of atomic wave functions. Several A_0^{iso} and B_0 values have been reported in literature. In general the reported values are reasonably close. This results in some uncertainty for the calculated atomic spin densities. Moreover, the effect of charge is not taken into account. A positively charged atom will tend to contract the valence orbitals leading to increased values of A_0^{iso} and B_0. The atomic parameters used in this thesis correspond to the latest values reported (Table I).[13]

A further insight into the structure of trapped radicals can be obtained from the transformation matrix that diagonalizes the A tensor. The eigenvector associated with the largest eigenvalue is coincident with the direction of the valence p orbital which gives rise to the coupling. When two or more interacting nuclei are present, the relative directions of the valence p orbitals can be determined. For radicals generated in single crystals additional information can be obtained when the x-ray structure analysis of the parent compound has been established. In favourable cases, it will be possible to relate the principal hyperfine couplings with the molecular frame of the precursor molecule, and thereby complete the single-crystal ESR analysis.

Table I. Relevant nuclear g_N factors. valence shell orbital couplings and atomic spin-orbit coupling constants.

Isotope	I	g_N	A_0^{iso} (MHz)	$2B_0$ (MHz)	ζ (cm^{-1})
^{1}H	½	5.585	1420		
^{14}N	1	0.403	1811	111	76
^{19}F	½	5.255	52870	3520	272
^{31}P	½	2.261	13360	734	299
^{33}S	3/2	0.428	3463	201	382
^{35}Cl	3/2	0.547	5723	351	586
^{37}Cl	3/2	0.456	4763	292	586
^{77}Se	½	2.841	20120	983	1688

The nuclear Zeeman term describes the energy of the nuclear magnetic moment **I** in an applied field **H**. These interactions are commonly observed in nuclear magnetic resonance (NMR) spectroscopy. However, in normal ESR transitions, for which the selection rules are $\Delta m_S = \pm 1$ and $\Delta m_I = 0$, the nuclear orientations do not change and the H·I term, which displaces equally all spin levels, causes no detectable effects.

3.2 Experimental determination of ESR parameters

The spin Hamiltonian 1.1 gives rise to different energy levels depending on the electronic and nuclear spin states. Calculation of the energy levels, to the approximation required for consideration of phosphoranyl radical spectra, requires second-order perturbation theory due to the large values of the phosphorus hyperfine coupling. For a $S = \frac{1}{2}$ radical with anisotropic g and A tensors of orthorhombic symmetry, that have common principal axes, the ESR field values along the principal axes (H_{x,m_I}, H_{y,m_I} and H_{z,m_I}) are given by the relations

$$h\nu_0 = g_{xx} \beta H_{x,m_I} + A_{xx} m_I + \frac{A_{yy}^2 + A_{zz}^2}{4 g_{xx} \beta H_{x,m_I}}[I(I+1) - m_I^2] \qquad 1.12a$$

$$h\nu_0 = g_{yy} \beta H_{y,m_I} + A_{yy} m_I + \frac{A_{xx}^2 + A_{zz}^2}{4 g_{yy} \beta H_{y,m_I}}[I(I+1) - m_I^2] \qquad 1.12b$$

$$h\nu_0 = g_{zz}\,\beta\,H_{z\,,m_I} + A_{zz}\,m_I + \frac{A_{xx}^2 + A_{yy}^2}{4\,g_{zz}\,\beta\,H_{z\,,m_I}}[I\,(I+1) - m_I^2]\qquad\qquad 1.12c$$

From these relations it can be seen that the principal values of g cannot be obtained by simply taking the halfway positions of the resonance field values along the principal axes, because the third term on the right hand side induces a down field shift. Moreover, since the magnetic field is not the same for the two transitions m_I and $m_I + 1$, the separation between two successive absorptions does not give an accurate value of the hyperfine coupling. The expressions 1.12a–c become more complicated when the magnetic field is not oriented along a principal axis or when the principal axes of g and A do not coincide. This situation can be expected for all radicals that do not possess an axis of trigonal or higher symmetry. The reader is referred to textbooks on ESR for a full discussion of this problem.[14-16]

In studies of single crystals, one usually does not know in advance the principal axes, and the problem is to find them. The first step is to evaluate the tensor elements of g and A relative to an orthogonal axes system defined for the single crystal. In typical measurements the crystal is mounted so that it can be rotated about one of the reference axes (eg. z) that is normal to the applied field. Spectra are then recorded with H at different angles relative to x and y. The observed transition fields are plotted as function of the crystal orientation in each of the three mutual orthogonal planes. Subsequently, the ESR parameters are adjusted to fit the theoretical formulas to the observed curves, usually by computer analysis. The last step is to diagonalize the g and A tensors to find the principal elements and direction cosines relative to the predefined axes.

4. OUTLINE OF THE THESIS

In chapter 2, the structural differences between TBP-a and σ^* phosphoranyl radical configurations are discussed on basis of quantum chemical calculations. Both configurations possess a C_{3v} symmetry and it is shown that the molecular geometry of the radical and of the radical precursor is of paramount importance for the choice between TBP-a and σ^*. A similar conclusion is obtained for octahedral (O_h) and C_{4v} σ^* phosphorane anion radicals ($\dot{P}R_5^-$).

Chapter 3 describes the quantum chemical calculation of isotropic and anisotropic electron–nuclear hyperfine couplings, which can serve for a direct comparison with the experimental values obtained from ESR measurements. For a number of small radicals the theoretical results are in good agreement with experiment.

The electron capture of substituted diphosphine disulphides, presented in chapter 4, shows that various different configurations for phosphoranyl radicals (three-electron bond, TBP-e) are formed simultaneously from one precursor. This indicates that the different structures are not far apart in relative energies. Subtle changes in ligand

properties or of the single-crystal matrix can cause the relative energies to interchange. The formed three-electron bond radical is accurately described with quantum chemical calculations.

Chapter 5 provides an insight in the strong dependence of the radical structure on the nature of the ligands. Substitution of chlorine by fluorine results in a marked change of the configuration from σ^* to TBP-e. It is shown that the formed P-Cl σ^* structure dissociates in the single crystal matrix via an in-line abstraction of chlorine yielding a three-coordinated phosphorus centred radical.

Chapter 6 describes a unique property of TBP-e phosphoranyl radicals. In contrast to the normal five-coordinated TBP phosphoranes, the site preference in a TBP-e configuration does not necessarily follows group electronegativity; fluorine is found in an equatorial position and chlorine on the apical site. These findings are confirmed by a quantum chemical description.

Chapter 7 describes the formation of σ^* structures in single crystals of the trialkylphosphine sulphides and selenides. Depending on the symmetry of the crystal these radicals show small distortions from trigonal symmetry. Only in an axially symmertic matrix the radicals possess a perfect trigonal symmetry. Theoretical calculations do not accurately describe the unpaired electron distribution of these $R_3\dot{P}\text{-}S^-$ phosphoranyl radicals.

In Chapter 8 the experimental and theoretical results of this thesis are discussed and related. The important factors in the formation of TBP-e and σ^* configurations are described.

REFERENCES

1. For a review on the structure, formation and reactivity of phosphoranyl radicals see: W.G. Bentrude, Acc. Chem. Res., 15, 117 (1982).
2. D. Nelson and M.C.R. Symons, J. Chem. Soc., Perkin Trans. 2, 286 (1977).
3. J.H.H. Hamerlinck, P. Schipper and H.M. Buck, J. Chem. Phys., 76, 2161 (1982).
4. K.A. McLauchlan and D.G. Stevens, Mol. Phys., 57, 223 (1986).
5. T. Gillbro and F. Williams, J. Am. Chem. Soc., 96, 5032 (1974).
6. A. Hasegawa, K. Ohnishi, K. Sogabe and M. Miura, Mol. Phys., 30, 1367 (1975).
7. T. Berclaz, M. Geoffroy and E.A.C. Lucken, Chem. Phys. Lett., 36, 677 (1975).
8. J.H.H. Hamerlinck, P. Schipper and H.M. Buck, J. Am. Chem. Soc., 102, 5679 (1980).
9. T. Berclaz, M. Geoffroy, L. Ginet and E.A.C. Lucken, Chem. Phys. Lett., 62, 515 (1975).
10. A.J. Colussi, J.R. Morton and K.F. Preston, J. Phys. Chem., 79, 1855 (1975).

11. J.M. Howell and K.F. Olsen, J. Am. Chem. Soc., **98**, 7119 (1976).

12. A. Carrington and A.D. McLachlan, *Introduction to Magnetic Resonance* (Harper & Row, New York, 1967).

13. J.R. Morton and K.F. Preston, J. Magn. Reson., **30**, 577 (1978).

14. W. Weltner, *Magnetic Atoms and Molecules* (Scientific and Academic Editions, New York, 1983).

15. W. Gordy, *Theory and Applications of Electron Spin Resonance* (Wiley-Interscience, New York, 1983).

16. A. Abragham and B. Bleaney, *Electron Paramagnetic Resonance of Transition Ions* (Oxford University Press, London, 1970).

CHAPTER 2

Quantum chemical study on the structure of C_{3v} phosphoranyl and C_{4v} phosphorane anion radicals

1. INTRODUCTION

Two different electronic configurations have been invoked to describe the structure of C_{3v} phosphoranyl radicals. The unpaired electron in the $Ph_3\dot{P}Cl$ radical is believed to reside in a $\sigma*$ P-Cl orbital, resulting in a three-electron bond.[1] This $\sigma*$ configuration explains the high spin density on chlorine and accounts for the fact that the ^{31}P hyperfine tensor and the ^{35}Cl tensor possess the same principal axis. In contrast, single-crystal ESR studies on the C_{3v} $\cdot\bar{P}(OCH_2CH_2)_3N^+BF_4^-$ radical revealed a TBP-a configuration in which the unpaired electron resides in an orbital directed towards the missing apical substituent of a TBP.[2] The near isotropic ^{14}N coupling of 62 MHz indicates a small spin density on the apical nitrogen atom.

Analogous to the C_{3v} structures, C_{4v} phosphorane anion radicals can adopt an octahedral structure (O_h) or a $\sigma* C_{4v}$ configuration. Likewise, large differences concerning the unpaired electron density on the apical ligands have been reported. The isotropic ESR spectrum of the $\dot{P}F_5^-$ radical anion shows four equivalent equatorial fluorines with a large coupling and one with a small coupling arising from the unique apical fluorine.[3] The same structure has been proposed for $\dot{P}Cl_5^-$ [4] and the isoelectronic $\dot{S}F_5$.[5] For the $Cl\dot{P}(O_2C_6H_4)_2^-$ radical, which adopts a local C_{4v} symmetry with chlorine in the apical position, the ^{31}P, ^{35}Cl, and ^{37}Cl hyperfine tensors are coincident and directed along the P-Cl linkage.[6] The chlorine hyperfine coupling shows, in sharp contrast to $\dot{P}F_5^-$, a large spin density on the apical ligand. In this chapter quantum chemical calculations are presented on the geometry and electronic structure of the various C_{3v} and C_{4v} radicals (Fig. 1). A detailed study is made of the C_{3v} $PH_3 + H\cdot$ potential energy surface. The stability of C_{3v} radicals $H\dot{P}H_3$, $F\dot{P}H_3$, and $Cl\dot{P}H_3$ is discussed.

2. QUANTUM CHEMICAL METHODS

The calculations were performed with the GAUSSIAN 76[7] and GAUSSIAN 80[8] program systems using the unrestricted Hartree-Fock (UHF) procedure. Throughout a split valence 4-31G basis set was used. The structures were fully optimized with respect to all bond lengths and bond angles within the symmetry constraints. Isotropic
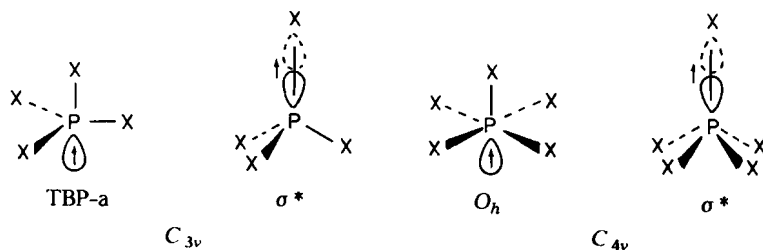
Figure 1. Electronic configurations of C_{3v} and C_{4v} phosphorus centred radicals.

hyperfine coupling constants (A_N^{iso}) were calculated from the Fermi contact integrals $(\rho(r_N))$.[9] Orbital spin densities were obtained by performing a Mulliken population analysis on the single determinant wave function. Transition states were calculated with the GAUSSIAN 80 saddle-point-search algorithm. At stationary points the second derivative matrix possesses a single negative value.

3. GEOMETRY AND ELECTRONIC STRUCTURE

3.1. Optimized geometries for C_{3v} radicals

The geometries of the radicals $X^a \dot{P} X_3^e$ were optimized for $X^a =$ H, F or Cl and $X^e =$ H or F within a C_{3v} symmetry constraint.[10] The optimized parameters for these radicals are collected in Table I together with the calculated UHF energies and the expectation values of S^2. The geometric parameters for $H\dot{P}H_3$ and $F\dot{P}F_3$ differ slightly from those previously reported by Howell et al.,[11] because in this study the apical-equatorial bond angle (ϕ) was included in the optimization. For $Cl\dot{P}H_3$ no stable geometry could be calculated. Characteristic for all these C_{3v} radicals is the apical-equatorial bond angle ϕ, which is near to 90°.
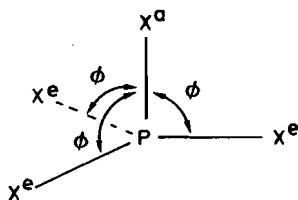
Table I. Optimized geometries, UHF energies and $<S^2>$ values for the C_{3v} $X^a \dot{P} X_3^e$ radicals.

$X^a \dot{P} X_3^e$	P-X^a (Å)	P-X^e (Å)	ϕ (°)	E(UHF) (a.u.)	$<S^2>$
H$\dot{P}$H$_3$	1.43	1.59	89.5	-342.472475	0.8328
F$\dot{P}$H$_3$	1.79	1.43	85.7	-441.245124	0.7579
Cl$\dot{P}$H$_3$					
H$\dot{P}$F$_3$	1.39	1.70	92.7	-638.782736	0.7787
F$\dot{P}$F$_3$	1.61	1.67	91.6	-737.549048	0.7798
Cl$\dot{P}$F$_3$	2.21	1.69	92.0	-1097.199849	0.7981

The singly occupied molecular orbital (SOMO) determines the distribution of the unpaired electron in the radical. The calculated SOMOs indicate that all studied radicals represent a TBP-a structure and not a $\sigma *$ arrangement, i.e. the unpaired electron density on phosphorus is directed towards the missing ligand and not localized between phosphorus and the apical substituent.

To characterize the electronic structure of these C_{3v} phosphoranyl radicals, the Fermi contact integrals $[\rho(r_N)]$ and the isotropic hyperfine coupling constants (A_N^{iso}) were evaluated together with the valence orbital spin densities. These values are collected in Tables II and III. All TBP-a radicals have a similar spin density distribution, in which the major part is located on phosphorus and the equatorial ligands. The apical ligand possesses a near zero spin density, which is a direct result from the fact that its atomic orbitals do not contribute significantly to the SOMO. This calculated general structure is in perfect agreement with the experimental values of the C_{3v} $\dot{P}$(OCH$_2$CH$_2$)$_3$N$^+$BF$_4^-$ radical and therefore confirms its assignment as TBP-a.

In comparison with other calculated TBP-a radicals the electronic structure of F$\dot{P}$H$_3$ shows some remarkable differences. Relative to H$\dot{P}$H$_3$ there is a serious decrease of the contribution to the SOMO of the phosphorus 3s orbital and the 1s orbital of the equatorial hydrogen atoms. Simultaneously, the contribution of the phosphorus $3p_z$ and of the apical ligand is increased. It has been frequently, suggested by various authors[12-15], that a radical like F$\dot{P}$H$_3$, with one strongly electronegative ligand, preferentially occupies a tetrahedral geometry with the unpaired electron in an antibonding $\sigma *$ orbital. However, the calculations show that for F$\dot{P}$H$_3$ the optimized value of ϕ (85.9°) does not confirm a tetrahedral geometry and that the electronic structure of F$\dot{P}$H$_3$ is clearly TBP-a.

As can be seen from Table I, the optimized apical bond length, for those radicals where $X^a = X^e$ (H$\dot{P}$H$_3$ and F$\dot{P}$F$_3$), is considerably shorter than the corresponding equatorial bond. In view of their TBP-a structures this is a remarkable result. It is a well-known fact that for five-coordinated phosphorus compounds with a TBP geometry the axial bonds are longer than the equatorial bonds when identical ligands are involved.[16] The same bond-length rule applies to TBP-e (C_{2v}) phosphoranyl radicals, as was

Table II. Fermi contact integrals $\rho(r_N)$ and isotropic hyperfine coupling constants A_N^{iso} for the C_{3v} $X^a \dot{P} X_3^e$ radicals.

	P		X^a		X^e	
	$\rho(r_P)$ (a.u.)	A_P^{iso} (MHz)	$\rho(r_{X^a})$ (a.u.)	$A_{X^a}^{iso}$ (MHz)	$\rho(r_{X^e})$ (a.u.)	$A_{X^e}^{iso}$ (MHz)
$H\dot{P}H_3$	1.252	2267	0.007	31	0.125	558
$F\dot{P}H_3$	0.280	507	0.195	820	0.048	214
$H\dot{P}F_3$	2.032	3680	-0.013	-58	0.158	664
$F\dot{P}F_3$	1.920	3477	-0.019	-80	0.152	639
$Cl\dot{P}F_3$	2.006	3633	0.007	3	0.154	648

Table III. Valence orbital spin densities for the C_{3v} $X^a \dot{P} X_3^e$ radicals[a].

	P		X^a		X^e	
	$3s$	$3p_z$	ns	np_z	ns	np_e [b]
$H\dot{P}H_3$	0.08	0.20	-0.01		0.42	
$F\dot{P}H_3$	0.04	0.57	-0.01	0.11	0.13	
$H\dot{P}F_3$	0.31	0.37	0.04		0.00	0.16
$F\dot{P}F_3$	0.31	0.33	0.00	-0.02	0.00	0.16
$Cl\dot{P}F_3$	0.33	0.52	0.00	-0.10	-0.01	0.18

[a] The listed values are summations over the inner and outer orbitals of the split valence 4-31G basis set. [b] np_e is the equatorial contribution, calculated as $np_x + np_y$.

shown by Howell et al.[11] The question arises of why the TBP-a radicals form an exception and possess a short apical bond. To answer this question one must be aware of the fact that both phosphoranyl radicals and five-coordinated phosphorus compounds are hypervalent species with more than eight electrons around phosphorus. To accommodate the extra electron(s) the HOMO[17] will possess some antibonding character. For phosphoranyl radicals this HOMO is identical with the SOMO. The HOMOs for the PH_5 molecule and the C_{2v} and C_{3v} $\dot{P}H_4$ radicals are depicted in Fig. 2. The schematic representations indicate that for ligands that contribute most to the HOMO the bond length is increased, while the ligands with a smaller contribution possess a normal bond length (ca. 1.43 Å). It is obvious that the increased bond length is a direct result of the antibonding character.
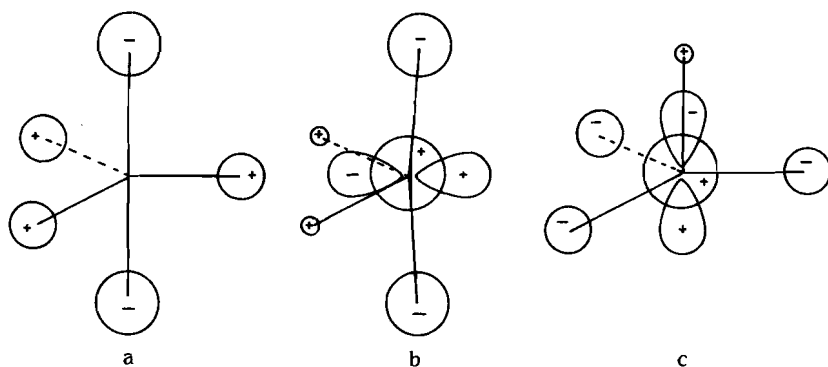
Figure 2. Geometries (ref. 11, Table I) and calculated antibonding molecular orbitals of (a) D_{3h} (TBP) PH_5; (b) C_{2v} (TBP-e) $\dot{P}H_4$; and (c) C_{3v} (TBP-a) $\dot{P}H_4$.

3.2. Optimized structure for C_{4v} $\dot{P}F_5^-$

Optimization of $\dot{P}F_5^-$, within a C_{2v} symmetry constraint, reveales an exact C_{4v} geometry (E(UHF)= -836.98279 a.u.; $<S^2>=0.7626$). This optimized structure is analogous to the C_{3v} optimized structure of $\dot{P}F_3$. The bond angle between the apical bond and the four equatorial bonds is 90.6°, and again the apical bond is substantially shorter ($PF^a = 1.64$ Å) than the equatorial bond ($PF^e = 1.73$ Å). This is in accordance with the fact that the equatorial ligands contribute more to the antibonding SOMO than the apical ligand. The calculated isotropic hyperfine coupling constants are in good agreement with the experimental values[3] (Table IV). The structure of the $\dot{P}F_5^-$ phosphorane anion radical can be described as octahedral (O_h), in which the unpaired electron density on phosphorus is directed towards the missing sixth ligand. The electronic structure of $\dot{P}F_5^-$ is essentially the same as for the TBP-a radicals. Phosphorus and the equatorial fluorines possess a large spin density and the apical ligand a very small spin density.

Table IV. Experimental (ref. 3) and calculated isotropic hyperfine coupling constants for $\dot{P}F_5^-$.

	P	F^a	F^e
Experimental (MHz)	3800	8	552
Calculated (MHz)	3708	-48	488

23

3.3. Geometry variations and electronic structures

Until now all calculations reveal radicals in which the unpaired electron occupies an orbital directed towards the missing ligand of a TBP or O_h structure. This results in a small spin density on the apical ligand. In a σ^* structure the unpaired electron occupies an antibonding orbital and is located between phosphorus and the apical ligand. This structure has been assigned to the $Ph_3\dot{P}Cl$ radical in order to explain the high spin density on the apical chlorine.[1] For a further insight in these differences, the effect of geometry variations on the spin density distribution was determined. For the $H\dot{P}H_3$ radical the angle ϕ between the apical and the three equatorial bonds was varied from 80° to 130°. During the variation of ϕ all bond lengths were fixed at the optimized values. The calculated isotropic hyperfine coupling constants of the phosphorus and hydrogen nuclei are given as a function of ϕ in Fig. 3.
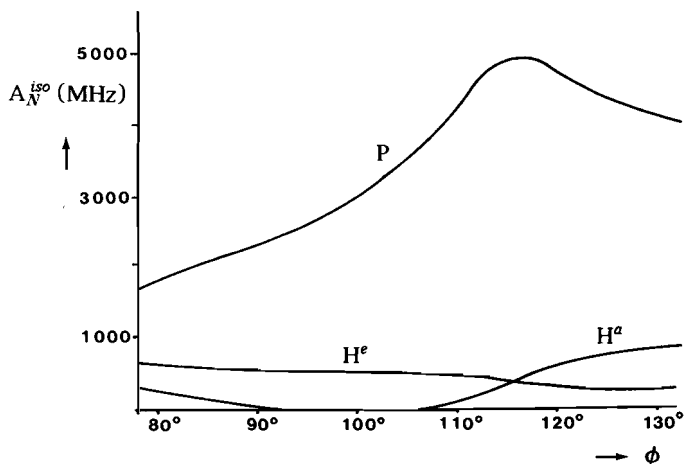
Figure 3. Calculated isotropic hyperfine coupling constants (A_N^{iso} (MHz)) of $H\dot{P}H_3$ vs. the apical-equatorial bond angle ϕ.

The phosphorus isotropic hyperfine coupling constant reaches a maximum value at $\phi = 117°$. At this point the phosphorus $3p_z$ orbital inverts and gives no contribution to the spin density distribution. This is the transition point where the structure changes formally from TBP-a to $\sigma^* C_{3v}$. Attempts to optimize the σ^* structure were not successful, but led to the dissociation into the PH_3 and $H\cdot$. The most important difference between the TBP-a and the $\sigma^* C_{3v}$ radical is the distribution of the unpaired electron over the hydrogen atoms. The $\sigma^* C_{3v}$ arrangement is characterized by a high spin density in the C_3 axis of the radical. This results in large isotropic couplings for phosphorus and the apical hydrogen atom. Going from TBP-a towards $\sigma^* C_{3v}$ a continuous transfer of spin density from the equatorial nuclei to the apical nucleus is calculated. This transfer starts at approximately $\phi = 108°$, before the actual inversion takes place. The calculated spin density distribution for the $H\dot{P}H_3$ σ^* arrangement is comparable

with the experimental values of the $Ph_3\dot{P}Cl$ radical and supports the σ^* assignment for $Ph_3\dot{P}Cl$.

For $\dot{P}F_5^-$ a similar structure variation of the bond angle ϕ was performed. Variation of ϕ reveals a transition from O_h to $\sigma^* C_{4v}$ at $\phi = 108°$. The calculated parameters (A_N^{iso} and spin density in the valence p orbitals) are depicted in Figs. 4 and 5. Analogous to the C_{3v} radicals there is a difference in the electronic structure of the optimized $\dot{P}F_5^-$ radical and its σ^* arrangement. For the optimized octahedral structure the equatorial ligands possess a large spin density, whereas the $\dot{\sigma}^* C_{4v}$ radical is characterized by a high spin density on the apical ligand. Both the O_h and σ^* structure exhibit a large phosphorus isotropic hyperfine coupling. This relative high spin density in the C_{4v} axis of the $\dot{P}F_5^-$ radical anion possessing a σ^* arrangement is comparable with the experimental values of the related C_{4v} $Cl\dot{P}(O_2C_6H_4)_2^-$ radical where a high spin density in the P–Cl axis has been found. From this point of view it may be suggested that the $Cl\dot{P}(O_2C_6H_4)_2^-$ radical anion possesses a $\sigma^* C_{4v}$ arrangement and not a O_h configuration.[6] This possibility was already recently suggested by Symons.[18]
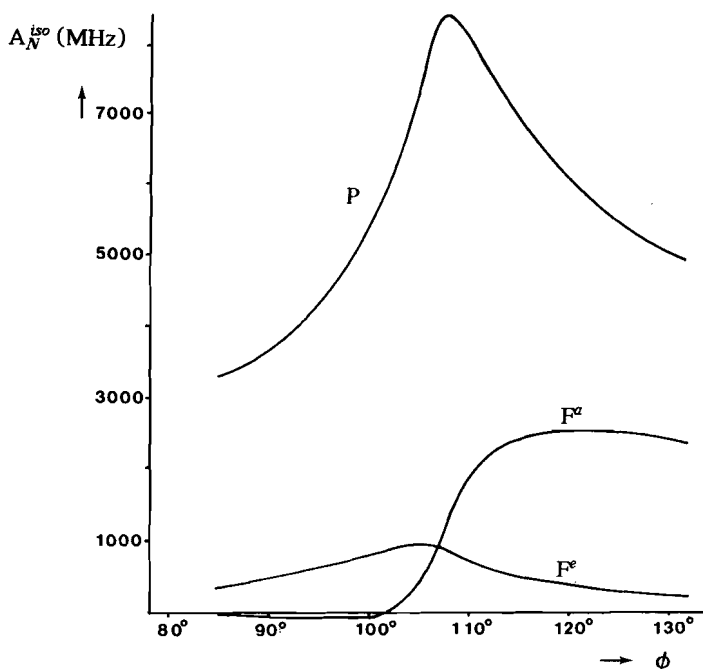
Figure 4. Hyperfine coupling constants (A_N^{iso} (MHz)) of $\dot{P}F_5^-$ vs. ϕ.
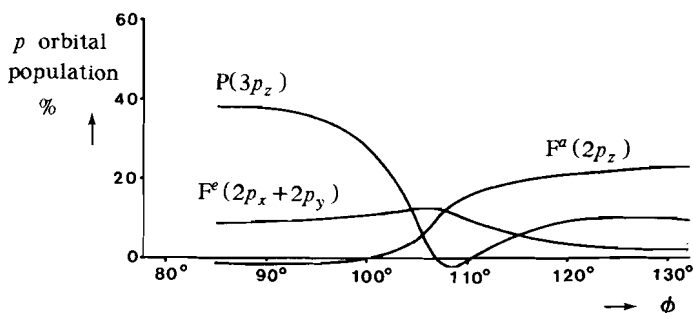
Figure 5. p Orbital population of $\dot{P}F_5^-$ vs. ϕ. Values are obtained from a Mulliken population analysis.

4. STABILITY OF $X^a \dot{P}H_3$ RADICALS

The calculations in section 3.1 reveal that the optimized C_{3v} $H\dot{P}H_3$ radical possesses a TBP-a structure. The question arises of whether this optimized structure represents the only stable structure for the C_{3v} $H\dot{P}H_3$ radical. In principle it is possible that more stable geometries for a C_{3v} $H\dot{P}H_3$ radical exist. Furthermore, it is important to know the stability of the C_{3v} $H\dot{P}H_3$ radical, for example, with respect to the dissociation into PH_3 and $H\cdot$.

4.1. Potential surface $PH_3 + H\cdot$

The PH_3 molecule is pyramidal and possesses a C_{3v} geometry. In its 4-31G optimized structure $(E(HF) = -342.02569$ a.u.$)$ the P-H bond length is 1.43 Å and the HPH angle is 94.4°. The calculated energy difference between the optimized C_{3v} $H\dot{P}H_3$ radical and the sum of isolated PH_3 and $H\cdot$ is 0.051449 a.u. (135 kJ mol^{-1}) in favour of the dissociation. The HOMO of PH_3 contains the two nonbonding electrons. Attack of a hydrogen atom along the PH_3 C_3 axis leads to a C_{3v} $H\dot{P}H_3$ radical. Within C_{3v} symmetry two possible routes for this attack can be distinguished (Fig. 6): an approach of $H\cdot$ towards the LUMO of the PH_3 molecule or an approach towards the HOMO. Likewise, the dissociation of a C_{3v} $H\dot{P}H_3$ radical can proceed along these two routes.
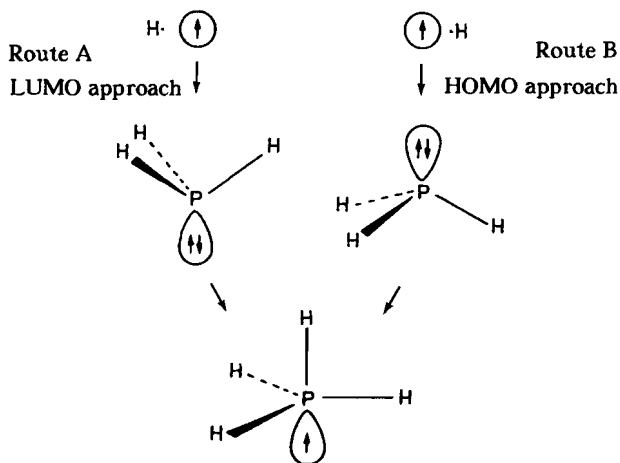
Figure 6. Two possible routes for H· attack towards PH_3. Route A, LUMO approach; route B, HOMO approach.

To determine the route with the lowest energy barrier three cross sections through the multidimensional potential energy surface were calculated. For each cross section the equatorial bond lengths (r_e) were kept constant, while the apical bond length (r_a) and the apical-equatorial bond angle (ϕ) were varied from 1.4 to 4.3 Å and from 55° to 125°, respectively. Cross sections were calculated for $r_e =$ 1.4, 1.5, and 1.6 Å (Fig. 7). The potential surfaces differ in the number of minima and transition states.

From these potential surfaces it is clear that the TBP-a structure represents the only stable HṖH₃ radical. There is no minimum that could belong to a stable $\sigma * C_{3v}$ arrangement. The potential surface shows furthermore that the energy barrier for LUMO approach is smaller than for HOMO approach. At PH^a distances of approximately 4 Å shallow minima are predicted, both for HOMO and LUMO approach. Fully optimized structures for these HOMO- and LUMO-loose complexes were determined. Their PH_3 fragments are identical with each other and with the optimized PH_3 molecule. The P-H^a distances differ: 4.18 Å for the LUMO and 3.86 Å for the HOMO. The energy of the loose complexes is essentially identical to the energy of the isolated PH_3 + H· . Using the saddle-point optimization method, the LUMO-TS was optimized with respect to all geometric parameters within C_{3v} symmetry $(PH^a = 1.73$ Å, $PH^e = 1.46$ Å, and $\phi = 81.4°)$. This LUMO-TS lies 178.3 kJ mol^{-1} above the isolated PH_3 + H· and 43.2 kJ mol^{-1} above the optimized C_{3v} HṖH₃ radical. Despite many trial geometries it was not possible to calculate a saddle point that could be attributed to a HOMO-TS. All efforts led to nonoptimized structures with very short apical bonds and large values of ϕ, or to the previously optimized LUMO-TS. The most important result that can be derived from the potential surfaces is that for all geometries where the electronic structure is $\sigma * C_{3v}$ the radical dissociates directly without any energy barrier (Fig. 7). Therefore the ligand exchange processes of nonrigid TBP-e phosphoranyl radicals via a $\sigma *$ intermediate[19] seem questionable.
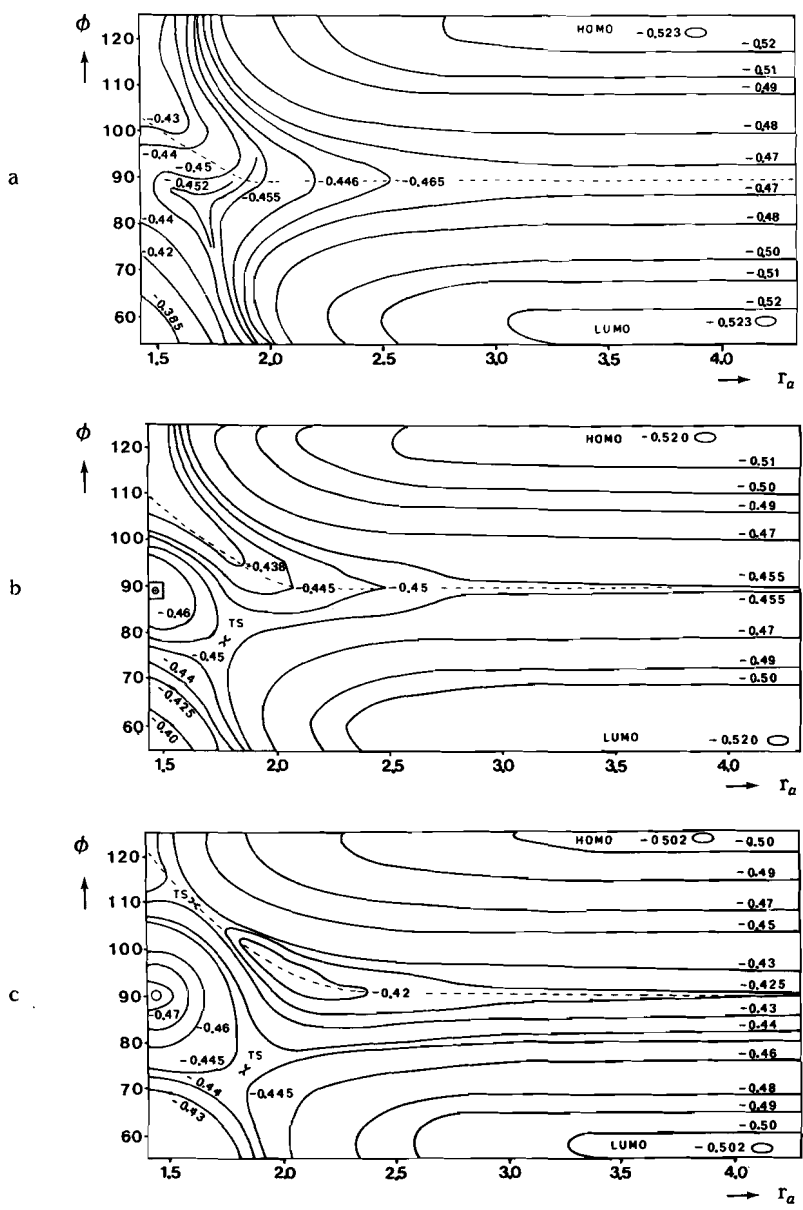
Figure 7. Potential energy surface of the PH$_3$+H$^+$ system. Geometric parameters are r_a, r_e and ϕ. Cross sections are drawn for three values of r_e: (a) 1.4 Å: (b) 1.5 Å: (c) 1.6 Å. The dotted lines indicate the edge between TBP-a and σ^* structures.

4.2. Stability of FṖH₃ and ClṖH₃

The energy of FṖH₃ lies 120.9 kJ mol⁻¹ above the energy of isolated PH₃ and F·. The geometry of this radical differs from the related radicals (Table 1). The equatorial bond length of 1.43 Å is considerably shorter than that of the same bond in HṖH₃ (1.59 Å), but identical with the bond length in the PH₃ molecule. The angle ϕ (85.9°) is smaller and the P-F bond length of 1.79 Å is longer than for FṖF₃. This structure actually resembles the LUMO-TS for HṖH₃. As in the case of HṖH₃, two loose complexes for FṖH₃ are found, both for HOMO and LUMO approach. Their PH₃ fragments are identical with the PH₃ molecule, the P-F distances are 3.21 and 3.73 Å, respectively. The UHF energies lie 3.8 and 0.2 kJ mol⁻¹ below isolated PH₃ and F·. By means of the saddle-point optimization method the F≐PH₃ transition state for LUMO approach was calculated. Its structure (PF= 2.10 Å, PH= 1.40 Å, ϕ= 78.5°) is close to that of the optimized FṖH₃ radical. The energy of this transition state is 130.7 kJ mol⁻¹ higher than for isolated PH₃ and F·. The energy difference between FṖH₃ radical and transition state is only 9.8 kJ mol⁻¹ indicating that the radical is rather unstable.

For ClṖH₃ no stable geometry could be calculated (section 3.1). On attempted optimization all trial geometries revealed a HOMO-loose complex (PH₃ + Cl· ; distance 3.21 Å) or a LUMO-loose complex (PH₃ + Cl· ; distance 4.18 Å). The energies of these loose complexes lie respectively 8.6 and 0.2 kJ mol⁻¹ below isolated PH₃ and Cl·.

5. DISCUSSION

The calculations show that all studied C_{3v} X^a ṖX_3^e phosphoranyl radicals possess a TBP-a structure. The calculated electronic structure of these radicals is in good agreement with the experiments on the ·P(OCH₂CH₂)₃N⁺BF₄⁻ radical. Geometry variations for HṖH₃ reveal a σ* arrangement, which, however, is unstable and dissociates directly into PH₃ and H·. The calculated electronic structure of this σ* arrangement is comparable with the experimental values for the Ph₃ṖCl radical reported by Berclaz et al.[1] and therefore gives support to their σ* assignment. The structure of C_{4v} ṖF₅⁻ is octahedral with the unpaired electron in apical position. This structure is fully analogous to the TBP-a structures. The calculated isotropic hyperfine coupling constants of ṖF₅⁻ are in excellent agreement with the experimental values reported by Morton et al.[3] Variation of the apical-equatorial bond angle for ṖF₅⁻ leads to a σ* arrangement. Comparison of the electronic structures of this σ* ṖF₅⁻ radical anion and the experimental values obtained for the ClṖ(O₂C₆H₄)₂⁻ radical anion indicates that the latter possibly possesses a σ* C_{4v} arrangement and not a O_h structure.[6]

From the calculations presented above it is clear that the electronic structure of C_{3v} phosphoranyl radicals and C_{4v} phosphorane anion radicals strongly depends on the apical-equatorial bond angle ϕ. The different configurations of the experimentally observed TBP-a, O_h and σ* radicals can be explained on basis of the angle ϕ of their

precursors. TBP-a and O_h structures can be expected when ϕ is close to $90°$. For $H\dot{P}(OCH_2CH_2)_3N^+BF_4^-$, the precursor of the TBP-a $\cdot\dot{P}(OCH_2CH_2)_3N^+BF_4^-$ radical, the angle ϕ between the three equatorial PO bonds and the apical PN linkage is $87°$.[20] Further, the O_h radicals $\dot{P}F_5^-$ and $\dot{P}Cl_5^-$ are formed by abstraction of fluorine and chlorine from the PF_6^- and PCl_6^- anions ($\phi = 90°$).[3,4] σ^* Structures, on the other hand, can be expected when $\phi > 100°$. The formation of the σ^* Ph$_3\dot{P}$Cl radical is in accordance with the tetrahedral configuration at phosphorus of Ph$_3$PBCl$_3$, from which this radical is generated.[1] Finally, the $Cl\dot{P}(O_2C_6H_4)_2^-$ radical is formed by electron capture of $ClP(O_2C_6H_4)_2$ which possesses ClPO bond angles ϕ from $98.8°$ to $105.3°$.

The importance of ϕ in the choice between the two possible configurations is related to the rigidity and compactness of the matrix in which the radicals are formed, since this may prevent geometrical isomerization and control cage reactions.

Despite geometry variations and a study of a number of different radicals it was not possible to calculate a stable σ^* radical. In general, the stability of σ^* radicals, containing a three-electron bond, is extremely dependent on the match of the energy levels of the two species involved in the formation of the bond. Only in case the energy levels are degenerate (or nearly), a σ^* structure can be expected.[22] Therefore, the possibility that the stabilization of a σ^* structure cannot be abstracted from the $\dot{P}H_4$ and $\dot{P}F_5^-$ model systems must be taken into account. In this respect it is important to note that stable σ^* structures for phosphoranyl radicals have been predicted by ab initio[22] and semi-emperical[23,24] quantum chemical calculations for symmetrical radicals as $H_3PPH_3^+$ and $(MeO)_3PP(MeO)_3^+$. These radicals possess, by symmetry, two degenerate interacting orbitals, giving rise to an optimal interaction and to a stable three-electron bond.

REFERENCES

1. T. Berclaz, M. Geoffroy and E.A.C. Lucken, Chem. Phys. Lett., **36**, 677 (1975).

2. J.H.H. Hamerlinck, P. Schipper and H.M. Buck, J. Am. Chem. Soc., **102**, 5679 (1980).

3. J.R. Morton, K.F. Preston and S.J. Strach, J. Magn. Reson., **37**, 321 (1980).

4. S.P. Mishra and M.C.R. Symons, J. Chem. Soc., Dalton Trans., 139 (1976).

5. A. Hasegawa and F. Williams, Chem. Phys. Lett., **45**, 275 (1977).

6. J.H.H. Hamerlinck, P. Schipper and H.M. Buck, Chem. Phys. Lett., **80**, 358 (1981).

7. J.S. Binkely, R.A. Whiteside, P.C. Hariharan, R. Seeger, J.A. Pople, W.J. Hehre and M.D. Newton, QCPE, **11**, 368 (1978).

8. J.S. Binkely, R.A. Whiteside, R. Krishnan, R. Seeger, D.J. DeFrees, H.B. Schlegel, S. Topiol, L.R. Kahn and J.A. Pople, GAUSSIAN 80, Department of Chemistry, Carnegie-Mellon University, Pittsburgh, (1980).

9. Details of the calculations will be presented in chapter 3.

10. Without this symmetry constraint optimization would probably reveal C_{2v} or C_s geometries.

11. J.M. Howell and J.F. Olsen, J. Am. Chem. Soc., 98, 7119 (1976).

12. M.C.R. Symons, Chem. Phys. Lett., 40, 226 (1976).

13. V.V. Penkovsky, Dokl. Akad. Nauk SSRR (Engl. Transl.), 243, 539 (1978).

14. J.A. Baban and B.P. Roberts, J. Chem. Soc., Chem. Commun., 537 (1979).

15. J.C. Evans and S.P. Mishra, J. Inorg. Nucl. Chem., 43, 481 (1981).

16. R.R. Holmes, ACS Monogr., No. 175 (1980).

17. Abbreviations used are HOMO for highest occupied molecular orbital and LUMO for lowest unoccupied molecular orbital.

18. M.C.R. Symons, *Electron Spin Resonance, Specialist Periodical Report, Vol. 7*, P.B. Ayscough, Ed. (The Chemical Society, London, 1982).

19. B.P. Roberts and K. Singh, J. Chem. Soc., Chem. Commun., 890 (1979).

20. J.C. Clardy, M.C. Milbrath, J.P. Springer and J.G. Verkade, J. Am. Chem. Soc., 98, 623 (1976).

21. R.K. Brown and R.R. Holmes, Inorg. Chem., 16, 2294 (1977).

22. T. Clark, J. Comput. Chem., 4, 404 (1983).

23. C. Glidewell, J. Chem. Soc., Perkin Trans. 2, 299 (1985).

24. C. Glidewell, J. Chem. Soc., Perkin Trans. 2, 551 (1985).

CHAPTER 3

Ab initio study of isotropic and anisotropic hyperfine interactions in phosphoranyl and phosphorane anion radicals

1. INTRODUCTION

Single-crystal ESR studies have revealed isotropic and anisotropic hyperfine couplings for a number of phosphoranyl radicals.[1-5] From the isotropic hyperfine coupling the participation of the valence s orbitals in the molecular orbitals can be estimated, whereas the anisotropic coupling can be related to the contribution of p (and d) orbitals. This results in a description of the singly occupied molecular orbital (SOMO). Previous ab initio calculations using the unrestricted Hartree-Fock (UHF) theory have been moderately successful in predicting isotropic couplings for phosphoranyl[6,7] and related radicals with other second row central atoms.[8,9] In these calculations orbital populations, derived from a Mulliken population analysis, are compared with the estimated values from the experimental hyperfine couplings. In this chapter calculations are presented for isotropic and anisotropic hyperfine interactions by a direct computation of the expectation values of the corresponding operators. The ab initio calculations are performed for a number of elementary phosphoranyl and phosphorane anion radicals. A comparison is made with experimental values and the influence of d orbitals on phosphorus is evaluated.

2. QUANTUM CHEMICAL METHODS

2.1. Electronic wave function

Three quantum chemical procedures were used to obtain a wave function for the open-shell state radicals. First, using the UHF method there is a serious limitation since the resulting wave function in general does not describe a pure spin state, but contains significant contaminations of higher multiplicities. Since the major aim of this study is the calculation of spin-dependent properties it is necessary to abstract wave functions which describe the doublet state more accurately. Therefore the UHF procedure was followed by removal of the next possible spin multiplicity (i.e., the quartet state). This was achieved by the use of the annihilation operator.[10,11] This second method is denoted

as UHF+AN. Finally, the restricted open-shell Hartree-Fock (ROHF) procedure was used, based on the theory by Binkley et al.[12] The resulting wave function from a ROHF calculation represents a pure spin state, which, however, is unable to explain spin polarization. The fact that this indirect spin distribution is neglected will be of minor interest, since the studied radicals are σ radicals and thus most of the experimentally observable isotropic and anisotropic hyperfine couplings are a result of direct delocalization of the unpaired electron. The ROHF procedure involves diagonalization of matrices in three subspaces: doubly occupied MOs/empty MOs; singly occupied MOs/empty MOs and doubly occupied MOs/singly occupied MOs, and is therefore very time consuming, especially when larger basis sets are involved. A difficulty which arises in computing ROHF wave functions is the accuracy of the initial guess. For UHF(+AN) calculations a projected Hückel guess is usually sufficient, but no convergence was achieved for the ROHF procedure when this type of guess was employed. It was found that the most convenient way to obtain SCF-convergence is the use of the α-MO coefficients derived from an UHF calculation as initial guess for a ROHF calculation. Despite many attempts with different initial wave functions it was not possible to obtain SCF-convergence with the ROHF procedure for one of the studied radicals ($\dot{P}F_5^-$, vide infra).

2.2. Basis set

Throughout the calculations a split valence 4-31G basis set[13] was used. To investigate the effect of d-type functions on the spin-dependent properties a single set of six second-order Gaussians, with a radial exponent α of 0.55, was added to the phosphorus basis. This basis set will be denoted as 4-31G(*). The choice for the exponent $\alpha = 0.55$ is based on the closely related 6-31G* basis set for phosphorus.[14]

2.3. Molecular geometries

The molecular geometries were fully optimized with respect to all bond lengths and bond angles within the symmetry constraints (C_{2v}, C_{3v}, C_{4v}). The structure optimizations were carried out with the 4-31G UHF wave function obtained before annihilation. All subsequent calculations (UHF+AN, ROHF and the inclusion of d-type Gaussians) were single-point calculations. It is likely, however, that the molecular geometries are changed if re-optimized at UHF+AN or ROHF level, or after the inclusion of d functions.

2.4. Properties

The hyperfine term of the Hamiltonian for a free radical in which one unpaired electron interacts with one nucleus consists of an isotropic part arising from the Fermi

contact interaction and an anisotropic part due to electron-nuclear dipole interaction. These interactions can be evaluated by computing the expectation values of their corresponding operators. When the MOs of the wave function are defined as linear combinations of atomic orbitals ϕ_μ, the expectation values of isotropic and anisotropic hyperfine interactions at a nucleus N can be expressed as

$$A_N^{iso} = (8\pi/3) g \beta g_N \beta_N \sum_{\mu,\nu} P_{\mu\nu}^{\alpha-\beta} <\phi_\mu | \delta(r_N) | \phi_\nu> \qquad 3.1$$

and

$$B_{ij}^N = -g \beta g_N \beta_N \sum_{\mu,\nu} P_{\mu\nu}^{\alpha-\beta} <\phi_\mu \left| \frac{r^2 \delta_{ij} - 3ij}{r^5} \right| \phi_\nu> \qquad 3.2$$

respectively, in which $P_{\mu\nu}^{\alpha-\beta}$ is the first-order spin density matrix and i, j represent the spatial coordinates x, y, z of the electron relative to the nucleus N. Since the B_{ij}^N matrix is symmetric ($B_{ij}^N = B_{ji}^N$) it can always be diagonalized. After diagonalization the three principal values are obtained, together with their directions relative to the x, y, z coordinate system. Spin density plots of some of the radicals presented in this study were calculated by evaluating the point spin density $\rho(r)$ defined as

$$\rho(r) = \sum_{\mu,\nu} P_{\mu\nu}^{\alpha-\beta} <\phi_\mu | \delta(r) | \phi_\nu> \qquad 3.3$$

2.5. Computational details

The SCF calculations and structure optimizations were performed with the GAUSSIAN 80 program system.[15] The program includes optionally annihilation of the largest spin contaminant and an algorithm for the ROHF procedure. For the evaluation of the hyperfine interactions the property package of the GAUSSIAN 79 program[16] was adapted for the calculation of spin-dependent properties. The GAUSSIAN 79 property package is based on the POLYATOM program.[17] The computed values of the properties are calculated in atomic units. Conversion factors to MHz are $800.24 \cdot g_N$ for A_N^{iso} and $95.52 \cdot g_N$ for B_{ij}^N. The conversion factors include the proportionality constants of eqns. 3.1 and 3.2. The g tensor is assumed to be isotropic and the actual electron g factor is set equal to the value of 2.00232 of the free electron.

3. RESULTS

The calculations were performed for the $\dot{P}H_4$ and $\dot{P}F_4$ phosphoranyl radicals both within C_{2v} and C_{3v} symmetry constraint and for the $\dot{P}F_5^-$ (C_{4v}) phosphorane anion radical. Earlier work at 4-31G level revealed the equilibrium geometries of C_{2v} $\dot{P}H_4$ and C_{2v} $\dot{P}F_4$.[6] The optimized geometrical parameters (Fig. 1) are presented in Table I.
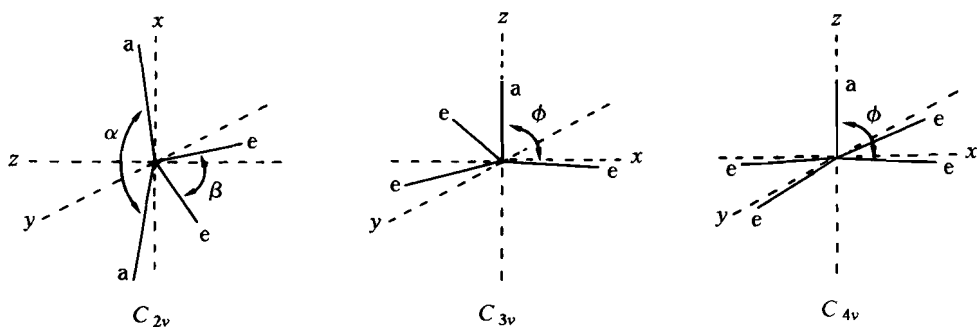
Figure 1. Standard orientation of the C_{2v}, C_{3v} and C_{4v} radicals in the x, y, z coordinate system. Geometrical parameters are indicated. (a= apical, e= equatorial).

Table I. Optimized geometrical parameters (see Fig. 1) for the studied radicals.

Radical	Symmetry	Bond length (Å)		Bond angle (°)		
		r_a	r_e	α	β	ϕ
$\dot{P}H_4$	C_{2v}	1.648	1.423	172.5	97.0	
$\dot{P}H_4$	C_{3v}	1.427	1.590			89.5
$\dot{P}F_4$	C_{2v}	1.704	1.609	162.6	101.7	
$\dot{P}F_4$	C_{3v}	1.614	1.670			91.6
$\dot{P}F_5^-$	C_{4v}	1.640	1.728			90.6

The calculated energies and expectation values of the S^2 operator are collected in Table II. The ROHF energies of the radicals lie 15-30 kJ mol^{-1} above the corresponding UHF energies. The lowering of the UHF energy as a result of the inclusion of d functions is approximately 188 kJ mol^{-1} for the two $\dot{P}H_4$ radicals[18] and 375-400 kJ mol^{-1}

35

Table II. UHF energies (a.u.) and $<S^2>$ expectation values for the radicals at their equilibrium geometries (Table I).

		UHF 4-31G//4-31G			UHF 4-31G(*)//4-31G			ROHF 4-31G//4-31G	
		E	$<S^2>$	$<S^2>_{AN}$	E	$<S^2>$	$<S^2>_{AN}$	E	$<S^2>$
$\dot{P}H_4$	C_{2v}	-342.504763	0.8080	0.7506	-342.575869	0.8023	0.7511	-342.493494	0.75
$\dot{P}H_4$	C_{3v}	-342.472475	0.8328	0.7543	-342.544737	0.8149	0.7530	-342.462516	0.75
$\dot{P}F_4$	C_{2v}	-737.556144	0.7773	0.7503	-737.705323	0.7675	0.7502	-737.548581	0.75
$\dot{P}F_4$	C_{3v}	-737.549048	0.7798	0.7505	-737.692526	0.7692	0.7503	-737.541742	0.75
$\dot{P}F_5^-$	C_{4v}	-836.982786	0.7626	0.7501	-836.135765	0.7592	0.7501	no convergence	

for the $\dot{P}F_4$ and $\dot{P}F_5^-$ radicals. Annihilation of the largest spin contaminant results in $<S^2>$ values close to 0.75 for both basis sets.

3.1. Isotropic hyperfine coupling

Isotropic hyperfine couplings were computed for the radicals at their 4-31G UHF equilibrium geometries. The results of these calculations for the ^{1}H, ^{19}F and ^{31}P nuclei are summarized in Table III.

The computed couplings agree very well with the experimental values.[3,19,20] These values indicate that the SOMO of the C_{2v} radicals contains mainly contributions of phosphorus and the two apical ligands, whereas for the C_{3v} and C_{4v} radicals the major part of the spin density is located on phosphorus and the three (or four) equatorial nuclei. The equatorial nuclei of the C_{2v}, and the apical nucleus of the C_{3v} and C_{4v} radicals possess a near zero spin density. Comparison of the $<S^2>$ values and the calculated isotropic hyperfine interactions reveals that the improvement of the wave function to a more pure doublet state leads to a higher value for the Fermi contact term of the central phosphorus nucleus, largely at the cost of the apical nuclei for the C_{2v} radicals and the equatorial nuclei for the C_{3v} and C_{4v} radicals. The implementation of d-type functions to the 4-31G basis set leads to an increase of the isotropic coupling of the central phosphorus nucleus for C_{2v} $\dot{P}H_4$ and C_{2v} $\dot{P}F_4$ but lowers this value for C_{3v} $\dot{P}H_4$, C_{3v} $\dot{P}F_4$, and C_{4v} $\dot{P}F_5^-$. These effects are for all five radicals accompanied by a decrease of the contribution of those ligands that contribute most to the SOMO. This is more pronounced for hydrogen than for fluorine.

Table III. Computed isotropic hyperfine couplings A^{iso} (MHz) for the nuclei of the studied radicals using different computational methods (experimental data, if available, are included).

			4-31G			4-31G(*)		
			UHF	UHF+AN	ROHF	UHF	UHF+AN	Experiment
$\dot{P}H_4$	C_{2v}	A_P	1432	1457	1645	1424	1494	1455[a]
		A_{H^a}	762	594	437	689	521	558
		A_{H^e}	-42	-11	6	-62	-17	17
$\dot{P}H_4$	C_{3v}	A_P	2267	2239	2446	1934	2043	
		A_{H^a}	31	39	48	11	31	
		A_{H^e}	558	378	252	488	331	
$\dot{P}F_4$	C_{2v}	A_P	3052	3110	3325	3228	3256	3671[b]
		A_{F^a}	639	465	373	605	448	858
		A_{F^e}	36	36	34	64	53	171
$\dot{P}F_4$	C_{3v}	A_P	3477	3562	3772	3411	3472	
		A_{F^a}	-80	-25	-3	-42	-14	
		A_{F^e}	639	490	404	594	462	
$\dot{P}F_5^-$	C_{4v}	A_P	3708	3758		3556	3570	3800[c]
		A_{F^a}	-48	-8		-20	-6	8
		A_{F^e}	488	359		437	328	552

[a] ref. 19; [b] ref. 3; [c] ref. 20.

3.2. Anisotropic hyperfine coupling

The results of the computation of the principal values of the dipolar hyperfine tensor and their directions are compiled in Tables IV to VII for $\dot{P}H_4$, C_{2v} $\dot{P}F_4$, C_{3v} $\dot{P}F_4$, and C_{4v} $\dot{P}F_5^-$ respectively. The coordinate system for these calculations is given in Fig. 1. For all radicals the z axis is the axis of highest symmetry (C_2, C_3, C_4) and which corresponds to the direction of the largest principal value of the phosphorus dipolar hyperfine coupling tensor.

The listed values for the two C_{2v} radicals clearly show the contaminating effect of higher multiplicities in the wave function. In an axially symmetrical system the principal values of the anisotropic coupling should be of the ratio of -B, -B, 2B.[21] Many phosphoranyl and phosphorane anion radicals with experimentally known couplings possess such an axially symmetrical dipolar tensor.[2-5] Table IV $(C_{2v}$ $\dot{P}H_4)$ and Table V $(C_{2v}$ $\dot{P}F_4)$ reveal that the condition for an axially symmetrical system is only fulfilled when the ROHF calculations are employed and thus $<S^2>=0.75$. A Mulliken population analysis nicely illustrates the contaminating effect. Upon improvement of the doublet

Table IV. Calculated phosphorus dipolar hyperfine coupling B (MHz) for the C_{2v} and C_{3v} isomers of the $\dot{P}H_4$ radical using different computational methods (coordinates x, y, z according to Fig. 1).

		C_{2v} $\dot{P}H_4$			C_{3v} $\dot{P}H_4$		
		B_{xx}	B_{yy}	B_{zz}	B_{xx}	B_{yy}	B_{zz}
UHF	4-31G	-238	50	188	-126	-126	251
UHF+AN	4-31G	-98	-11	109	-64	-64	128
ROHF	4-31G	-45	-48	93	-45	-45	90
UHF	4-31G(*)	-247	25	222	-140	-140	280
UHF+AN	4-31G(*)	-118	-28	146	-84	-84	168

Table V. Calculated phosphorus and fluorine dipolar hyperfine couplings B (MHz) for C_{2v} $\dot{P}F_4$ using different computational methods[a].

		P	F_1^a					F_1^c				
		B	B	T			θ^a	B	T			θ^a
UHF	B_{xx}	-238	939	0.976	0	-0.220	12.7	-50	1	0	0	
4-31G	B_{yy}	-70	-493	0	1	0		-56	0	1.000	0.004	
	B_{zz}	308	-496	0.220	0	0.976		106	0	0.004	-1.000	0.2
UHF+AN	B_{xx}	-151	772	0.972	0	-0.236	13.7	-42	1	0	0	
4-31G	B_{yy}	-98	-386	0	1	0		-39	0	0.989	0.148	
	B_{zz}	249	-386	0.236	0	0.972		81	0	0.148	-0.989	8.5
ROHF	B_{xx}	-126	572	0.966	0	-0.260	15.0	-42	1	0	0	
4-31G	B_{yy}	-123	-286	0	1	0		-39	0	0.966	0.259	
	B_{zz}	249	-286	0.260	0	0.966		81	0	0.259	-0.966	15.0
UHF	B_{xx}	-210	790	0.967	0	-0.255	14.8	-65	1	0	0	
4-31G(*)	B_{yy}	-106	-401	0	1	0		-53	0	0.968	0.249	
	B_{zz}	316	-389	0.255	0	0.967		118	0	0.249	-0.968	14.4
UHF+AN	B_{xx}	-157	605	0.962	0	-0.274	15.9	-50	1	0	0	
4-31G(*)	B_{yy}	-120	-305	0	1	0		-42	0	0.956	0.293	
	B_{zz}	277	-300	0.274	0	0.962		92	0	0.293	-0.956	17.0
Expt.	B_{xx}	-179	454	-67				-41				
(ref. 3)	B_{yy}	-179	-227	-67				-41				
	B_{zz}	358	-227	134				81				

[a] The coordinate system x, y, z is given in Fig. 1. T represents the transformation matrix and gives the directions of the principal values (B_{ii}). θ is the angle (deg.) between the direction of the largest principal value and the nearest coordinate axis. (θ^a relative to x; θ^c relative to z).

Table VI. Calculated phosphorus and fluorine dipolar hyperfine couplings B (MHz) for C_{3v} $\dot{P}F_4$ using different computational methods[a].

		P	F^a	F^e				
		B	B	B	T			θ^e
UHF	B$_{xx}$	-160	28	785	0.949	0	0.317	18.5
4-31G	B$_{yy}$	-160	28	-406	0	1	0	
	B$_{zz}$	321	-56	-379	-0.317	0	0.947	
UHF+AN	B$_{xx}$	-121	5	583	0.943	1	0.334	19.5
4-31G	B$_{yy}$	-121	5	-297	0	1	0	
	B$_{zz}$	243	-9	-286	-0.334	0	0.943	
ROHF	B$_{xx}$	-115	-5	432	0.933	0	0.359	21.0
4-31G	B$_{yy}$	-115	-5	-216	0	1	0	
	B$_{zz}$	231	11	-216	-0.359	0	0.933	
UHF	B$_{xx}$	-160	-3	642	0.938	0	0.345	20.2
4-31G(*)	B$_{yy}$	-160	-3	-328	0	1	0	
	B$_{zz}$	320	6	-314	-0.345	0	0.938	
UHF+AN	B$_{xx}$	-135	-5	476	0.931	0	0.364	21.4
4-31G(*)	B$_{yy}$	-135	-5	-241	0	1	0	
	B$_{zz}$	269	10	-235	-0.364	0	0.931	

[a] Parameters as for Table V, except θ^e, the angle between the direction of the largest principal value of F^e and the x axis.

Table VII. Calculated phosphorus and fluorine dipolar hyperfine couplings B (MHz) for C_{4v} $\dot{P}F_5^-$ using different computational methods[a].

		P	F^a	F^e				
		B	B	B	T			θ^e
UHF	B$_{xx}$	-160	14	479	0.914	0	0.407	24.0
4-31G	B$_{yy}$	-160	14	-241	0	1	0	
	B$_{zz}$	320	-28	-238	-0.407	0	0.914	
UHF+AN	B$_{xx}$	-137	3	359	0.911	0	0.413	24.4
4-31G	B$_{yy}$	-137	3	-179	0	1	0	
	B$_{zz}$	274	-6	-179	-0.413	0	0.911	
UHF	B$_{xx}$	-160	-3	398	0.907	0	0.420	24.8
4-31G(*)	B$_{yy}$	-160	-3	-202	0	1	0	
	B$_{zz}$	320	6	-196	-0.420	0	0.907	
UHF+AN	B$_{xx}$	-145	-8	297	0.902	0	0.432	25.6
4-31G(*)	B$_{yy}$	-145	-8	-149	0	1	0	
	B$_{zz}$	190	15	-149	-0.432	0	0.902	

[a] Parameters as for Table VI.

state the large negative value for the spin density in the $3p_x$ orbital diminishes and becomes zero when the ROHF procedure is used (Table VIII). The fact that C_{3v} and C_{4v} radicals possess an axially symmetrical phosphorus dipolar hyperfine tensor in all calculations is a consequence of the higher rotational symmetry of these radicals.

Table VIII. Mulliken population analysis for the two C_{2v} radicals using different computational methods. Values are computed as a summation of the inner and outer orbitals of the 4-31G basis set ($<S^2>$ values are given for comparison).

	C_{2v} $\dot{P}H_4$			C_{2v} $\dot{P}F_4$		
	UHF	UHF+AN	ROHF	UHF	UHF+AN	ROHF
$<S^2>$	0.8080	0.7506	0.7500	0.7773	0.7503	0.7500
$3s$	0.052	0.076	0.105	0.289	0.302	0.328
$3p_x$	-0.324	-0.104	0.000	-0.089	-0.030	0.000
$3p_y$	0.041	0.015	0.000	0.015	0.005	0.000
$3p_z$	0.202	0.168	0.187	0.314	0.291	0.313

Only for the C_{2v} $\dot{P}F_4$ radical anisotropic experimental data are available for a direct comparison[3] (Table V). The computed phosphorus anisotropic coupling is in reasonable agreement with the experimental data and the couplings of two equatorial fluorines are almost perfectly predicted. Hasegawa et al.[3] report two anisotropic parts for each of the two api al fluorines, because of an asymmetric hyperfine tensor with principal values along x and z axes. The calculations do not confirm this result but clearly show an axial symmetrical tensor. However, the computations reveal that the largest principal value is not coincident with any of the x, y or z axes, but lies in the xz plane. Since the single–crystal experiments on the $\dot{P}F_4$ radical consisted of rotation around only one axis it is possible that the reported non-axial symmetry is in error. The phosphorus dipolar hyperfine couplings of the other calculated radicals also possess values that are similar to experimentally known anisotropic couplings ($B_{zz}^P = 200-360$ MHz).[2]

The implementation of d functions results in a small rise of the phosphorus dipolar hyperfine interaction tensor. The largest effects are found for the two $\dot{P}H_4$ radicals where an increase of 34-37 MHz is found on UHF+AN level. The influence of the second–order Gaussians is more pronounced on the dipolar couplings of the most contributing ligands. A serious decrease of the largest principal value is calculated for the apical fluorines of C_{2v} $\dot{P}F_4$ and the equatorial fluorines of C_{3v} $\dot{P}F_4$, and C_{4v} $\dot{P}F_5^-$.

An important and unexpected result that can be derived from Tables V to VII is that the direction of the fluorine anisotropic coupling does not coincide with any axis of the coordinate system, nor with the P-F bond, but makes a pronounced angle with the direction of this bond. The angles θ between the direction of the fluorine dipolar tensor and the axes of the coordinate system are given in the last column of Tables V to VII.

3.3. Spin density plots

The point spin density $\rho(\mathbf{r})$ was calculated for the C_{2v} $\dot{P}H_4$ and C_{2v} $\dot{P}F_4$ radicals in the xz and yz planes. The values at the curves of constant spin density in Figs. 2 and 3 are expressed in milli-electrons bohr^{-3}. The wave function used in these calculations was derived from the ROHF procedure to minimize contaminating effects. Figure 3 illustrates the results concerning the direction of the apical fluorine dipolar hyperfine coupling, since it is clear that the plotted fluorine $2p$ orbital is not directed along the P-F$^\alpha$ bond. Figures 2 and 3 furthermore emphasize the antibonding character of the SOMO of phosphoranyl radicals.
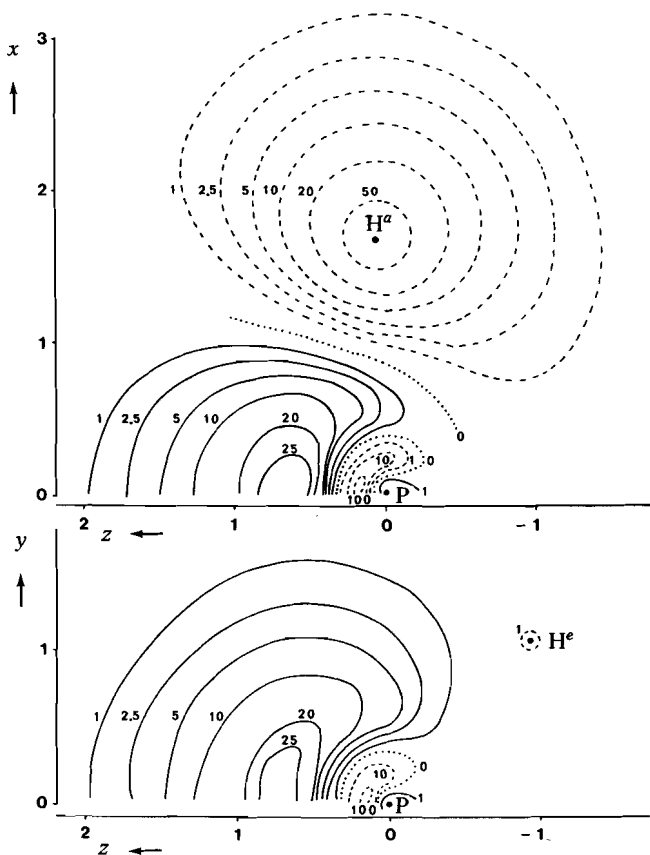
Figure 2. Spin density plot of C_{2v} $\dot{P}H_4$ calculated in the xz and yz planes with the 4-31G ROHF wave function. Because of the twofold symmetry only the positive x and y directions are shown. The values of the spin density at the curves are in milli-electrons bohr^{-3}.
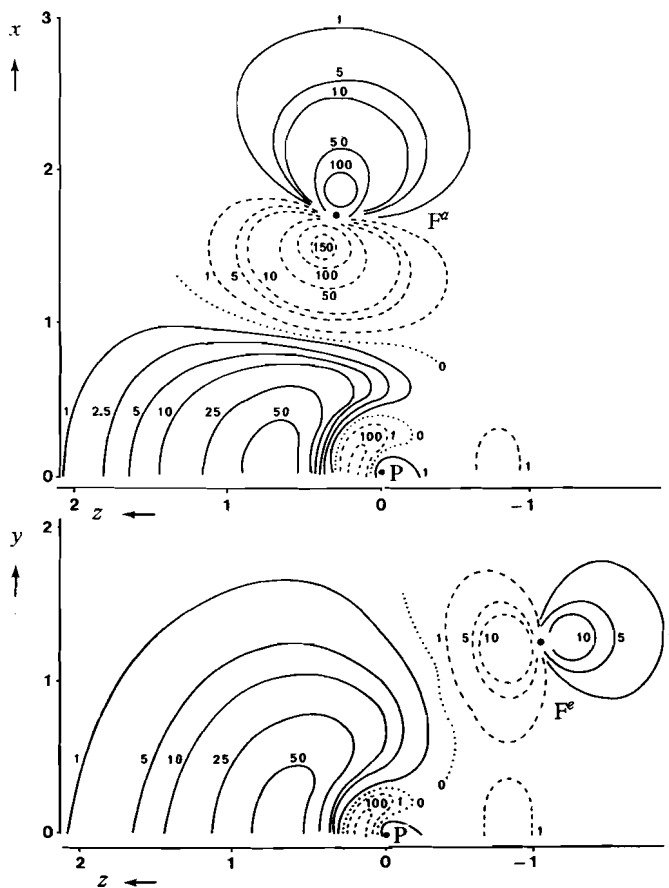
Figure 3. Spin density plot of C_{2v} $\dot{P}F_4$ (See Fig. 2).

4. DISCUSSION

All computational methods give fairly good results for the isotropic hyperfine couplings. For the dipolar couplings, however, the wave function must present a pure spin state in order to produce axially symmetrical hyperfine tensors and to predict experimental couplings. Further improvement of the accuracy of the calculation of isotropic and anisotropic hyperfine interactions can be achieved by the use of larger and more accurate basis sets. Especially the behaviour of the wave function near the nuclei

is of major importance since both isotropic $(\delta(r_N))$ and the dipolar $(<r^{-3}>)$ couplings strongly depend on the electron distribution close to the nuclei. Comparison of the isotropic and anisotropic phosphorus couplings for the C_{2v} and C_{3v} radicals of $\dot{P}H_4$ and $\dot{P}F_4$ indicates that their magnitude is comparable for both isomers of the $\dot{P}H_4$ and $\dot{P}F_4$ radicals respectively. The same result has been experimentally demonstrated by Hamerlinck et al.[22,23] in a single-crystal ESR study of the TBP-e (C_{2v}) and TBP-a (C_{3v}) isomers of the $\dot{P}(OCH_2CH_2)_3N^+BF_4^-$ radical.

The calculations predict larger couplings for the C_{3v} isomers, whereas the reverse was found experimentally (Fig. 4). The strong dependence of the isotropic coupling on variation of the apical-equatorial bond angle ϕ in C_{3v} and C_{4v} radicals[24] can partly account for this discrepancy.

	TBP-e	TBP-a
A_P^{iso}	2783 MHz	2236 MHz
B_{zz}^P	354 MHz	252 MHz
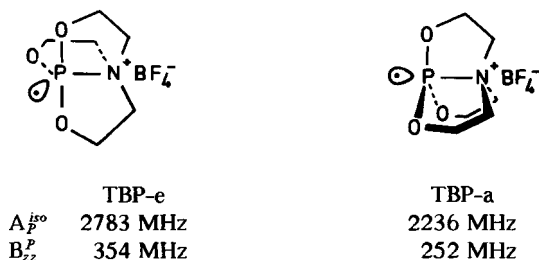
Figure 4. The TBP-e (C_{2v}) and TBP-a (C_{3v}) isomers of the $\dot{P}(OCH_2CH_2)_3N^+BF_4^-$ radical; including the experimental hfcs (refs. 22, 23).

Another explanation may be found in the participation of d orbitals. It was shown that the inclusion of d-type Gaussians leads to an increase of the isotropic phosphorus hyperfine coupling for the C_{2v} radicals, but lowers this value for C_{3v} radicals. The d-type Gaussians further affect the hyperfine interaction of the unpaired electron with the ligand nuclei. For the ligands that contribute most to the SOMO the hyperfine couplings are lowered: for hydrogen the isotropic and for fluorine the anisotropic coupling. This can be explained by the new type of symmetry which is introduced on phosphorus by the inclusion of d orbitals, and which fits exactly to the symmetry of the SOMO of the phosphoranyl radicals. The computed MO coefficients (Table IX) indicate that from the six second-order Gaussians the d_{x^2} and d_{z^2} orbitals contribute most to the SOMO of the C_{2v} radicals and the d_{x^2}, d_{y^2}, and d_{z^2} to the SOMO of the C_{3v} and C_{4v} radicals. The d_{xy}, d_{xz}, and d_{yz} orbitals do not contribute to any of the SOMOs because of their wrong symmetry.

The fact that the calculated dipolar fluorine hyperfine tensor is not coincident with the corresponding fluorine-phosphorus bond is a new aspect in the structure of these radicals. This result remains unaffected after the inclusion of d orbitals. Single-crystal ESR studies on $O\dot{P}Cl_3^-$[5] and $\dot{P}F_4$[3] have demonstrated that the apical ligands of these radicals are magnetically equivalent for all orientations of the radical relative to the external magnetic field. Subsequently the conclusion was drawn that the X^a-P-X^a

Table IX. The d orbital SOMO coefficients for the studied radicals resulting from a 4-31G(*) UHF calculation.

		d_{x^2}	d_{y^2}	d_{z^2}	d_{xy}	d_{xz}	d_{yz}
$\dot{P}H_4$	C_{2v}	-0.115	0.062	0.069	0	0	0
$\dot{P}H_4$	C_{3v}	-0.033	-0.033	0.065	0	0	0
$\dot{P}F_4$	C_{2v}	-0.100	0.008	0.185	0	0	0
$\dot{P}F_4$	C_{3v}	-0.055	-0.055	0.134	0	0	0
$\dot{P}F_5^-$	C_{4v}	-0.067	-0.067	0.144	0	0	0

bond is linear. In view of the calculations this conclusion seems unjustifiable, since the dipolar hyperfine tensors can be aligned even when the X^a-P-X^a bond angle deviates seriously from 180°. An explanation for these results can be found in the fact that the phosphoranyl and phosphorane anion radicals are hypervalent, i.e., there are more than eight electrons around phosphorus. The SOMO will therefore possess antibonding character, and is not responsible for the bonding of phosphorus to the ligands.

REFERENCES

1. For a review on phosphoranyl radicals see: W.G. Bentrude, Acc. Chem. Res., **15**, 117 (1982).
2. J.H.H. Hamerlinck, P. Schipper and H.M. Buck, J. Am. Chem. Soc., **105**, 385 (1983).
3. A. Hasegawa, K. Ohnishi, K. Sogabe and M. Miura, Mol. Phys., **30**, 1367 (1975).
4. T. Berclaz, M. Geoffroy and E.A.C. Lucken, Chem. Phys. Lett., **36**, 677 (1975).
5. T. Gillbro and F. Williams, J. Am. Chem. Soc., **96**, 5032 (1974).
6. J.M. Howell and J.F. Olsen, J. Am. Chem. Soc., **98**, 7119 (1976).
7. T. Clark, J. Comput. Chem., **4**, 404 (1983).
8. T. Clark, J. Chem. Soc., Perkin Trans. 2, 1267 (1982).
9. T. Clark, J. Chem. Soc., Chem. Commun., 515 (1981).
10. A.T. Amos and G.G. Hall, Proc. R. Soc. London Ser. A, **263**, 483 (1961).
11. A.T. Amos and L.C. Snyder, J. Chem. Phys., **41**, 1773 (1964).
12. J.S. Binkley, J.A. Pople and P.A. Dobosh, Mol. Phys., **28**, 1423 (1974).
13. (a) R. Ditchfield, W.J. Hehre and J.A. Pople, J. Chem. Phys., **54**, 724 (1971). (b) W.J. Hehre and W.A. Lathan, J. Chem. Phys., **56**, 5255 (1972).

14. M.M. Francl, W.J. Pietro, W.J. Hehre, J.S. Binkley, M.S. Gordon, D.J. DeFrees and J.A. Pople, J. Chem. Phys., **77**, 3654 (1982).

15. J.S. Binkley, R.A. Whiteside, R. Krishnan, R. Seeger, D.J. DeFrees, H.B. Schlegel, S. Topiol, L.R. Kahn and J.A. Pople, GAUSSIAN 80, Department of Chemistry, Carnegie-Mellon University, Pittsburgh.

16. P. Marsh and D.E. Williams, QCPE, Program No. 421, 1981.

17. D.B. Neumann, H. Basch, R.L Kornegay and L.C. Snyder, QCPE, Program No. 199, 1971.

18. Howell and Olsen (ref. 6) found a smaller energy lowering of 153 kJ mol^{-1} for C_{2v} $\dot{P}H_4$ on implementation of d-type functions with a radial exponent of 0.36.

19. A.J. Colussi, J.R. Morton and K.F. Preston, J. Chem. Phys., **62**, 2004 (1975).

20. J.R. Morton, K.F. Preston and S.J. Strach, J. Magn. Reson., **37**, 321 (1980).

21. R.S. Drago, *Physical Methods in Chemistry* (W.B. Saunders, London, 1977).

22. J.H.H. Hamerlinck, P. Schipper and H.M. Buck, J. Chem. Soc., Chem. Commun., 1149 (1981).

23. J.H.H. Hamerlinck, P. Schipper and H.M. Buck, J. Org. Chem., **48**, 306 (1983).

24. R.A.J. Janssen, G.J. Visser and H.M. Buck, J. Am. Chem. Soc., **106**, 3429 (1984). Chapter 2.

CHAPTER 4

Electron capture phosphoranyl radicals in x-irradiated diphosphine disulphides

1. INTRODUCTION

In recent years, there has been a considerable interest in the structure of three-electron bonds in which one electron occupies a $\sigma*$ orbital. Three-electron bond radicals have been observed between atoms of several elements. Examples include $N\dot{\cdot}N$,[1,2] $P\dot{\cdot}$ P,[3-7] $P\dot{\cdot}$halogen,[8-10] $As\dot{\cdot}As$,[3,11] $S\dot{\cdot}S$,[12-14] $S\dot{\cdot}$halogen,[10,15] and $Se\dot{\cdot}Se$.[16] For phosphoranyl radicals several $\sigma*$ structures have been identified.[3-10] Phosphoranyl radicals are of particular interest since they can adopt a number of geometrically and electronically different structures (TBP-e, TBP-a and $\sigma*$) depending on the nature of the substituents and steric constraints.[17-21]

The aim of this study is to investigate the electronic and geometric structure of electron capture phosphoranyl radicals·in x-irradiated single crystals of substituted diphosphine disulphides [$R_2P(S)P(S)R_2$, R= Me, Et, Ph]. These compounds possess a planar *trans* SPPS conformation and a local C_{2h} symmetry.[22] Tetramethyldiphosphine disulphide (1) was part of an investigation by Lyons and Symons[3] on three-electron $P\dot{\cdot}P$ bond radicals. Analysis of the ESR spectrum, obtained after γ irradiation of a powdered sample of 1, revealed the existence of an electron capture radical with a three-electron $P\dot{\cdot}P$ bond. This structure has been assigned on basis of the large splitting between the two observed lines, which could not possibly be due to a phosphorus doublet but represented the $m_I = \pm 1$ features of a triplet. The central $m_I = 0$ lines were hidden under the intense signals of a carbon centred radical. Gillbro et al.[5] reported the first spectroscopic evidence of a three-electron bond by the detection of the $m_I = 0$ transitions for the $(MeO)_3P\dot{\cdot}P(OMe)_3^+$ radical cation. Although single crystals of the parent compound trimethylphosphite were studied, no directional information on the hyperfine couplings was reported. Other three-electron bond radicals have been detected in γ-irradiated trialkylphosphines and -phosphites[3,6,7] (also on basis of the $m_I = \pm 1$ absorptions) and described with MNDO[23,24] and ab initio[28] quantum chemical methods.

In this chapter experimental evidence for the formation of three-electron bond radicals in diphosphine disulphide derivatives is presented. It will be shown that these structures cannot be described as $\sigma*$ since the SOMO does not possess rotational symmetry. In fact, the phosphorus anisotropic hyperfine coupling makes an angle of $20°-30°$ with the P-P bond. The conclusions are based on single-crystal ESR experiments and completely supported by ab initio quantum chemical calculations. For tetramethyldiphosphine disulphide (1) two differently oriented three-electron bond radicals with appreciable differences in ESR parameters are detected. This result can be explained on basis of the x-ray structure analysis of the parent compound.

46

Furthermore, an unexpected result is obtained by the detection and identification of a number of electron capture radicals with an asymmetrical distribution of the unpaired electron over the SPPS moiety.

2. EXPERIMENTAL SECTION

2.1. Synthesis

Compounds tetramethyldiphosphine disulphide (1), tetraethyldiphosphine disulphide (2), tetraphenyldiphosphine disulphide (3), and triethylphosphine sulphide (4) were synthesized according to published methods.[26-29]

2.2. Irradiation and ESR

Single crystals, of suitable dimension for ESR measurements were obtained by slow evaporation in a stream of dry nitrogen of solutions of 1, 2, and 3 in ethanol, diethylether, and benzene, respectively. The single crystals were mounted on a quartz rod and subsequently sealed in a quartz tube. The crystals were x irradiated in a glass Dewar vessel containing liquid nitrogen (77 K) with unfiltered radiation from a Cu source operating at 40 kV and 20 mA for approximately 6h. The ESR measurements were made using a Bruker ER 200D spectrometer operating with a X-band standard cavity. The spectra were recorded digitally using a Bruker Aspect 3000 computer. In a typical run a sweep width of 0.1875 T was sampled with 4 K points resulting in a resolution of 0.045 mT. Microwave power was set as low as possible, being 1 mW in most experiments. The single crystals were rotated perpendicular to the magnetic field with a single axis goniometer in 10° steps. Temperature was controlled with the aid of a variable temperature unit operating between 90 K and room temperature.

2.3. Spectral analysis

The ESR parameters obtained in this study were determined from a second-order analysis of the spectra. Even the qualitative appearance of the ESR spectrum of a three-electron bond radical containing two equivalent $I = \frac{1}{2}$ nuclei exhibiting a large hyperfine coupling cannot be accounted for by first-order theory.[30,31] It is necessary to use a coupled representation for the nuclear spin state and describe the two nuclei with a triplet $(I = 1)$ and a singlet $(I = 0)$. The four nuclear spin states are then denoted by

$|I, m_I>$. If the hyperfine coupling is sufficiently large, as for phosphorus centred radicals, the ESR spectrum will consist of four equally intense lines caused by a separation of the originally degenerated spectral lines for $m_I = 0$ (second-order splitting). In fact, the three $I = 1$ lines are shifted downfield, whereas the $I = 0$ line remaines unaffected. Since the experiments were carried out with irradiated crystals in a quartz tube it was not always possible to observe the two $m_I = 0$ transitions, because of a large overlapping central absorption due to the irradiated quartz. For this reason, the hyperfine coupling and g factor were evaluated from the $m_I = \pm 1$ lines, and when possible, checked with the $m_I = 0$ position(s).
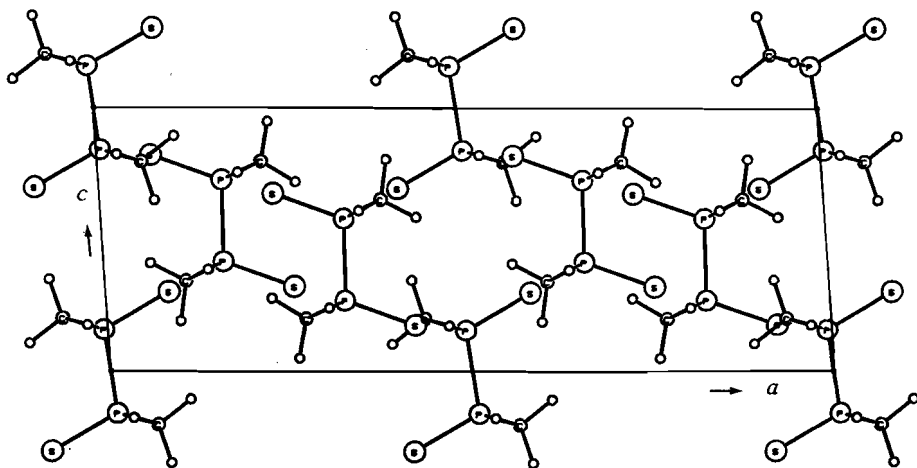
Figure 1. Projection along [010] of the unit cell of tetramethyldiphosphine disulphide (**1**). Molecules I have centres at $(0, 0, 0)$ and $(\frac{1}{2}, \frac{1}{2}, 0)$. Molecules II have centres at $(x, 0, z)$, $(\bar{x}, 0, \bar{z})$, $(\frac{1}{2}+x, \frac{1}{2}, z)$ and $(\frac{1}{2}-x, \frac{1}{2}, \bar{z})$.

3. RESULTS AND ASSIGNMENT

3.1. Tetramethyldiphosphine disulphide (1)

The crystals of tetramethyldiphosphine disulphide (1) belong to the monoclinic space group $C_{2/m}$ and have unit cell parameters $a = 18.882$ Å, $b = 10.703$ Å , $c = 6.984$ Å, and $\beta = 94.7°$.[32] There are six molecules in the unit cell divided over two sets of special orientations. Molecules I have centres at $(0, 0, 0)$ and $(½, ½, 0)$ whereas the centres of molecules II are located on the $(x, 0, z)$, $(\bar{x}, 0, \bar{z})$, $(½+x, ½, z)$ and $(½-x, ½, \bar{z})$ positions (Fig. 1).

Figure 2. Single-crystal ESR spectra of x-irradiated **1**: (a) at 100 K; (b) at 120 K after annealing to 200 K.

49

The two sets of molecules possess pronounced differences in their geometries, especially the P-P bond lengths deviate (respectively, 2.245 Å for 1 and 2.165 Å for II). After x irradiation of a needle-shaped single crystal of **1** at 77 K an ESR spectrum as shown in Fig. 2(a) was obtained.[33] This spectrum was successfully interpreted by assuming the existence of two differently oriented and magnetically not completely equivalent radicals **1a(A)** and **1a(B)**. Both radicals possess two equivalent phosphorus atoms with large hyperfine couplings.

The second-order splitting is very distinct in the spectra. The signals are assigned to originate from three-electron bond radicals **1a(A,B)** (Fig. 3), formed by electron capture in the antibonding MO of the P-P bonds of the precursor molecules.
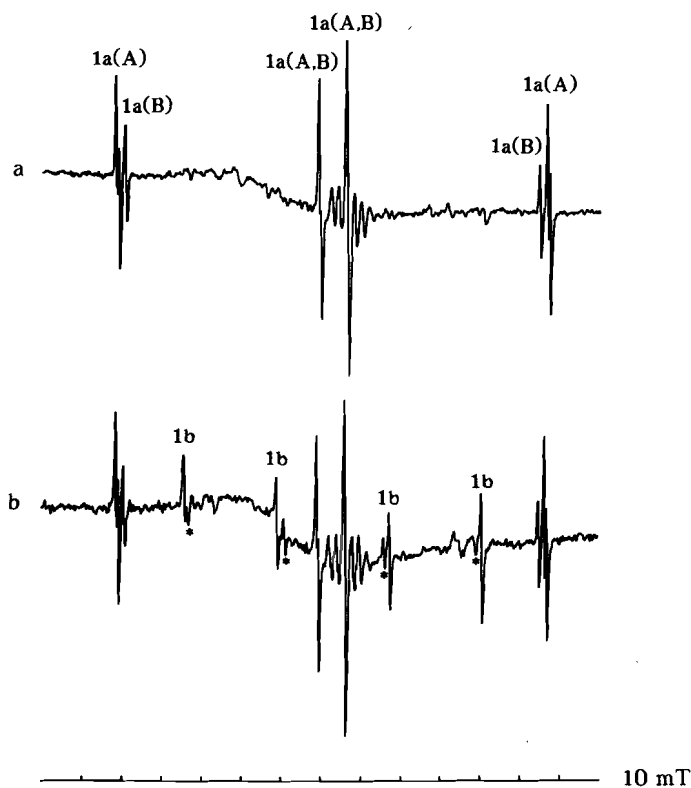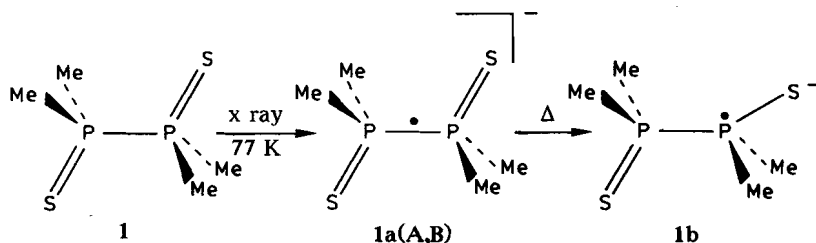

Figure 3. Formation of radicals **1a** and **1b** upon x irradiation and subsequent annealing.

The spectra of the two slightly different radicals are not equally intense and one of them [**1a(A)**] exhibits a small additional splitting due to a single $I = \frac{1}{2}$ nucleus. A complete analysis of these radicals was obtained by rotating the crystals in three mutual

Table I. Hyperfine tensors for radicals **1a(A)**, **1a(B)**, and **1b**.

Radical	Nucleus	Temperature (K)	Total tensor (MHz)	Isotropic part (MHz)	Dipolar tensor (MHz)	Direction cosines		
						a^*	b	c
1a(A)	P_1, P_2	100	1303	1395	-93	-0.887	0.085	-0.454
			1332		-62	0.126	0.990	-0.061
			1550		155	-0.445	0.115	0.889
1a(B)	P_1, P_2	100	1266	1372	-106	-0.805	-0.292	0.517
			1315		-57	-0.260	0.956	0.135
			1535		163	0.533	0.026	0.846
1b	P_1	120	1428	1549	-121	0.199	0.126	0.972
			1485		-64	0.113	0.982	-0.151
			1734		185	-0.974	0.139	0.181
	P_2	120	477	544	-77	-0.989	0.107	-0.102
			496		-48	0.112	0.993	-0.041
			659		115	-0.097	0.052	0.994
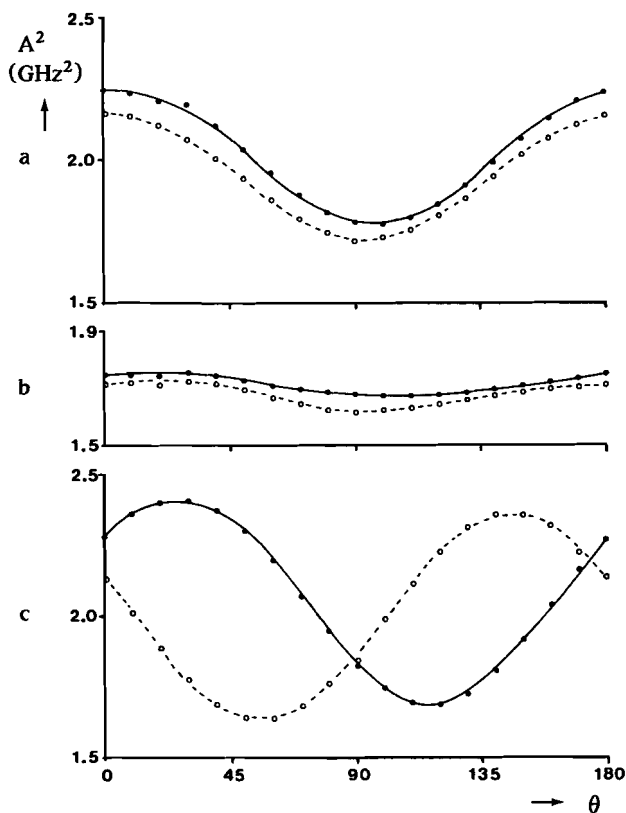
Figure 4. Angular variation of the phosphorus hyperfine coupling for **1a(A)** (solid line) and **1a(B)** (dashed line). (a) cb plane; (b) $a*b$ plane; (c) $ca*$ plane.

orthogonal planes. For this purpose, the orthogonal crystallographic axes b and c were designated as two of the reference axes. The third axis, represented by a*, was taken as the vector product b×c. Figure 4 shows the angular variations of the phosphorus hyperfine coupling for the two radicals.

The small additional splitting of 20 MHz, observed for one of the radicals, is nearly isotropic. Diagonalization of the A^2 and g^2 tensors results in their principal values together with the corresponding direction cosines (Tables I and II). On annealing the crystal to 200 K the intensity of the ESR spectra of the primary products decreases and the features of a secondary radical (**1b**) become apparent. After recooling to 120 K, the ESR spectrum [Fig. 2(b)] shows clearly this radical having one large and one smaller phosphorus hyperfine coupling (**1b**, Fig. 3). This radical possesses a TBP-e like structure with a central phosphorus atom and a second phosphorus nucleus in apical position.

Table II. g Tensors for radicals **1a(A)**, **1a(B)**, and **1b**.

Radical	Temperature (K)	g Tensor	Direction cosines		
			a^*	b	c
1a(A)	100	2.000	-0.507	0.124	0.853
		2.006	-0.856	0.040	-0.515
		2.008	0.099	0.991	-0.086
1a(B)	100	2.001	0.534	0.010	0.840
		2.003	-0.779	0.379	0.499
		2.008	0.313	0.925	-0.214
1b	120	2.004	-0.978	0.196	0.070
		2.004	-0.043	0.073	-0.996
		2.005	-0.191	-0.981	0.035

The remaining apical substituent is a sulphur atom. From the angular variation of these couplings (Fig. 5) their principal values and direction cosines (Tables I and II) are obtained.

For this TBP-e radical only one orientation could clearly be identified. A second site might be present as can be seen from the small absorptions (indicated with an asterisk) in Fig. 2(b). However, a complete analysis of this possible second site proved to be impracticable. From the direction cosines the relative orientations of the maximal and minimal dipolar hyperfine couplings for **1a(A)**, **1a(B)** and **1b** can be calculated (Table III).

Table III. Relative orientations (deg) of the principal directions[a] of the hyperfine couplings for radicals generated in **1**. A clockwise rotation from the horizontal to the vertical tabled couplings is quoted positive.

Radical	**1a(A)**	**1a(B)**	**1b$_1$**	**1b$_2$**
1a(A)	0			
1a(B)	58.8	0		
1b$_1$	-52.5	-111.3	0	
1b$_2$	21.2	-37.8	73.7	0

[a] Because no absolute sign can be attributed to the direction of a principal value, there is an ambiguity of $\pm$ 180° in the listed values.
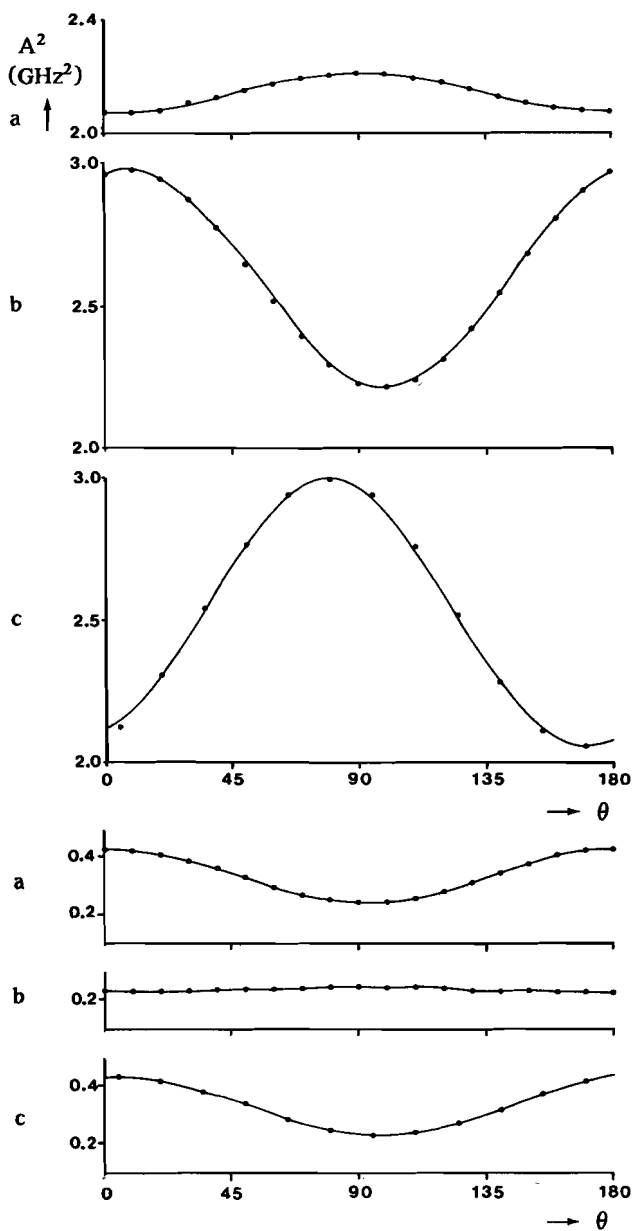
Figure 5. Angular variation of the phosphorus hyperfine couplings for **1b**: (a) *cb* plane; (b) *a*b* plane; (c) *ca** plane. The upper three curves show the coupling of the central phosphorus atom; the remaining three curves show the coupling of the phosphorus atom on the apical site of the TBP-e.

These directions are for **1a(A)** and **1a(B)** inclined by an angle of 58.8°. Since the relative orientation of the two P-P bonds for the two different sets of molecules is only 7.4° (see Fig. 1 for a projection along [010] of the unit cell), it is clear that the maximum spin density in the three-electron bond is not located along the direction of this bond, but makes a pronounced angle with it. Because the axes of rotation are known it is possible to relate the crystal structure with the ESR experiments. Figure 6 shows the two different sets of molecules together with the directions of the principal hyperfine couplings.
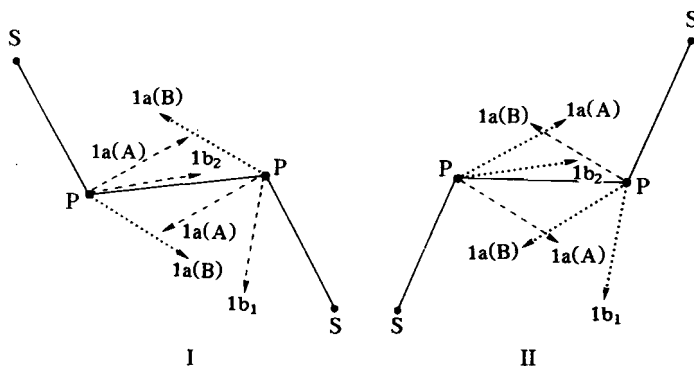

Figure 6. Relative orientations of the precursor molecules I and II and the directions of the hyperfine couplings **1a(A)**, **1a(B)**, **1b₁**, and **1b₂**. Dashed lines represent the assignment of **1a(A)** and **1b** to I and **1a(B)** to II.

The assignment of the radicals **1a(A)** and **1a(B)** to a particular molecule I or II is not straightforward because in principle two possibilities are present. Nevertheless it is possible to make a positive identification based on ab initio quantum chemical calculations. These calculations (vide infra) clearly predict that the largest hyperfine coupling of the three-electron bond radical is situated between the P-P and P-S bonds, making an angle of 30.1° with the P-P bond. Furthermore, it is likely that the most intense three-electron bond radical **1a(A)** gives rise to the secondary radical **1b** and therefore these couplings arise from a single molecule. This is confirmed by the relative orientations of these couplings which are similar to the ESR experiments on tetraethyldiphosphine disulphide (2) (vide infra). Based on these arguments, radical **1a(A)** is assigned to originate from precursor molecule I, and consequently **1a(B)** from II. This is shown in Fig. 6.

The additional splitting of 20 MHz observed for **1a(A)** is probably due to a short distance interaction of a nonbonded hydrogen atom with the radical in the crystal matrix. Lee and Goodacre[32] reported in their determination of the crystal structure such a short distance (2.84 Å) between the sulphur atoms of I and neighbouring methyl hydrogens. The extra splitting must be the result of a direct delocalization of the spin density on the hydrogen nucleus. The alternative explanation that these lines are the result of a weak magnetic dipole-dipole interaction,[34] coupling the electron spin and a

nuclear spin, can be ruled out since no central line is observed. Furthermore, the splitting of 20 MHz is identical for all absorptions in the ESR spectrum and larger than the calculated proton resonance frequencies at the $m_I = 1$, 0, and -1 field positions which are approximately 12.1, 14.3, and 16.1 MHz, respectively.

From the isotropic and anisotropic contributions to the hyperfine coupling the spin densities in the phosphorus $3s$ and $3p$ orbitals can be estimated[35] (Table IV).

Table IV. Orbital population and p/s ratio for radicals generated in substituted diphosphine disulphides **1**, **2**, and **3**.

Radical	Temperature (K)	ρ_s (%)	ρ_p (%)	p/s	ρ_s (%)	ρ_p (%)	p/s	Total (%)
			P$_1$			P$_2$		
1a(A)	100	10.5	21.1	2.01	10.5	21.1	2.01	63.2
1a(B)	100	10.3	22.2	2.16	10.3	22.2	2.16	65.0
1b	120	11.6	25.2	2.17	4.1	15.7	3.83	56.6
2a	100	10.2	23.6	2.31	10.2	23.6	2.31	67.6
2b	100	11.6	26.4	2.23	4.2	17.0	4.05	59.2
2c	175	13.2	42.9	3.25				56.1
2d	100	7.3	47.4	6.49				54.7
3a	100	9.2	22.9	2.49	9.2	22.9	2.49	64.2
3b	100	12.2	39.1	3.20	0.1	0.7		52.1
3c	100	8.4	37.2	4.43	0.4	1.3		47.3
3d	100	6.3	39.4	6.16				45.7

The structure of the two three–electron bond radicals is characterized by two completely equivalent phosphorus nuclei. The spin density is mainly localized on phosphorus [63.2% for **1a(A)** and 65.0% for **1a(B)**] with a p/s ratio of approximately 2. The angle of the principal direction of the SOMO with the P–P bond varies from 22.3° for **1a(A)** to 30.1° for **1a(B)**. The central phosphorus atom of the TBP–e radical **1b** possesses 36.8% of the spin density and a p/s ratio of 2.2. The apical phosphorus atom contributes for 19.8% and this spin density is mainly localized in a $3p$ orbital. The hyperfine couplings of the two phosphorus atoms make an angle of 73.7° and are therefore nearly perpendicular as is expected for TBP–e like structures. The remaining spin density is located on the second apical position, occupied by the sulphur atom, resulting in an equatorial position for the two methyl groups.

3.2. Tetraethyldiphosphine disulphide (2)

Tetraethyldiphosphine disulphide (2) crystallizes in the triclinic space group $P\bar{1}$ with one molecule in the unit cell.[36] The crystals are colourless well-defined plates. The ESR spectrum recorded at 100 K after x irradiation of a single crystal of 2 is shown in Fig. 7(a).
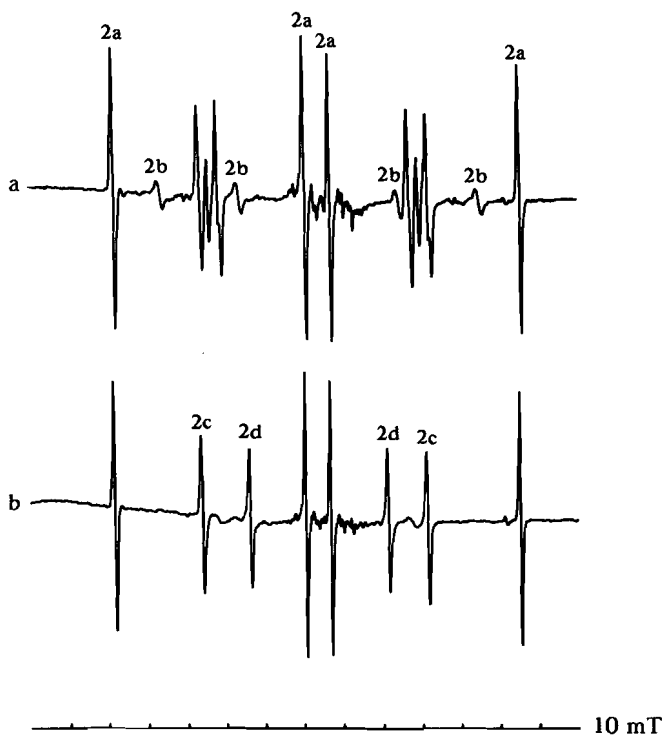
Figure 7. Single-crystal ESR spectra of x-irradiated 2: (a) at 100 K; (b) at 200K.

As for the methyl derivative the most intense absorptions (2a) originate from a three-electron bond radical, exhibiting again a pronounced second-order splitting. Besides, a weak double doublet (2b), arising from a TBP-e radical, is present. Furthermore, two rather complex patterns are found approximately 0.05 T apart. Annealing to 200 K results in a change of the spectrum [Fig. 7(b)]. The three-electron bond radical 2a is still present but the double doublet 2b has disappeared. This behaviour is opposite to x-irradiated tetramethyldiphosphine disulphide for which the TBP-e radicals increase upon annealing. The complex patterns have changed and only one phosphorus doublet

(2c) remains. Finally a new phosphorus doublet (2d) is formed. Upon recooling to 100 K this process turns out to be partially reversible. Although, the TBP-e signals (2b) are not recovered and the new-formed doublet (2d) remains, the complex patterns are present again. The formation and disappearance of these signals is fully reversible between 100 and 230 K. After annealing to room temperature all signals are irreversibly lost except the doublet 2d which could still be detected, even after storage for several weeks at room temperature.

In order to obtain a complete analysis of these radicals, a crystal was rotated around three orthogonal reference axes. One of them was chosen perpendicular to the crystal plate, while the other two were defined arbitrarily (but orthogonal) in the plane of the plate. At 100 K, the signals 2a, 2b, and 2d were examined, in which 2d was present from a previous irradiation. After annealing to 175 K the same analysis was repeated together with a survey of the phosphorus doublet 2c. Comparison of the spectra at 100 and 175 K for all orientations indicates that signals 2c are part of the complex patterns at 100 K, although at 175 K the phosphorus hyperfine coupling seems to be somewhat smaller.

After diagonalization of the appropriate tensors the principal values and direction cosines of A and g were obtained (Tables V and VI).

Table V. Hyperfine tensors for radicals 2a, 2b, 2c, and 2d.

Radical	Nucleus	Temperature (K)	Total tensor (MHz)	Isotropic part (MHz)	Dipolar tensor (MHz)	Direction cosines		
						x	y	z
2a	P_1, P_2	100	1251	1351	-101	0.887	-0.351	0.299
			1280		-72	-0.420	-0.347	0.838
			1524		173	0.190	0.870	0.455
2b	P_1	100	1429	1546	-117	-0.258	0.964	-0.060
			1470		-77	-0.609	-0.114	0.785
			1740		194	0.750	0.239	0.617
	P_2	100	483	556	-73	0.840	-0.217	0.497
			504		-52	-0.540	-0.239	0.807
			680		125	0.057	0.946	0.318
2c	P_1	175	1589	1762	-173	0.783	0.504	0.364
			1620		-142	-0.387	-0.063	0.920
			2076		315	-0.486	0.862	-0.146
2d	P_1	100	793	975	-183	0.608	-0.102	0.787
			811		-165	0.776	0.282	-0.563
			1323		348	-0.165	0.954	0.251

Table VI. g Tensors for radicals 2a, 2b, 2c, and 2d.

Radical	Temperature (K)	g Tensor	Direction cosines		
			x	y	z
2a	100	2.001	0.266	0.824	0.500
		2.004	0.784	-0.487	0.385
		2.011	-0.561	-0.290	0.775
2b	100	2.002	0.780	0.121	0.614
		2.004	-0.485	0.738	0.470
		2.005	-0.396	-0.664	0.634
2c	175	2.003	-0.465	0.883	-0.065
		2.004	-0.033	0.056	0.998
		2.008	0.885	0.466	0.004
2d	100	2.005	-0.160	0.952	0.261
		2.018	-0.133	-0.283	0.950
		2.018	0.978	0.117	0.172

The principal directions of the largest eigenvalues of the A tensors of 2a, 2b, 2c, and 2d lie approximately in one plane with normal vector (0.6375, 0.2705, -0.7214). The calculated deviations of the principal directions with respect to this plane are small ($\sim 1.6°$ for 2a, 2c, and 2d; $3.6°$-$5.7°$ for the two splittings of 2b). This hyperfine coupling plane is most likely identical to the molecular SPPS plane of 2. In principle is should be possible to confirm this by relating the ESR coordinate system and the x-ray structural data.

Dutta and Woolfson[36] reported that the crystal plates are parallel to (001). From this statement and the x-ray data it can be calculated that the SPPS plane and the (001) plane are inclined by an angle of 18.8°. The ESR reference y axis was chosen perpendicular to the plate and from the normal vector an angle of 74.3° (arccos 0.2705) is found between the plane of the couplings and the plate. The deviation is at least 55.5° and thus the x-ray data and ESR experiments cannot be correlated. To be sure of the analysis presented above, a second single crystal was examined with its rotation axis perpendicular to the plate. This revealed the same angular dependencies for the hyperfine splittings as before. Despite the fact that a correlation could not be made the principal directions of the A tensors are very likely to be situated in the SPPS plane. This is based on two important facts.

First, in the case of the methyl analogue 1 the three-electron bond radical and the TBP-e radical have their principal directions in the SPPS plane. Since all experimental data such as A and g tensors and their relative orientations are similar for the two compounds it is conceivable that their radicals are identical.

The second argument is based on symmetry considerations. If a phosphorus centred radical is formed with its principal direction not oriented in the SPPS plane, it will always introduce at least two magnetically unequivalent sites in the crystal because the precursor molecule 2 possesses a local C_{2h} symmetry. Since for all radicals only one site is observed, such a radical has not been formed.

Table VII. Relative orientations (deg) of the principal directions[a] of the hyperfine couplings for radicals generated in 2. A clockwise rotation from the horizontal to the vertical tabled couplings is quoted positive.

Radical	2a	2b₁	2b₂	2c	2d
2a	0				
2b₁	50.8	0			
2b₂	-11.9	-62.3	0		
2c	126.2	75.6	137.9	0	
2d	-24.1	-75.0	-13.3	149.9	0

[a] Because no absolute sign can be attributed to the direction of a principal value, there is an ambiguity ± 180° in the listed values.

In Table VII the relative orientations of the couplings for the four radicals **2a-2d** are collected. Since the orientation of the precursor molecule with respect to the ESR reference axes is not exactly known, the results of the methyl derivative **1** were used together with the quantum chemical calculations, and the angle between the P-P bond and the direction of the largest hyperfine coupling for **2a** was assumed to be 30°. On this basis Fig. 8 has been composed which shows the relative orientations of the maximal anisotropies and the parent molecule.
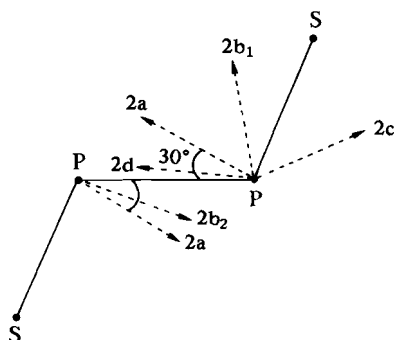

Figure 8. Relative orientations of the precursor molecule **2** and the principal directions of the hyperfine couplings **2a**, **2b₁**, **2b₂**, **2c**, and **2d**.

Table IV comprises the orbital populations derived from the hyperfine interactions. Radical **2a** (Fig. 9) possesses clearly a three-electron bond. The spin density is located mainly (67.6%) on the two phosphorus atoms and their p/s ratio is 2.31. The radical is very similar to the radicals **1a(A)** and **1a(B)**. The TBP-e species **2b** possesses a central phosphorus atom which contributes for 38.0% ($p/s = 2.23$) to the SOMO and an apical phosphorus atom with a spin density of 21.2%, largely confined to the $3p$ orbital. The angle between the two couplings is 62.3° and therefore somewhat less than the corresponding value for the methyl analogue **1b**. Radical **2d** can be attributed to a dissociation product resulting from a bond breaking of the P-P linkage. The principal values of the A tensor for **2d** (1323, 811, and 793 MHz) are nearly identical to those for the $Ph_2\dot{P}S$ radical (1322, 841, and 820 MHz), formed in diphenylphosphine sulphide by x irradiation.[37] This $Ph_2\dot{P}S$ radical is, like **2d**, a stable species at room temperature. Radical **2d** is essentially tetrahedral, because the SOMO is directed along the original P-P bond. The spin density is mainly located in the phosphorus $3s$ (7.3%) and $3p$ (47.4%) orbitals, resulting in a relatively high p/s ratio of 6.49.
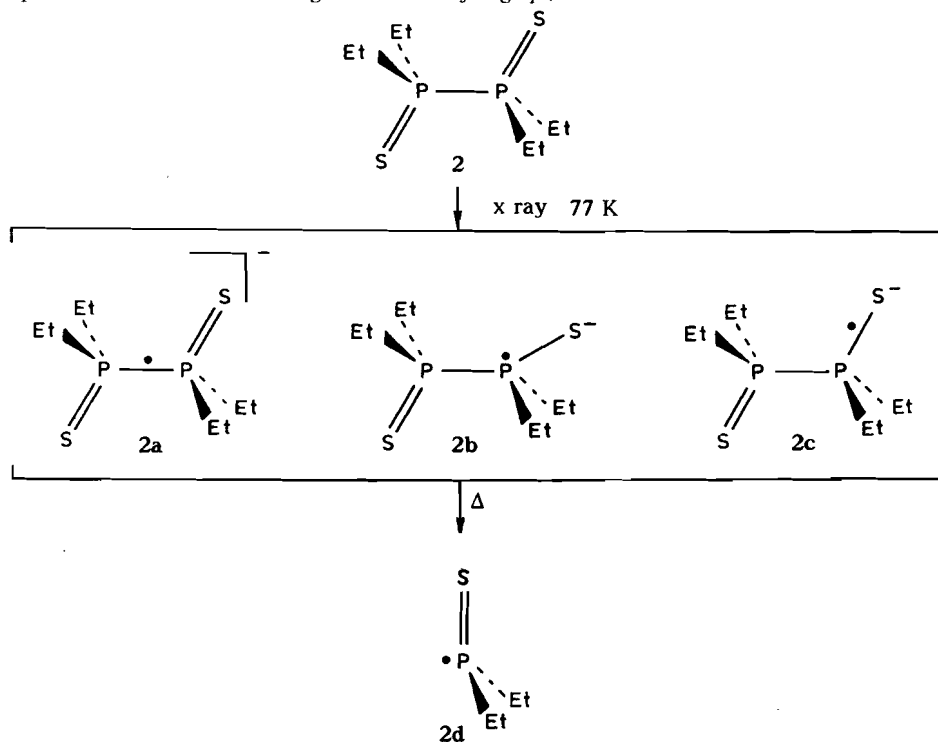

Figure 9. Formation of radicals **2a, 2b, 2c,** and **2d** upon x irradiation and subsequent annealing.

As can be seen from Table V radical **2c** exhibits the largest phosphorus hyperfine splitting of the radicals in **2**. The SOMO possesses 13.2% $3s$ and 42.9% $3p$ character. The large hyperfine coupling indicates that this radical is a phosphoranyl radical. These signals can be attributed to a three-electron bond radical in which the unpaired electron is located between a phosphorus and sulphur atom. Its p/s ratio of 3.25 is comparable to other three-electron bond radicals.[38] Moreover, similar three-electron P∴S bond radicals have been reported for $Ph_3\overset{.}{P}S^-$.[39]

Confirmation of this assignment was obtained by x irradiation of a powdered sample of triethylphosphine sulphide (Et_3PS, **4**). It can be expected that if radical **2c** is indeed a three-electron P∴S species, the hyperfine couplings of a similar radical in **4** should be comparable. Analysis of the resulting ESR spectrum of this compound gave $A_1 = 1943$ MHz, $A_2 = 1517$ MHz, and $A_3 = 1517$ MHz, which is in reasonable agreement with the principal values of **2c** (Table V).

One of the features of the ESR spectra of x-irradiated **2** remains indistinct. No account could be made for the absorptions which are reversibly lost and formed upon warming and cooling between 100 and 230 K. This behaviour points to a time-dependent phenomenon whose rate varies with the temperature. The phosphorus hyperfine splitting of more than 1400 MHz is an indication for the presence of a phosphoranyl radical, however a satisfying analysis of these absorptions could not be made. The unidentified set of lines in Fig. 7(a) turns out to be much more complicated upon rotation of the crystal and is obscured by the absorptions due to **2c**. The possibility of a radical pair confined into a cage by the single-crystal matrix can be ruled out on basis of the absence of $\Delta m_s = \pm 2$ transitions at half-field.

3.3. Tetraphenyldiphosphine disulphide (3)

According to Blake et al., tetraphenyldiphosphine disulphide (**3**) crystallizes in the monoclinic space group $P2_1/c$.[40] The unit cell contains two pairs of molecules in two sets of special orientations. This results in four orientations of the P-P bond. Colourless, but irregularly shaped single crystals of **3** were x irradiated at 77 K. The ESR spectrum recorded at 100 K [Fig. 10(a)] shows clearly the presence of a three-electron P∴P bond radical **3a**. The most intense absorptions, however, are due to a central 1:2:1 triplet.

Surprisingly, only one orientation is found for **3a**, whereas at least four magnetically unequivalent sites can be expected. Furthermore, the spectrum shows a number of weak absorptions. These lines are interpreted to originate from three different radicals. The outermost, **3b**, is a double doublet present in two independent orientations. It possesses one large and one small splitting. Next to it, with a smaller phosphorus hyperfine splitting, a second double doublet **3c**, again with two different orientations, is found. Finally, two sites of a simple phosphorus doublet can be observed (**3d**).

On annealing, all radicals, except **3c**, start to disappear from the spectrum. After warming to 200 K and subsequent recooling to 100 K, the spectrum shown in Fig.
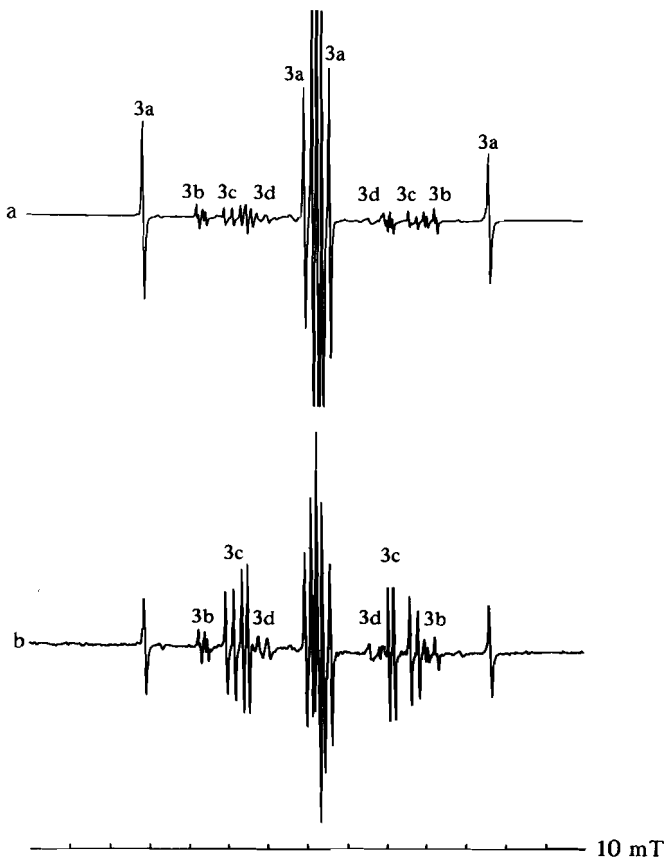
Figure 10. Single-crystal ESR spectra of x-irradiated **3**: (a) at 100 K; (b) at 100 K after annealing to 200 K.

10(b) was recorded. Clearly, the intensity of **3c** has increased and the differences between the absorptions due to **3b**, **3c**, and **3d** are more distinct. All attempts to orient one single crystal, or even three independent crystals, of **3** along three orthogonal axes finished unsatisfactorily due to their fragility and irregular morphology.

In order to obtain a correct analysis of the hyperfine couplings several crystals were rotated around random reference axes and the spectra of maximal and minimal coupling were compared with the spectrum of a powdered sample. In this way it is possible to determine the principal values (Table VIII), although no precise information about their directions can be obtained.
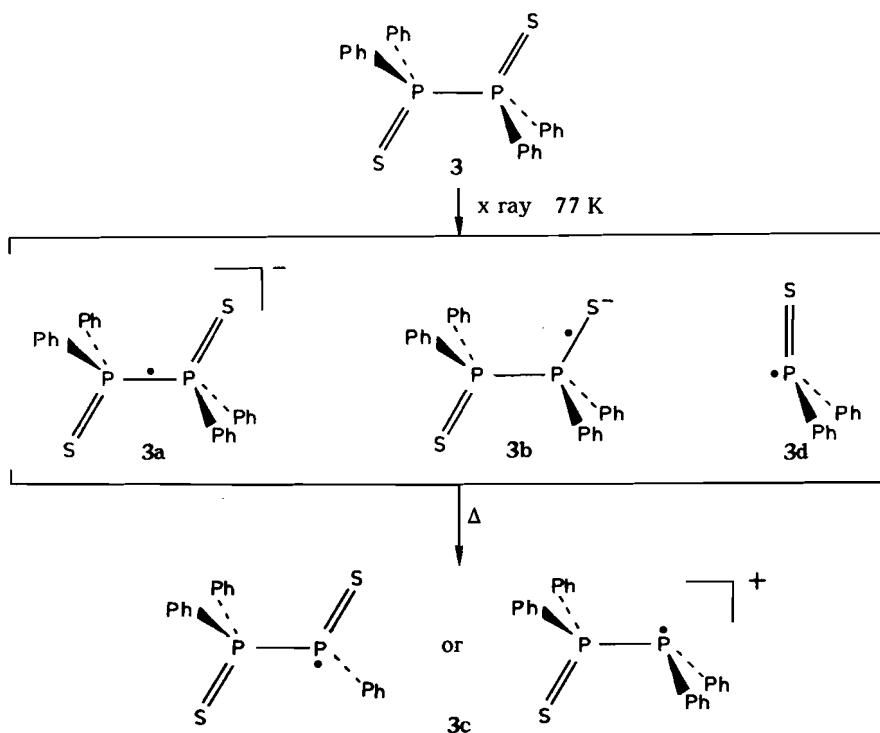
Figure 11. Formation of **3a**, **3b**, **3c**, and **3d** upon x irradiation and subsequent annealing.

The calculated spin densities are compiled in Table IV. Radical **3a** (Fig. 11) can be attributed to a three-electron bond species with a structure similar to **1a(A,B)** and **2a**, despite its appreciable smaller isotropic hyperfine coupling. This must be the result of a slight decrease of 3s contribution to the SOMO. Species **3b** is assigned to a three-electron bond P∴S radical because the ESR parameters are comparable to the corresponding ethyl analogue **2c** and the related $Ph_3\dot{P}S^-$ radical ($A_{//}=1738$ MHz and $A_\perp=1359$ MHz).[39] The SOMO possesses 12.2% 3s and 39.1% 3p character. The additional splitting of 14-22 MHz comes most likely from a small contribution ($\sim 1\%$) of the second phosphorus atom. Since the concentration of **3c** increases upon partial annealing it is assigned to a dissociation product. Because **3c** exhibits a splitting of 42-50 MHz due to a second phosphorus atom the P-P linkage is still intact. In absence of information on the principal directions, **3c** is tentatively assigned to be formed by a dissociation of a P-Ph or a P-S bond resulting in an essentially tetrahedral phosphorus radical.

Table VIII. Hyperfine and g tensors for radicals **3a**, **3b**, **3c**, and **3d**.

Radical	Nucleus	Temperature (K)	Total tensor (MHz)	Isotropic part (MHz)	Dipolar part (MHz)	g Tensor
3a	P_1, P_2	100	1137	1224	-87	2.008
			1143		-81	2.006
			1393		168	2.001
3b	P_1	100	1461	1621	-160	2.008
			1494		-127	2.012
			1908		287	2.002
	P_2		14-22			
3c	P_1	200	986	1123	-137	2.015
			986		-137	2.015
			1396		273	2.003
	P_2		42-56			
3d	P_1	100	697	841	-144	2.017
			697		-144	2.017
			1130		289	2.008

Finally, radical **3d** can be attributed to a thiophosphonyl radical formed by a dissociation of the P-P bond comparable to **2d**. The hyperfine couplings of **3d** reveal 6.3% $3s$ and 39.4% $3p$ character. For the same $Ph_2\overset{.}{P}S$ radical, formed in a single crystal of diphenylphosphine sulphide, a slightly higher spin density on phosphorus has been reported.[37] This difference is most likely due to constraints by the single crystal matrix or the presence of the second dissociated fragment.

4. QUANTUM CHEMICAL CALCULATIONS

4.1. Computational details

The UHF calculations, and the computation of the hyperfine interactions, were performed using the methods described in chapter 3. Throughout the calculations a split valence 4-31G basis set[41,42] was used, implemented with a single set of six second-order Gaussians on phosphorus and sulphur with a radial exponent of 0.55 and 0.65, respectively.[43] The molecular geometries were fully optimized in an analytical-gradient procedure with respect to all bond lengths and bond angles within the symmetry constraints. In order to reduce the computational time the Me, Et, and Ph substituents were replaced by hydrogen atoms.

4.2. Results of the calculations

The ESR experiments reveal several configurations for phosphoranyl radicals generated by electron capture of the diphosphine disulphides. For all three compounds a three-electron bond radical was detected and from the hyperfine couplings a description of the SOMO could be obtained.
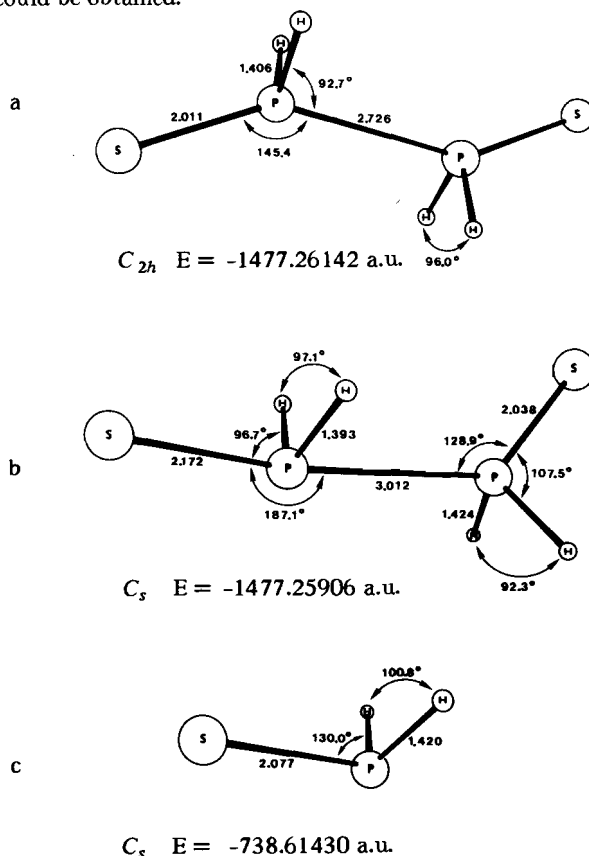

C_{2h} E = -1477.26142 a.u.

C_s E = -1477.25906 a.u.

C_s E = -738.61430 a.u.

Figure 12. Optimized geometries (Å and deg) and energies (a.u.) for (a) C_{2h} $H_2P(S)\dot{-}P(S)H_2^-$; (b) C_s $H_2P(\dot{S})-P(S)H_2^-$; (c) $H_2\dot{P}S$.

Geometry optimization for the model $H_2P(S)\dot{-}P(S)H_2^-$ radical results in a structure with C_{2h} symmetry, implicating two identical phosphorus atoms. This structure [Fig. 12(a)] is characterized by a relatively long P-P bond of 2.726 Å and a SPP bond angle of 145.5°, which is a serious deformation from a tetrahedral geometry. A similar bond length (2.88-2.89 Å) was found for the three-electron bond $H_3P\dot{-}PH_3^+$ radical cation on basis of 4-31G SCF and Møller-Plesset calculations.[25]

Table IX. Calculated isotropic and dipolar hyperfine interactions for C_{2h} and C_s $H_2P(S)\dot{}P(S)H_2^-$ and for C_s $H_2\dot{P}S$.

Radical	Nucleus	A^{iso} (a.u.)	(MHz)	B (a.u.)	(MHz)	Direction cosines[a] x	y	z
$H_2P(S)\dot{}P(S)H_2^-$	P_1, P_2	0.529	1072.1	0.818	177.0	0.8643	-0.5029	0
C_{2h}				-0.447	-96.6	0.5029	0.8643	0
$<S^2> = 0.7512$				-0.372	-80.4	0	0	1
	S_1, S_2	0.006		0.899		0.9769	-0.2173	0
				-0.488		0.2173	0.9769	0
				-0.411		0	0	1
	H_1, H_2	0.001	2.2					
$H_2P(\dot{S})-P(S)H_2^-$	P_1	0.085	153.9	0.171	37.0	0.4380	0.8990	0
C_s				-0.094	-20.3	-0.8990	0.4380	0
$<S^2> = 0.7500$				-0.077	-16.6	0	0	1
	P_2	0.006	10.9	0.012	2.6	-0.9743	-0.2292	0
				-0.007	-1.5	-0.2292	0.9734	0
				-0.005	-1.1	0	0	1
	S_1	0.024		3.516		0.0204	0.9980	0
				-1.757		-0.9980	0.0204	0
				-1.759		0	0	1
	S_2	0.000		0.018		-0.9847	0.1742	0
				-0.010		0.1742	0.9847	0
				-0.008		0	0	1
	H_1	0.004	18.2					
	H_2	0.000	0.3					
$H_2\dot{P}S$	P	0.079	143.1	0.185	40.0	-0.5763	0.8172	0
C_s				-0.094	-20.3	0.8172	0.5763	0
$<S^2> = 0.7501$				-0.091	-19.7	0	0	1
	S	0.032		3.591		-0.0897	0.9960	0
				-1.799		0.9960	0.0897	0
				-1.792		0	0	1
	H	0.007	31.3					

[a] Direction cosines refer to the orientations of the radicals in Fig. 13.

Evaluation of the expectation values of the Fermi contact and dipolar hyperfine interactions (Table IX) reveals a good agreement between the C_{2h} $H_2P(S)\dot{}P(S)H_2^-$ model and the ESR experiments on the three-electron bond radicals **1a(A,B)**, **2a**, and **3a**. The calculated isotropic hyperfine coupling of 1072 MHz is somewhat less than the experimental values of 1395 MHz for **1a(A)**, 1372 MHz for **1a(B)**, 1351 MHz for **2a**, and 1224 MHz for **3a**. The dipolar hyperfine coupling is more accurately predicted: 177 MHz for $H_2P(S)\dot{}P(S)H_2^-$ vs. 155, 163, 173, and 169 MHz for the experimental values of **1a(A)**, **1a(B)**, **2a**, and **3a**, respectively. The direction of the largest hyperfine coupling which is situated in the SPPS plane, as is expected for a C_{2h} structure, makes an angle of 30.1° with the P-P bond. This is in good agreement with the experiments on **1a(A)**

and **1a(B)**. These quantum chemical calculations evidently confirm the ESR experiments on the $R_2P(S)\dot{\cdot}P(S)R_2^-$ three-electron bond radicals and provide a better insight into the nature of the SOMO.
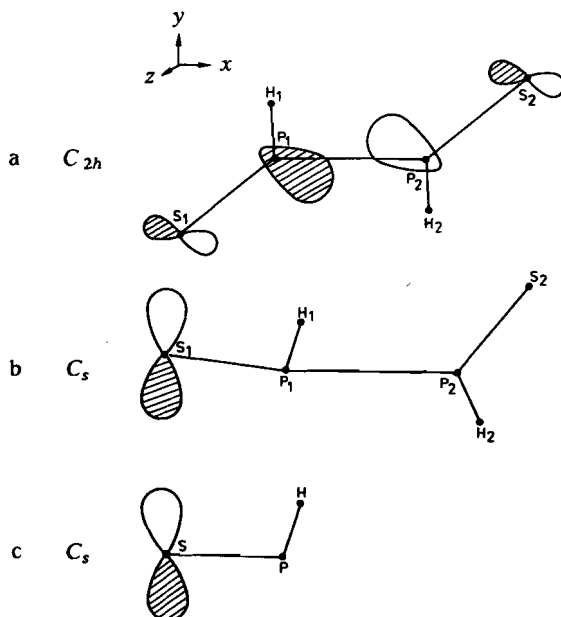

Figure 13. Schematic representation of the SOMO for (a) C_{2h} $H_2P(S)\dot{\cdot}P(S)H_2^-$; (b) C_s $H_2P(S)\dot{\cdot}P(S)H_2^-$; (c) C_s $H_2\dot{P}S$.

The SOMO of the C_{2h} $H_2P(S)\dot{\cdot}P(S)H_2^-$ radical [Fig. 13(a)] possesses B_u symmetry and contains three nodal planes. This antibonding character results in the elongation of the SPPS moiety and accounts for the calculated bond length and SPP angle. The major contributions to the SOMO arise from the phosphorus and sulphur $3s$, $3p_x$, and $3p_y$ orbitals. The hydrogen atoms do not contribute and only a small isotropic hyperfine coupling is predicted for them.

Besides this C_{2h} three-electron bond radical the ab initio calculations predict a second minimum on the multidimensional potentional energy surface. This second structure [Fig. 12(b)] possesses C_s symmetry and is only 6.2 kJ mol^{-1} higher in energy on 4-31G(*) UHF SCF level than the C_{2h} isomer.

Two completely different SPH$_2$ fragments are encountered in this C_s structure. The first [right in Fig. 12(b)] represents a rather normal tetrahedral geometry but the second fragment (left) is unusual because of the nearly in-line orientation of the SPPS moiety. The distance between the two fragments is also unexpectedly large with a P-P bond length of 3.021 Å. The calculation of the Fermi and dipolar hyperfine interactions (Table IX) indicates that the unpaired electron is located in a sulphur $3p$ orbital with some delocalization on the adjacent phosphorus atom resulting in an isotropic hyperfine coupling of 153 MHz.

Figure 13(b) shows a schematic representation of the SOMO for this radical. The ESR experiments did not reveal a radical with such a small phosphorus hyperfine coupling. Attempts to obtain a quantum chemical description of the experimentally detected TBP-e and three-electron bond P∴S radicals were not successful because no other minimum within C_s symmetry could be calculated.

Calculations on $H_2\dot{P}S$, as a model for the dissociation products **2d** and **3d**, reveal again a sulphur centred radical [Figs. 13(c) and 14(c)] where the $3p$ orbital gives the major contribution to the SOMO. The calculated hyperfine couplings (Table IX) for $H_2\dot{P}S$ are similar to those for the C_s $H_2P(S)∴P(S)H_2^-$ structure. Apparently, the calculations tend to move the unpaired electron on the sulphur atom, whereas a large contribution from phosphorus is found experimentally.

5. DISCUSSION

The three-electron bond radicals **1a(A)**, **1a(B)**, **2a**, and **3a** possess an antibonding SOMO. The observation of the second-order splitting for the $m_I = 0$ transitions gives evidence of a symmetrical delocalization of the unpaired electron over the two phosphorus nuclei. The ESR experiments and ab initio calculations indicate that the direction of the largest phosphorus hyperfine coupling makes an angle of 20°-30° with the P-P bond.

It is clear that the description "$\sigma *$" does not hold for this type of radicals, since the B_u SOMO has no rotational symmetry. Theoretical calculations[25,44−46] indicate that, in general, the anisotropy of the hyperfine coupling for a hypervalent radical not necessarily coincides with the molecular frame. Until now, the only experimental verification was obtained from the structure of the $Ph_3\dot{P}Br$ radical.[21] An exception to this rule will be a highly symmetrical species like the $R_3P∴PR_3^+$ radical cation, provided it possesses a D_{3d} conformation.

An interesting aspect of the three-electron bond radicals **1a(A)** and **1a(B)** is that their ESR parameters are not completely identical. This can only be the result of geometric constraints caused by the single-crystal matrix. The absorptions due to **1a(A)** are more intense than those for **1a(B)**. This is not expected from the relative occurence of the precursor molecules, but agrees with the observation that the P-P bond length in molecule I, which leads to **1a(A)**, is significantly larger than in molecule II, which is the precursor for **1a(B)**. It is conceivable that a molecule with a longer P-P bond more easily accommodates the extra electron, because upon electron capture this bond will tend to elongate.

The detection and identification of the TBP-e radicals **1b** and **2b** demonstrate that electron capture in these diphosphine disulphides can result in an asymmetric distribution of the odd electron. The spin density is located for almost 38% on the central phosphorus atom and for approximately 20% on the second phosphorus nucleus. The remaining part will be confined to the apical sulphur nucleus. These radicals are the

first examples of an apically located S⁻ substituent in a TBP-e radical. This leads to the conclusion that not the electronegativity alone determines the apicophilicity of a substituent in a TBP-e structure, because then an electropositive ligand, like S⁻, would invariably reside in an equatorial site. The formation of the TBP-e radicals is different for the two compounds. The methyl derivative **1b** is a secondary radical detected after partial annealing, whereas for the ethyl analogue the TBP-e radical **2b** is a primary product of the irradiation. This demonstrates the subtle energy differences between the several radical structures. No quantum chemical confirmation for a TBP-e radical could be obtained. Nevertheless, it is clear that the SOMO of **1b** and **2b** will actually show a close resemblance to the electronic configuration of the three-electron bond radicals. This conclusion can be derived from Tables I, III-V, and VII which indicate that a relative small adaption of the spin density distribution and the principal directions of the hyperfine couplings can result in a conversion of a three-electron P∸P bond radical into a TBP-e structure and vice versa.

The three-electron P∸S bond radicals **2c** and **3b** exhibit the largest hyperfine couplings of the radicals encountered in the diphosphine disulphides. The direction of the largest anisotropic coupling, although indirectly determined, is for **2c** not parallel to the original P-S bond. The dissociation products **2d** and **3d** possess a tetrahedral geometry and are well established,[37] although the quantum chemical calculations on $H_2\dot{P}S$ do not confirm these structures. An unambiguous assignment for **3c** is not possible. From the two suggested possibilities, P-S bond dissociation and P-Ph bond dissociation, the latter seems to be more likely. A cleavage of the P-S bond will result in a trisubstituted phosphorus cation. Although little experimental data are available, such a radical should exhibit a very high p/s ratio. The related $Ph_3\dot{P}^+$ radical, e.g., shows a p/s ratio of 9.0.[7,47] Dissociation of the P-Ph bond reveals a thiophosphonyl type radical. Comparison with related thiophosphonyl radicals[37,48] supports this assignment for **3c**.

REFERENCES

1. R.W. Alder and R.B. Sessions, J. Am. Chem. Soc., **101**, 3651 (1979).

2. R. Kirste, R.W. Alder, R.B. Sessions, M. Bock, H. Kurreck and S.F. Nelsen, J. Am. Chem. Soc., **107**, 2635 (1985).

3. A.R. Lyons and M.C.R. Symons, J. Chem. Soc., Faraday Trans. 2, **68**, 1589 (1972).

4. M.C.R. Symons, Mol. Phys., **24**, 885 (1972).

5. T. Gillbro, C.M.L. Kerr and F. Williams, Mol. Phys., **28**, 1225 (1984).

6. M.C.R. Symons and G.D.G. McConnachie, J. Chem. Soc., Chem. Commun., 851 (1982).

7. A. Hasegawa, G.D.G. McConnachie and M.C.R. Symons, J. Chem. Soc., Faraday Trans. 1, **80**, 1005 (1984).

8. T. Berclaz, M. Geoffroy and E.A.C. Lucken, Chem. Phys. Lett., **36**, 677 (1975).

9. M.C.R. Symons, Chem. Phys. Lett., **40**, 226 (1976).

10. M.C.R. Symons and R.L. Petersen, J. Chem. Soc., Faraday Trans. 2, **75**, 210 (1979).

11. R.L. Hudson and F. Williams, J. Phys. Chem., **84**, 3483 (1980).

12. M. Göbl, M. Bonifačić and K.-D. Asmus, J. Am. Chem. Soc., **106**, 5984 (1984).

13. K.-D. Asmus, Acc. Chem. Res., **12**, 436 (1979).

14. S.F. Nelsen, C.R. Kessel and D.J. Brien, J. Am. Chem. Soc., **101**, 1874 (1979).

15. M. Bonifačić and K.-D. Asmus, J. Chem. Soc., Perkin Trans. 2, 758 (1980).

16. K. Nishida and F. Williams, Chem. Phys. Lett., **34**, 302 (1975).

17. A. Hasegawa, K. Ohnishi, K. Sogabe and M. Miura, Mol. Phys., **30**, 1367 (1975).

18. A.J. Colussi, J.R. Morton, and K.F. Preston, J. Phys. Chem., **79**, 1855 (1975).

19. J.H.H. Hamerlinck, P. Schipper and H.M. Buck, J. Am. Chem. Soc., **105**, 385 (1983).

20. J.H.H. Hamerlinck, P. Schipper and H.M. Buck, J. Am. Chem. Soc., **102**, 5679 (1980).

21. T. Berclaz, M. Geoffroy, L. Ginet and E.A.C. Lucken, Chem. Phys. Lett., **62**, 515 (1979).

22. The conformation of highest symmetry for $R_2P(S)P(S)R_2$ is C_{2h} and is only found when R= Me. Et and Ph groups are not symmetrically oriented relative to the SPPS plane and the molecules belong to the C_i point group. The C atoms directly linked to phosphorus build up a local C_{2h} symmetry.

23. C. Glidewell, J. Chem. Soc., Perkin Trans. 2, 299 (1985).

24. C. Glidewell, J. Chem. Soc., Perkin Trans. 2, 551 (1985).

25. T. Clark, J. Comput. Chem., **4**, 404 (1983).

26. H. Niebergall and B. Langenfeld, Chem. Ber., **95**, 64 (1962).

27. K. Issleib and A. Tzschach, Chem. Ber., **92**, 704 (1959).

28. W. Kuchen and H. Buchwald, Chem. Ber., **91**, 2871 (1958).

29. R.A. Zingara and R.E. McGlothlin, J. Org. Chem., **26**, 5205 (1961).

30. R.W. Fessenden, J. Chem. Phys., **37**, 747 (1962).

31. R.W. Fessenden and R.H. Schuler, J. Chem. Phys., **43**, 2704 (1965).

32. J.D. Lee and G.W. Goodacre, Acta Crystallogr. Sect. B, **27**, 302 (1971).

33. The ESR spectra shown in the figures in this chapter were obtained from randomly oriented crystals which were transferred after the irradiation at 77 K to an unirradiated sample tube in order to remove the central absorptions due to irradiated quartz.

34. G.T. Tramell, H. Zeldes and R. Livingstone, Phys. Rev., **110**, 630 (1958).

35. J.R. Morton and K.F. Preston, J. Magn. Reson., **30**, 577 (1978).

36. S.N. Dutta and M.M. Woolfson, Acta Crystallogr., **14**, 178 (1961).

37. M. Geoffroy, Helv. Chim. Acta, **56**, 1553 (1973).

38. W.G. Bentrude, *Reactive Intermediates*, R.A. Abramovitch, Ed. (Plenum, New York, 1983), Vol. 3, p. 199.

39. J.C. Evans, S.P. Mishra and C.C. Rowlands, Chem. Phys. Lett., 72, 168 (1980).

40. A.J. Blake, R.A. Howie and G.P. McQuillan, Acta Crystallogr. Sect. B, 37, 966 (1981).

41. R. Ditchfield, W.J. Hehre and J.A. Pople, J. Chem. Phys., 54, 724 (1971).

42. W.J. Hehre and W.A. Lathan, J. Chem. Phys., 56, 5255 (1972).

43. M.M. Francl, W.J. Pietro, W.J. Hehre, J.S. Binkley, M.S. Gordon, D.J. DeFrees and J.A. Pople, J. Chem. Phys., 77, 3654 (1982).

44. T. Clark, J. Comput. Chem., 2, 261 (1981).

45. T. Clark, J. Comput. Chem., 3, 112 (1982).

46. R.A.J. Janssen and H.M. Buck, J. Mol. Struc. (THEOCHEM), 110, 139 (1984). Chapter 3.

47. G.W. Eastland and M.C.R. Symons, J. Chem. Soc., Perkin Trans. 2, 833 (1977).

48. S.P. Mishra and M.C.R. Symons, J. Chem. Soc., Dalton Trans., 1494 (1973).

CHAPTER 5

σ* and TBP-e radicals obtained by electron capture
of four-coordinated phosphorus compounds

1. INTRODUCTION

A variety of phosphoranyl radical structures (TBP-e, TBP-a and σ*) are known and have been described by single-crystal ESR[1-6] and quantum chemical methods[7-9]. However, the conditions that rule the specific formation of one of the limiting structures are not fully understood. According to Symons[10] the formation of a σ* configuration, possessing a three-electron bond, will be favoured when one of the four atoms attached to phosphorus is more electronegative than the other three. Three-electron bond phosphoranyl radicals have only been identified when chlorine, bromine, or iodine is linked to phosphorus,[11] or when the radical possesses a symmetrical phosphorus-phosphorus bond.[12,13] From the fact that only higher row atoms, with possible d orbital participation, give rise to σ* structures, it can be expected that the electronegativity is not the only factor responsible for the formation of a σ* radical.

In this chapter a striking difference between the electron capture of dipyrrolidino-chlorophosphine sulphide (1) and dimorpholinofluorophosphine sulphide (2) is presented. The compounds 1 and 2 give rise to phosphoranyl radicals closely resembling the limiting σ* and TBP-e configurations.

2. EXPERIMENTAL SECTION

All experiments were done in an atmosphere of dry nitrogen. Solvents were dried by standard methods. ^{1}H NMR spectra were recorded on a Hitatchi Perkin-Elmer R-24B spetrometer. ^{31}P NMR spectra were recorded on a Bruker HX-90 spectrometer; downfield shifts are quoted positive.

Dipyrrolidinochlorophosphine sulphide (1). To a stirred solution of 14.2 g (0.2 mol) of pyrrolidine in 75 mL of carbon tetrachloride was added dropwise at -5 °C a solution of 8.5 g (0.05 mol) of thiophosphoryl chloride ($SPCl_3$) in 20 mL of carbon tetrachloride. After the addition had been completed, the mixture was warmed to 50 °C for 1 h. Filtration, evaporation of the solvent, and recrystallization from diethyl ether afforded 9.6 g (81%) of 1, mp 78 °C: ^{1}H NMR ($CDCl_3$) δ 1.80–2.00 (t, 4, CH_2),

3.06-3.34 (m, 4, NCH$_2$); ^{31}P NMR (CDCl$_3$) δ 77.2. Anal. Calcd for C$_8$H$_{16}$ClN$_2$PS: C, 40.25; H, 6.76; N, 11.73. Found: C, 40.12; H, 6.81; N, 11.92. Single crystals were obtained by slow evaporation of a diethyl ether solution.

Dimorpholinofluorophosphine sulphide (2) In analogy to **1**, **2** was prepared from 8.7 g (0.10 mol) of morpholine in 100 mL of carbon tetrachloride and 3.8 g (0.025 mol) of thiophosphoryl chloride fluoride (SPCl$_2$F)^{14} in 20 mL of carbon tetra-chloride, yield 4.5 g (72%) of **2**, mp 46 °C: ^{1}H NMR (CDCl$_3$) δ 3.19 (m, 4, NCH$_2$), 3.69 (t, 4, OCH$_2$); ^{31}P NMR (CDCl$_3$) δ 80.0, J$_{PF}$ = 1027 Hz. Anal. Calcd for C$_8$H$_{16}$FN$_2$O$_2$PS: C, 37.79; H, 6.34; N, 11.02. Found: C, 37.74; H, 6.15; N, 10.83. Single crystals were obtained by slow crystallization at -20 °C of **2** in tetrahydrofuran (THF)/pentane (12 mL 1:2 THF/pentane for 1 g of **2**).

The techniques employed for x irradiation and ESR studies have been described in chapter 4. ESR parameters were obtained from a second-order analysis of the spectra.

3. RESULTS AND ASSIGNMENT

3.1. Dipyrrolidinochlorophosphine sulphide (1)

An x-irradiated single crystal of **1** was studied at 100 K. The ESR spectra show the features of a phosphoranyl radical which can be attributed to the three-electron bond radical **1a** (Fig. 1).
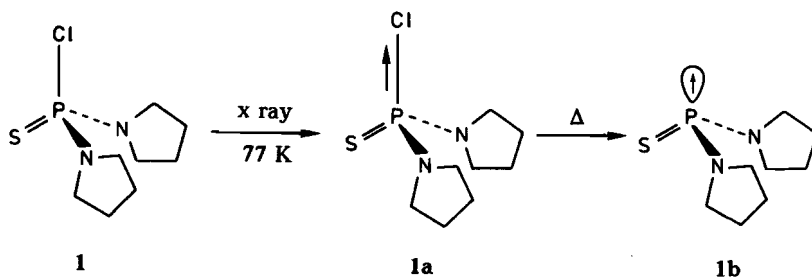

Figure 1. Formation of radicals **1a** and **1b** upon x irradiation and subsequent annealing.

The ESR spectrum of **1a** consists of a ^{31}P doublet with additional hyperfine splitting from one ^{35}Cl or ^{37}Cl nucleus (Fig. 2). The single-crystal ESR spectra of **1a** do not show any resolvable additional splitting due to the ^{14}N nuclei or to the difference in gyromagnetic constant for ^{35}Cl and ^{37}Cl.
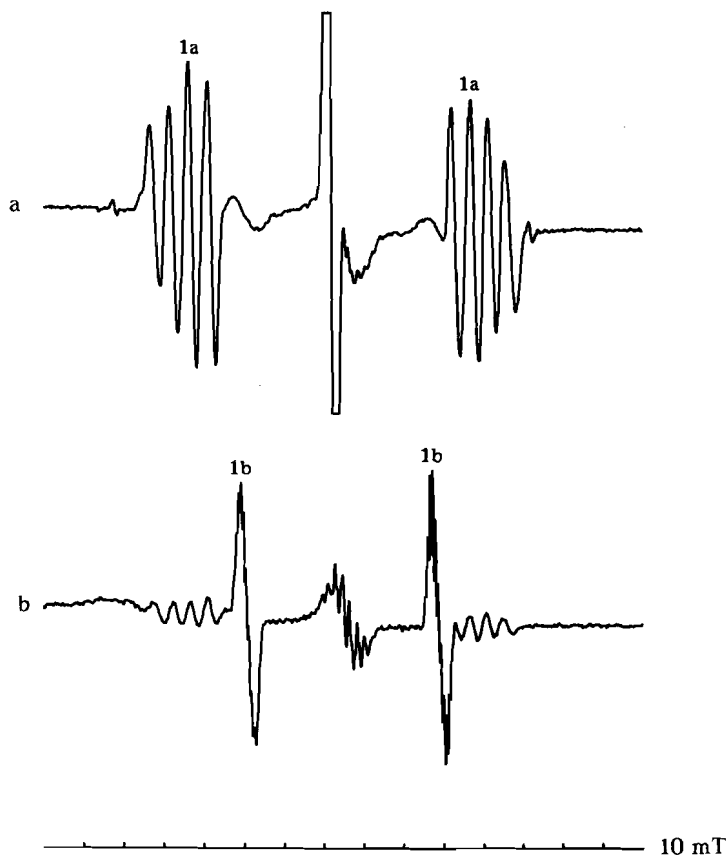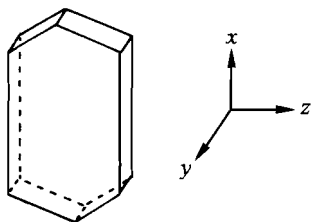

Figure 2. Single-crystal ESR spectra of x-irradiated **1**. Magnetic field parallel to yz: (a) radical **1a** at 100 K; (b) radical **1b** at 140 K after annealing to 240 K.

In order to obtain a complete analysis, a flat, regular shaped, single crystal was rotated around three mutual orthogonal axes designated x, y, and z.

The ESR spectra reveal the existence of two differently oriented radicals. Their spectra coalesce upon rotation around the x axis which appears to be an axis of twofold symmetry. Rotation in the xz and yz planes results in very complex spectra due to overlapping sites. For this reason the interpretation was performed using computer simulation. The accuracy of the hyperfine coupling resulting from these spectra is somewhat less than for the rotation in the yz plane. The principal hyperfine couplings of the two sites are nearly identical (± 5 MHz for ^{31}P; ± 0.5 MHz for ^{35}Cl). Averaged values are compiled in Table I.

Table I. Hyperfine tensors for radicals **1a** and **1b**.

Radical	Nucleus	Temperature (K)	Total tensor (MHz)	Isotropic part (MHz)	Dipolar tensor (MHz)	Direction cosines		
						x	y	z
1a	P	100	1822	1985	-163	∓ 0.308	0.882	-0.355
			1851		-134	∓ 0.668	0.065	0.742
			2282		297	± 0.678	0.466	0.569
	Cl	100	57	89	-32	∓ 0.416	0.707	-0.572
			73		-16	∓ 0.873	-0.136	0.468
			137		48	± 0.253	0.694	0.674
1b	P	140	981	1153	-172	∓ 0.593	0.789	-0.158
			1026		-127	± 0.629	0.332	-0.703
			1452		299	± 0.502	0.517	0.693

On annealing to 240 K the ESR spectrum of **1a** is irreversibly lost, but signals due to a secondary radical **1b** (Fig. 2) become apparent. The two orientations of **1a** give rise to two orientations of **1b** which coalesce also, upon rotation around x. Radical **1b** is assigned to a thiophosphonyl radical formed from **1a** by dissociation of the phosphorus–chlorine bond (Fig. 1). Recooling to 140 K and subsequent rotation of the crystal afforded the angular dependence of the ^{31}P hyperfine coupling and its principal values (Table I).

Table II. g Tensors for radicals 1a and 1b.

Radical	Temperature (K)	g Tensor	Direction cosines		
			x	y	z
1a	100	1.998	± 0.643	0.625	0.443
		2.004	∓ 0.656	0.151	0.739
		2.012	∓ 0.396	0.766	-0.507
1b	140	2.000	∓ 0.009	0.688	0.725
		2.001	∓ 0.808	-0.432	0.399
		2.010	∓ 0.589	0.583	-0.560

The spectra of **1b** display some additional hyperfine splitting due to the ^{14}N nuclei. This ^{14}N hyperfine coupling, which shows little anisotropy and possesses an average value of approximately 40 MHz, is not always resolved and an accurate determination of the principal values was not possible. For the coalesced spectra in the *yz* plane a remarkably small splitting can be detected for **1b**. This splitting is best resolved when the spectra are recorded at 170 K. The multiplet (Fig. 3) shows at least 11 lines separated by 0.63 mT. This multiplet structure arises most likely from the coupling of the unpaired electron with two equivalent ^{14}N nuclei and from four equivalent ^{1}H nuclei where the A_N is about twice the A_H. Theoretically this combination results in 13 transitions.[15] The ^{14}N hyperfine coupling of 35 MHz (1.26 mT) is in good agreement with the ^{14}N coupling of the related $(Me_2N)_2\dot{P}=O$ phosphonyl radical which is found to be 1.2 mT.[16] The ^{1}H hyperfine splitting originates presumably from the four hydrogen nuclei on C(2) and C(5) of the two pyrrolidine rings which are oriented syn to the SOMO.

The ESR parameters for **1a** and **1b** are collected in Tables I and II. The spin densities in the valence *s* and *p* orbitals (respectively ρ_s and ρ_p) have been estimated from the isotropic and anisotropic contributions to the hyperfine coupling[17] (Table III).

Radical **1a** has clearly been formed by electron capture. The unpaired electron occupies an antibonding orbital between phosphorus and chlorine. The spin density is mainly located on phosphorus (55.4%) with a *p/s* ratio of 2.72. Chlorine contributes for 15.3% and this spin density is largely confined to the $3p$ orbital. This distribution is comparable to those of the $(alkyl)_3\dot{P}Cl$ and $Ph_3\dot{P}Cl$ σ^* phosphoranyl radicals,[5,11] although in the present case the contribution of chlorine is smaller. The direction cosines in Table I give useful information on the directions of the valence *p* orbitals contributing to the SOMO. This results from the fact that the direction of the largest principal value is identical with the direction of the *p* orbital. For **1a** the directions of the ^{31}P and ^{35}Cl tensors are inclined by an angle of 29°. The spin density of the tetrahedral dissociation product **1b** is predominantly (49.4%) confined to phosphorus with little delocalization on the nitrogen nuclei (each 2%). The direction of the ^{31}P anisotropy of **1b** makes an angle of 12° with the ^{31}P tensor of **1a** and 17° with the
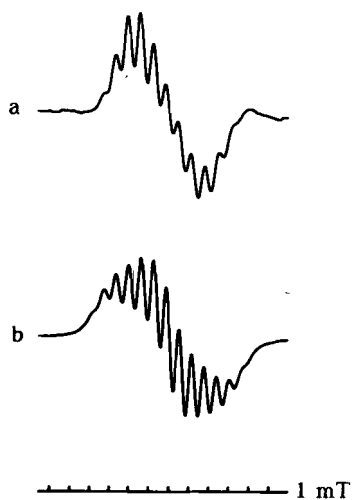
Figure 3. High-field multiplet of **1b** at 170 K. Magnetic field parallel to yz : (a) experimental; (b) computer simulation.

Table III. Approximate orbital spin densities

Radical	Nucleus	ρ_s (%)	ρ_p (%)	p/s
1a	P	14.9	40.5	2.72
	Cl	1.6	13.7	8.56
1b	P	8.7	40.7	4.68
	N	1.9		
2a	P	17.3	32.5	1.88
	F	1.8	12.9	7.17

corresponding ^{35}Cl tensor.

The three principal directions of the largest eigenvalues of **1a** and **1b** lie approximately in one plane (normal vector 0.184, ± 0.672, ∓ 0.718). The deviations are small (less than 3°). This plane is most likely the molecular plane through the P, Cl, and S nuclei. Since the direction of the eigenvector associated with the largest eigenvalue of **1b** lies in the direction of the cleaved phosphorus–chlorine bond,[3,18] it is possible to relate the molecular geometry with the principal hyperfine coupling directions. Based on the orbital spin densities and directional information the following structures can be

assigned to the radicals **1a** and **1b**:

1a   **1b**
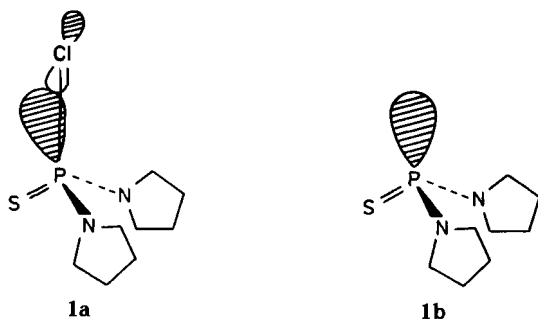
3.2. Dimorpholinofluorophosphine sulphide (2)

x Irradiation of a single crystal of **2** generates a phosphoranyl radical **2a** (Fig. 4), formed by electron capture. The ESR spectrum recorded at 100 K (Fig. 5) exhibits hyperfine coupling to one ^{31}P and one ^{19}F nucleus.

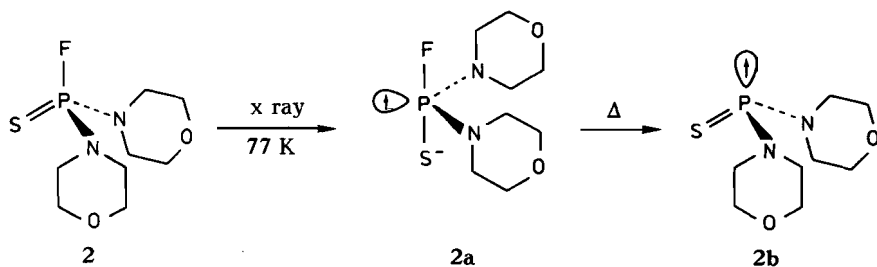**2**   **2a**   **2b**

Figure 4. Formation of radicals **2a** and **2b** upon x irradiation and subsequent annealing.

Examination of several single crystals obtained from THF/pentane solutions (see Experimental section) reveals the existence of two different crystal structures for **2**. One class of single crystals shows two differently oriented radicals after irradiation, resulting in eight lines. The second class reveals only one site (four transitions). In general the single crystals are very fragile and this prevents remounting and recooling. For this reason three different single crystals, with identical habit (class 2), were chosen to obtain an analysis of the principal hyperfine couplings. The single crystals were oriented using a polarization microscope, and three mutual orthogonal reference axes were chosen:
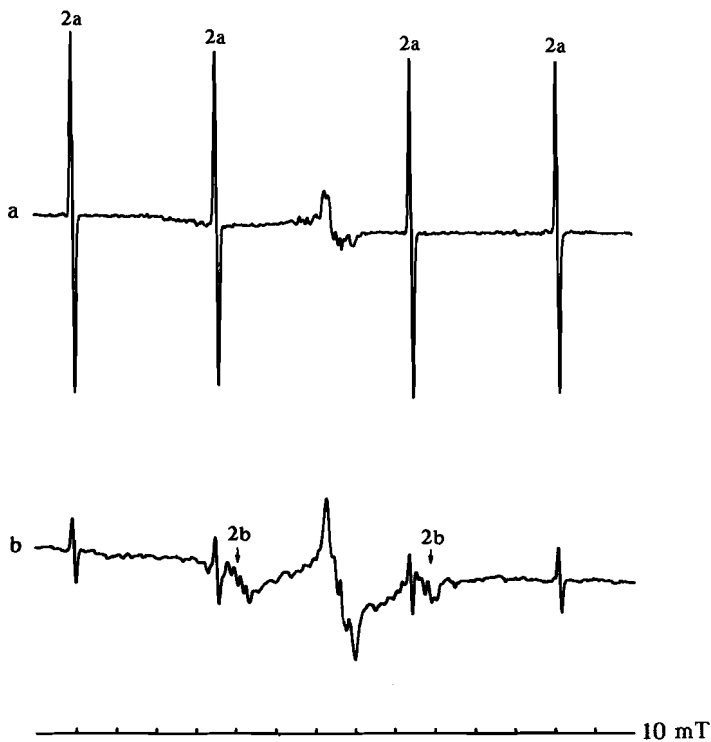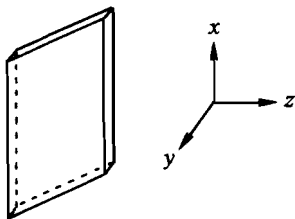
78

Figure 5. Single-crystal ESR spectra of x-irradiated **2**: (a) radical **2a** at 100 K; (b) radical **2b** at 140 K after annealing to 240 K.

From this type of measurement it is possible to deduce two sets of principal hyperfine couplings and principal axes because it is not possible to distinguish between positive and negative senses of rotation about the reference axes.[19] Additional

information to solve this ambiguity was obtained from an independent single-crystal rotation about a fourth axis in the xy plane. The principal values of the hyperfine and g tensors are compiled in Tables IV and V together with the corresponding direction cosines.

Table IV. Hyperfine tensor for radical **2a**

| Radical | Nucleus | Temperature (K) | Total tensor (MHz) | Isotropic part (MHz) | Dipolar tensor (MHz) | Direction cosines | | |
						x	y	z
2a	P	100	2140	2296	-156	0.534	-0.455	0.713
			2214		-82	0.463	0.863	0.204
			2535		239	0.708	-0.221	-0.671
	F	100	705	935	-230	0.073	0.951	-0.299
			709		-226	0.870	0.087	-0.486
			1390		455	0.488	-0.296	0.821

Table V. g Tensor for radical **2a**.

| Radical | Temperature (K) | g Tensor | Direction cosines | | |
			x	y	z
2a	100	2.000	0.453	-0.131	-0.882
		2.001	0.800	-0.376	0.467
		2.007	0.393	0.917	0.065

On annealing to 190 K the features of radical **2a** start to disappear from the ESR spectrum and, on increasing the spectrometers receiver gain, weak signals attributable to **2b** (Figs. 4 and 5) can be detected. A complete analysis of these signals proved to be impracticable because of their weak intensity. However, the powder spectra of **1b** and **2b** are virtually identical which suggests similar hyperfine couplings.

The orbital populations (Table III) which can be derived from the hyperfine interactions indicate that for **2a** the main part of the spin density is confined to phosphorus ($\rho_s = 17.3\%$ and $\rho_p = 32.5\%$). The fluorine atom contributes for a total of 14.7% to the SOMO, largely with the $2p$ orbital. The magnitudes of the isotropic and anisotropic ^{19}F hyperfine couplings are comparable to the apical ^{19}F couplings of the TBP-e $\dot{P}F_4$ radical ($A^{iso} = 857$ MHz; $2B = 386$ MHz).[1] The angle between the principal

directions of the anisotropies of phosphorus and fluorine is 82° (or 180°−82°= 98°). This nearly perpendicular orientation leads to the assignment of a TBP-e configuration for **2a**. The fluorine nucleus possesses an apical position in the TBP structure and the unpaired electron resides as a fifth ligand in an equatorial position.

The nature of the second apical ligand, in principle nitrogen or sulphur, cannot be derived directly from the ESR spectra. Nevertheless the sulphur nucleus is assigned to occupy the second apical site. Two facts support this assignment. First, no ^{14}N splitting is observed whereas an apically located ^{14}N nucleus normally exhibits a hyperfine coupling of approximately 70 MHz.[20,21] The second argument is based on symmetry considerations. The precursor molecule possesses C_s symmetry. Upon the formation of a TBP-e phosphoranyl radical with apical ^{19}F and ^{14}N nuclei this symmetry would be lost. In that case the ESR spectrum will show two differently oriented radicals because both morpholino groups have an equal chance to occupy the apical position. The observation of only one site is in accordance with the assignment of an apical sulphur nucleus.

The exact molecular geometry of **2a** cannot be determined experimentally. Upon electron capture the original tetrahedral geometry will be deformed toward a TBP configuration by an enlargement of the angle between the P-F and P-S bonds. Radical **2a** will possess approximately the following structure:

2a
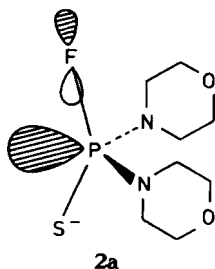
4. DISCUSSION

From this study it is clear that the structure of a phosphoranyl radical strongly depends on the nature of the ligands.

Radical **1a** represents a near σ* structure in which the extra electron occupies an antibonding orbital between phosphorus and chlorine. The original tetrahedral geometry of precursor **1** will be preserved upon electron capture, although the phosphorus-chlorine bond will elongate. The weakening of the three-electron bond, because of its partial antibonding character, is nicely demonstrated by the observed dissociation of **1a** into **1b** on annealing. The small angle of 12° between the principal directions of the ^{31}P hyperfine couplings of **1a** and **1b** in the single crystal indicates the near in-line mode of

this process.

Radical **2a** possesses a TBP-e structure with fluorine and sulphur in apical positions. The exact contribution of the sulphur nucleus to the SOMO remains unknown because the ^{32}S isotope possesses no spin angular momentum. Table III reveals that 35.5% of the unpaired electron density could not be detected. This might be an indication of the delocalization on sulphur. The apical location of the sulphur substituent in a TBP-e phosphoranyl radical is unusual but has also been found in electron capture radicals of tetramethyl- and tetraethyldiphosphine disulphides.[13]

The C_s symmetry of the radicals **1a** and **2a** forces the principal direction of one g value and one A_P value to be parallel. For **1a** these parallel principal values are $g = 2.004$ and $A_P = 1851$ MHz, whereas for **2a** $g = 2.004$ and $A_P = 2214$ MHz are nearly aligned. The remaining principal directions (Fig. 7) are located in one plane. Figure 6 reveals that the direction of the largest A_P is close to the minimum of g. This is expected because it is the direction of the contributing phosphorus $3p$ orbital.
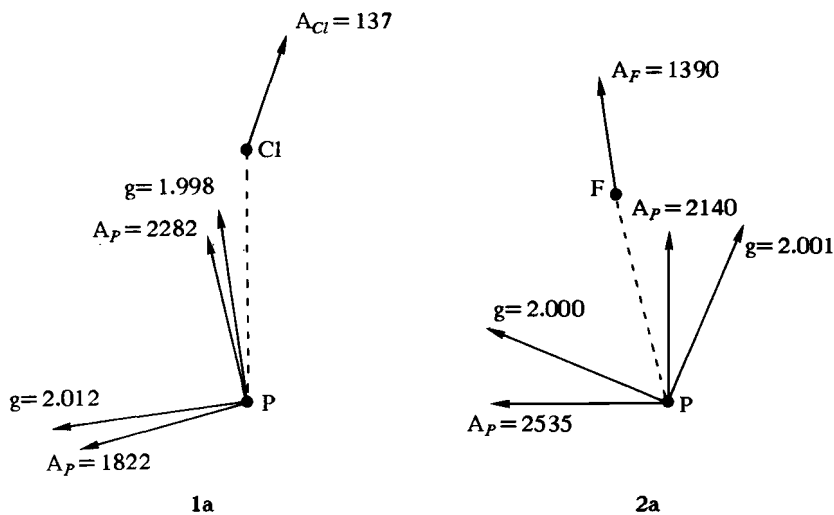

Figure 6. Schematic representation of the principal directions for **1a** and **2a**.

An attempt to obtain a quantum chemical description of the radicals **1a** and **2a** was not successful. Ab initio calculations on STO-3G and 4-31G SCF levels, using methods described before,[8,9] did not reveal stable geometries for model species of **1a** and **2a** in which the pyrrolidino and morpholino groups are replaced by NH_2 groups. For both radicals gradient optimization leads to dissociation of the phosphorus-halogen bond.

The observed difference in radical structure can be rationalized on basis of the nature of the halogen substituents and the intrinsic properties of the phosphorus-halogen bonds. According to Giles and Roberts,[21] the tendency for a substituent (A) to

occupy an apical position in a TBP is determined by the electron affinity (E_A) of A· and the average homolytic bond dissociation enthalpy [D(P-A)]. An increase of E_A and decrease of D(P-A) will lead to a higher apicophilicity. Comparison of these values[22,23] for fluorine ($E_A = 328$ kJ mol^{-1}, D(P-A)= 490 kJ mol^{-1}) and chlorine ($E_A = 349$ kJ mol^{-1}, D(P-A)= 323 kJ mol^{-1}) reveals a larger apicophilicity for chlorine. If the tendency for a substituent to occupy an apical position is appreciably larger than for the other three, a σ* structure will be preferred. If, however, the apicophilicity is more or less equal for two substituents a TBP configuration can be expected.

Correspondingly, an explanation for the formation of σ* and TBP-e structures can be derived from a qualitative description of the MO scheme (Fig. 7). The P-F bond is approximately 167 kJ mol^{-1} more stable than the P-Cl bond. Consequently the P-F σ MO lies below the P-Cl σ MO. The LUMOs of the precursors 1 and 2 will be singly occupied upon electron capture. For compound 1 the energy gap between the P-Cl σ and σ* MOs will be smaller than for the P-F bond in compound 2. It is therefore conceivable that the LUMO of 2 is not the σ* MO but a TBP-e like orbital. Apparently the TBP-e and σ* MOs are interconverted for the two compounds. Since both orbitals possess the same type of symmetry (A' in C_s point group), some mixing will occur, resulting in the observed deviations from pure σ* and pure TBP-e configurations.
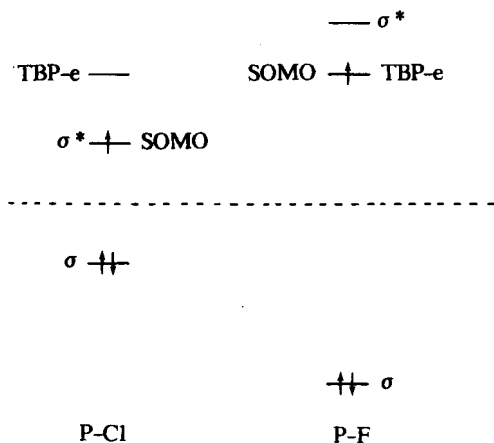

Figure 7. Orbital diagram for the formation of σ* and TBP-e structures in **1a** and **2a**, respectively.

Similar arguments have been put forward by Clark in ab initio studies on phosphorus and chlorine σ* radical cations,[24] and on C_{3v} and C_s silyl halide anions.[25,26] An important factor, determining the stability of a two–centre, three–electron bond, is the energy gap between the interacting orbitals of the two molecular groups that form the σ* bond. In case the two orbitals are (nearly) degenerate, a stable σ* radical can be expected. TBP-e configurations become more favourable for large values of the energy gap.

REFERENCES

1. A. Hasegawa, K. Ohnishi, K. Sogabe and M. Miura, Mol. Phys., **30**, 1376 (1975).
2. A.J. Colussi, J.R. Morton and K.F. Preston, J. Phys. Chem., **79**, 1855 (1975).
3. J.H.H. Hamerlinck, P. Shipper and H.M. Buck, J. Am. Chem. Soc., **105**, 385 (1983).
4. J.H.H. Hamerlinck, P. Schipper and H.M. Buck, J. Am. Chem. Soc., **102**, 5679 (1980).
5. T. Berclaz, M. Geoffroy and E.A.C. Lucken, Chem. Phys. Lett., **36**, 677 (1975).
6. T. Berclaz, M. Geoffroy and E.A.C. Lucken, Chem. Phys. Lett., **62**, 515 (1979).
7. J.M. Howell and J.F. Olsen, J. Am. Chem. Soc., **98**, 7119 (1976).
8. R.A.J. Janssen, G.J. Visser and H.M. Buck, J. Am. Chem. Soc., **106**, 3429 (1984). Chapter 2.
9. R.A.J. Janssen and H.M. Buck, J. Mol. Struc. (THEOCHEM), **110**, 139 (1984). Chapter 3.
10. M.C.R. Symons, Chem. Phys. Lett., **40**, 226 (1976).
11. M.C.R. Symons and R.L. Petersen, J. Chem. Soc., Faraday Trans. 2, **75**, 210 (1979), and references therein.
12. A. Hasegawa, G.D.G. McConnachie and M.C.R. Symons, J. Chem. Soc., Faraday Trans. 1, **80**, 1005 (1984), and references therein.
13. R.A.J. Janssen, M.H.W. Sonnemans and H.M. Buck, J. Chem. Phys., **84**, 3694 (1986). Chapter 4.
14. H.W. Roesky, Chem. Ber., **100**, 1447 (1967).
15. Theoretical intensities: 1-4-8-12-16-20-22-20-16-12-8-4-1.
16. B.P. Roberts and K.J. Singh, J. Organomet. Chem., **159**, 31 (1978).
17. J.R. Morton and K.F. Preston, J. Magn. Reson., **30**, 577 (1978).
18. G.W. Fouse and W.A. Bernard, J. Chem. Phys., **70**, 1667 (1979).
19. D.S. Schonland, Proc. Phys. Soc. London, Ser. A, **73**, 788 (1959).
20. J.H.H. Hamerlinck, P.H.H. Hermkens, P. Schipper and H.M. Buck, J. Chem. Soc., Chem. Commun., 358 (1981).
21. J.R.M. Giles and B.P. Roberts, J. Chem. Soc., Perkin Trans. 2, 1211 (1981).
22. J.E. Bartmess, J.A. Scott and R.T. McIver, J. Am. Chem. Soc., **101**, 6046 (1979).
23. W.G. Bentrude, *Free Radicals*, J.K. Kochi, Ed. (Wiley-Intersience, New York, 1973), p. 595-663.
24. T. Clark, J. Comput. Chem., **4**, 104 (1983).
25. T. Clark, J. Chem. Soc., Chem. Commun., 515 (1981).
26. T. Clark, J. Chem. Soc., Perkin Trans. 2, 1267 (1982).

CHAPTER 6

The $S\overset{\cdot}{P}Cl_2F^-$ radical

1. INTRODUCTION

The site preference of the substituent groups in a TBP-e phosphoranyl radical is important for the spin density distribution when two or more different groups are present. In principle a substituent can be located either in an apical or an equatorial position. In general the most electronegative ligands are located on the apical site, consistent with the apicophilicities of five-coordinated phosphoranes.[1,2] In chapter 5 it was shown that if the tendency of one substituent to occupy an apical position is appreciably larger than for the other three a $\sigma*$ structure can be expected.

This chapter describes the ESR spectrum and an ab initio quantum chemical calculation of the dichlorofluorophosphine sulphide radical anion ($S\overset{\cdot}{P}Cl_2F^-$, Fig. 1), 1a, which represents a strongly deformed TBP-e type radical with two apical chlorine nuclei and an equatorial fluorine nucleus. The apparent violation of the electronegativity rule is discussed. The quantum chemical calculations reveal that the determination of the radical geometry on basis of anisotropic hyperfine couplings is not always justified because the principal directions of the dipolar interactions are not necessarily coincident with the molecular frame.
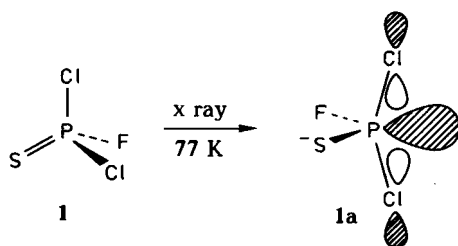

Figure 1. Schematic representation of the SOMO of **1a**.

2. RESULTS

A solution of $SPCl_2F^3$ in 2-methyltetrahydrofuran (MeTHF) was rapidly frozen in liquid nitrogen and subsequently x irradiated for 6h (Cu source). The ESR spectrum obtained at 100 K (Fig. 2) shows clearly the features of a phosphoranyl radical formed by electron capture. The high and low field components of the large ^{31}P doublet show an additional splitting resulting from two equivalent chlorine nuclei.
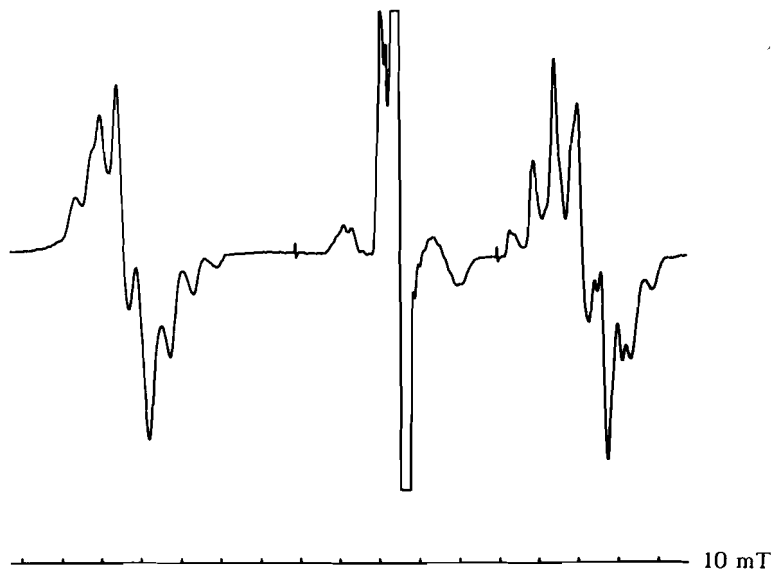

10 mT

Figure 2. First derivative ESR spectrum at 100 K of x-irradiated $SPCl_2F$ in MeTHF.

Analysis of the spectrum in terms of anisotropic ^{31}P and $^{35}Cl/^{37}Cl$ hyperfine couplings is not possible. The parallel ^{35}Cl splittings are well defined but the perpendicular features are not resolved. This is a frequently observed phenomenon in powder spectra of chlorine containing radicals which results from the relatively large nuclear quadrupole interaction and second-order effects.[4,5] For radicals in which the direction of the principal hyperfine coupling coincides with the major quadrupole axis, the spectra yield a normal equally spaced multiplet when the magnetic field is parallel to this axis. For a perpendicular orientation of the magnetic field, however, complicated spectra can occur particularly when the quadrupole interaction is of the same order of magnitude as the hyperfine energy.[6-8] The important result that the two chlorine nuclei are equivalent, and bear a large amount of spin density, is not affected by the complexity of the spectrum. Furthermore no ^{19}F hyperfine coupling is observed and hence the spin density on

fluorine will be small. The results lead to the assignment that the $S\dot{P}Cl_2F^-$ radical anion possesses a TBP-e like structure in which the two chlorine nuclei are located apically and the fluorine and sulphur nuclei are in equatorial positions.

After correction according to the Breit-Rabi equations the spectrum of $S\dot{P}Cl_2F^-$ yields $A_P = 2986$ MHz, $A_{Cl} = 167$ MHz and a g value of 2.010. Assuming a perpendicular orientation for the ^{31}P and ^{35}Cl hyperfine tensors these values correspond to $A_\perp$ ($= A^{iso} - B$) for ^{31}P and $A_{//}$ ($= A^{iso} + 2B$) for ^{35}Cl. The $^{35}Cl/^{37}Cl$ couplings of $S\dot{P}Cl_2F^-$ are comparable to other TBP-e phosphoranyl radicals in which two chlorine atoms occupy apical positions as $O\dot{P}Cl_3^-$,[9] $\dot{P}Cl_4$,[10] and $S\dot{P}Cl_3^-$.[11]

A quantum chemical description of the $S\dot{P}Cl_2F^-$ radical was obtained by using the UHF method at SCF-level with the standard 4-31G basis set[12,13] implemented with a single set of six second-order Gaussians on P, S and Cl.[14] Gradient optimization without any symmetry constraint results in a structure of C_s symmetry (Fig. 3, E = -1745.9538 a.u. and $<S^2> = 0.7506$).
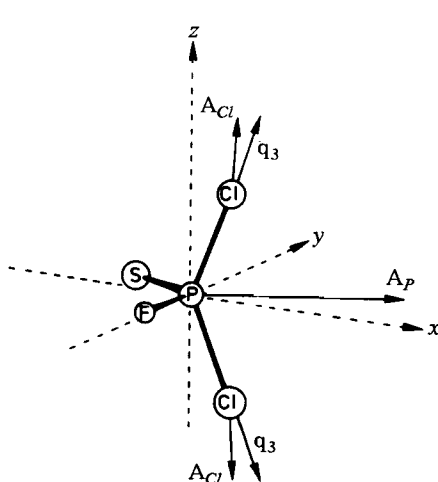

Figure 3. Optimized geometrical parameters for $S\dot{P}Cl_2F^-$ and directions of A_P, A_{Cl} and q_3. Bond distances PCl = 2.32 Å, PS = 1.92 Å, PF = 1.60 Å; bond angles ClPCl = 134.1°, ClPS = 111.0°, ClPF = 91.4°, SPF = 109.8°. Cl_1 and Cl_2 in xz plane; S and F in xy plane.

The P-Cl bond length in this structure is 2.34 Å and the Cl-P-Cl angle is 134.1°. The dihedral angle of the ClPCl and SPF planes is exactly 90°. The SOMO is an antibonding orbital with large contributions from the central phosphorus nucleus and the two chlorine substituents, in accordance with the experimental observation. The calculated isotropic and anisotropic hyperfine couplings of this radical obtained after annihilation of the corresponding UHF wave function[15] are in accordance with the experimental data and give a further insight into the structure of this radical (Table I).

Table I. Calculated isotropic and anisotropic hyperfine coupling constants for $S\dot{P}Cl_2F^-$.

Nucleus	A^{iso} (a.u.)	(MHz)	B (a.u.)	(MHz)	Direction cosines[a] x	y	z
P	1.423	2577	1.216	263	0.925	0.381	0.000
			-0.565	-122	0.381	-0.925	-0.000
			-0.651	-141	-0.000	-0.000	1.000
Cl_1	0.129	56	1.370	72	0.147	-0.118	0.982
			-0.682	-36	0.869	0.489	-0.071
			-0.688	-36	0.471	-0.864	-0.175
Cl_2	0.129	56	1.370	72	0.147	-0.118	-0.982
			-0.682	-36	0.869	0.489	0.071
			-0.688	-36	0.471	-0.864	0.175
F	0.005	21	0.138	69	0.642	0.767	0.001
			-0.059	-29	0.767	-0.641	-0.001
			-0.079	-40	-0.000	-0.001	1.000
S	0.001		0.542		0.963	0.271	0.000
			-0.259		0.271	-0.970	-0.001
			-0.283		0.000	-0.001	1.000

[a] Direction cosines refer to coordinate system in Fig. 3

The directions of the chlorine anisotropic hyperfine interactions are inclined by an angle of 158.3° and nearly perpendicular to the phosphorus dipolar interaction. The near alignment of the ligand hyperfine couplings (usually chlorine or fluorine) has often been invoked to be an indication and a confirmation of a TBP-e structure.[4,9,16] The calculations reveal that the Cl-P-Cl bond angle in $S\dot{P}Cl_2F^-$ is only 134° and that the actual molecular geometry is in fact intermediate between a tetrahedral configuration and a TBP-structure.

The computation of the electric field gradient tensor (Table II) at the position of the chlorine nuclei reveals an angle of only 2.7° between the direction of q_3 and the P-Cl bond, and of 13.3° between q_3 and the direction of the largest chlorine hyperfine coupling. The nuclear quadrupole coupling constant, calculated as the product of the nuclear quadrupole moment Q and the largest value of the electric field gradient tensor[17,18] at the chlorine nuclei, is of the same order of magnitude (-41 MHz) and of similar direction as the chlorine hyperfine coupling.

Table II. Electric field gradient tensor and nuclear quadrupole coupling (NQC) for $S\dot{P}Cl_2F^-$.

	q (a.u.)	NQC (MHz)	Direction cosines[a]		
			x	y	z
Cl_1	-1.148		-0.295	0.946	0.129
	-1.061		0.889	0.321	-0.326
	2.209	-41	0.350	-0.019	0.936
Cl_2	-1.148		-0.295	0.946	-0.129
	-1.061		0.889	0.321	0.326
	2.209	-41	0.350	-0.019	-0.936

[a] Direction cosines refer to coordinate system in Fig. 3.

3. DISCUSSION

Both experiment and theoretical calculations reveal that the $S\dot{P}Cl_2F^-$ radical possesses an electronic structure in which the major part of the unpaired electron density is located on phosphorus and the two equivalent chlorine atoms. The chlorine nuclei occupy the axial positions of a strongly deformed TBP-e structure. The tendency of chlorine to contribute to the SOMO and to occupy an apical position thus appears to be superior to that of fluorine. This is in accordance with the results on the structure of chlorine and fluorine diaminophosphine sulphide electron capture radicals.[19] Five-coordinated phosphoranes show an opposite behaviour for the relative apicophilicity of fluorine and chlorine since PF_3Cl_2 is known to have both chlorines in equatorial positions.[20] Although, in general, TBP-e phosphoranyl radical structures agree well with the principles of five-coordination, an important difference is the nature of the highest occupied molecular oirbital. For a phosphoranyl radical this orbital is half-filled and highly antibonding between phosphorus and the two p orbitals of the apical ligands. Ab initio calculations for TBP phosphoranes reveal that the highest symmetrical MO is essentially nonbonding or slightly antibonding between the central atom and the apical nuclei.[21−23] On this basis the apical bonds in a phosphoranyl radical can be expected to be longer and weaker than the corresponding bonds in a phosphorane. Upon formation of a TBP-e structure, after electron capture of a four–coordinated compound, the site preference of the substituents will partly depend on the intrinsic P-substituent bond energy. The P-Cl bond energy is known to be approximately 170 kJ mol^{-1} smaller than the P-F bond energy, explaining the observed axial location of chlorine.

REFERENCES

1. W.G. Bentrude, Acc. Chem. Res., **15**, 117 (1982).

2. R.S. McDowell and A. Streitwieser Jr., J. Am. Chem. Soc., **107**, 5849 (1985).

3. H.W. Roesky, Chem. Ber., **100**, 1447 (1967).

4. D.J. Nelson and M.C.R. Symons, J. Chem. Soc., Dalton Trans., 1164 (1975).

5. C.M.L. Kerr and F. Williams, J. Am. Chem. Soc., **94**, 5212 (1972).

6. F.G. Herring, C.A. McDowell and J.C. Tait, J. Chem. Phys., **57**, 4564 (1972).

7. F.J. Adrian, E.L.Cochran and V.A. Bowers, J. Chem. Phys., **56**, 6251 (1972).

8. T.G. Castner and W. Känzig, J. Phys. Chem. Solids, **3**, 178 (1957).

9. T. Gillbro and F. Williams, J. Am. Chem. Soc., **96**, 5032 (1974).

10. S.P. Mishra and M.C.R. Symons, J. Chem. Soc., Dalton Trans., 139 (1976).

11. S.P. Mishra and M.C.R. Symons, J. Phys. Chem., **78**, 576 (1974).

12. R. Ditchfield, W.J. Hehre and W.A. Lathan, J. Chem. Phys., **54**, 724 (1971).

13. W.J. Hehre and W.A. Lathan, J. Chem. Phys., **56**, 5255 (1972).

14. Radial coefficients P 0.55, S 0.65, and Cl 0.75. M.M. Francl, W.J. Pietro, W.J. Hehre, J.S. Binkley, M.S. Gordon, D.J. DeFrees and J.A. Pople, J. Chem. Phys., **77**, 3654 (1982).

15. R.A.J. Janssen and H.M. Buck, J. Mol. Struc. (THEOCHEM), **110**, 139 (1984). Chapter 3.

16. J.W. Cooper, M.J. Parrott and B.P. Roberts, J. Chem. Soc., Perkin Trans. 2, **730** (1977).

17. J. Kowaleski and K.M. Larson, Chem. Phys. Lett., **109**, 104 (1984).

18. G.E. Scuseria, T.J. Lee, R.J. Saykally and H.F. Schaefer III, J. Chem. Phys., **84**, 5711 (1986).

19. R.A.J. Janssen, M.H.W. Sonnemans and H.M. Buck, J. Am. Chem. Soc., **108**, 6145 (1986). Chapter 5.

20. R.R. Holmes, R.P. Cartner Jr. and G.E. Peterson, Inorg. Chem., **3**, 1748 (1964).

21. A. Strich and A. Veillard, J. Am. Chem. Soc., **95**, 5574 (1973).

22. A. Rauk, L.C. Allen and K. Mislow, J. Am. Chem. Soc., **94**, 3035 (1972).

23. R.F. Hout, W.J. Pietro and W.J. Hehre, *A Pictorial Approach to Molecular Structure and Reactivity* (Wiley-Interscience, New York, 1984).

CHAPTER 7

Trialkylphosphine sulphide and selenide radical anions

1. INTRODUCTION

Phosphoranyl radicals generated by radiation-induced electron capture of four-coordinated phosphorus compounds ($R_3P=X$) can, in principle, adopt a σ^* configuration in which the unpaired electron resides in an antibonding orbital between phosphorus and the originally double bonded substituent X (Fig. 1).
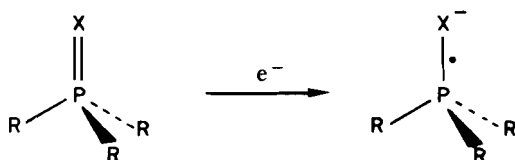

Figure 1. Formation of a $R_3\dot{P}\dot{-}X^-$ configuration.

Structures of this type have been postulated, based on ESR studies of polyoriented systems, for $Me_3\dot{P}O^-$,[1] $Et_3\dot{P}O^-$, $Me_3\dot{P}S^-$ and $Ph_3\dot{P}S^-$.[2] The analysis of powder ESR spectra can be very ambiguous and no precise directional information on the magnetic hyperfine interactions can be obtained. Hence, there is no evidence that these structures do not seriously deviate from a pure trigonal one. Moreover, a detailed ESR study of chalcogeno triphenylarsoranyl radicals ($Ph_3\dot{A}sX^-$, $X = O$, S, Se), trapped in single crystals, has shown that the maximum [75]As coupling forms an angle of 20° with the parent As-X bond, indicating a deviation from the C_3 structure.[3] A prerequisite for the formation of a C_3 $P\dot{-}X^-$ σ^* structure is that the substituent X and the PX bond can accommodate the extra electron appreciably better than the ligands R and the PR bonds. This can be achieved when trialkyl- and triarylphosphine chalcogenides are studied.

The formation of a $P\dot{-}X^-$ σ^* bond is closely related to the parent $P=X$ bond energy, because upon electron capture the antibonding character of the SOMO will tend to elongate the bond. Extensive experimental[4,5] and theoretical[6] studies have shown that the thiophosphoryl (PS) bond is weaker and contains less multiple bond character than does the phosphoryl (PO) bond. Typical dissociation energies of PS bonds are 443 kJ mol^{-1} versus 732 kJ mol^{-1} for the PO group.[7] The quantum chemical estimate of the bond order of the PS bond in H_3PS is 1.32, substantially less than the 1.58 bond

order in H_3PO.[6] From this it is clear that $P \doteq X^- \sigma^*$ phosphoranyl radicals are more readily formed in phosphine sulphides than in the corresponding oxides.

In this chapter single-crystal ESR experiments are reported on phosphoranyl radicals generated in trialkylphosphine sulphides and selenides. The results are correlated with the x-ray structure analysis of the parent compounds. It will be shown that several trigonal $R_3P \doteq X^-$ phosphoranyl radicals are formed. The presence of ^{77}Se satellites in the phosphine selenides enabled the detection of spin density on the chalcogen ligand. Finally, quantum chemical calculations are presented which offer a possibility for a theoretical description of the radical structure.

2. EXPERIMENTAL SECTION

Trimethylphosphine sulphide (1) was obtained from the reaction of tetramethyldiphosphine disulphide and methyl iodide.[8] Triethylphosphine sulphide (2), tricyclohexylphosphine sulphide (3), trimethylphosphine selenide (4), triethylphosphine selenide (5), and tricyclohexylphosphine selenide (6) were synthesized from the corresponding phosphines and elemental sulphur or selenium.[9-11] Triphenylphosphine sulphide (7) and selenide (8) were commercial materials (Janssen Chimica). All compounds were characterized with ^1H and ^{31}P NMR and elemental analysis. Single crystals were prepared by slow evaporation or slow cooling of solutions of the desired compound in ethanol (1, 3, 4, 5, 6) or 1,4-dioxane (2, 8).

Irradiation of the compounds, subsequent ESR measurements and analysis of the spectra were performed as described in chapter 4.

3. RESULTS AND ASSIGNMENT

3.1. Trimethylphosphine sulphide (1)

Trimethylphosphine sulphide (1) crystallizes in the monoclinic space group $P2_1/m$ with unit cell parameters $a = 6.266$ Å, $b = 7.588$ Å, $c = 6.642$ Å, and $\beta = 90.36°$.[12] Although the reported x-ray structure analysis is incomplete, the results suggest a small distortion of the molecules from C_{3v} to C_s symmetry. One SPC angle is slightly larger than the other two.

The ESR spectrum obtained at 105 K of a x-irradiated single crystal of 1 (Fig. 2a) shows a ^{31}P doublet which can be attributed to the trimethylphosphine sulphide radical

anion (**1a**). The high and low field transitions are broadened by a poorly resolved ^{1}H hyperfine coupling. From some orientations of the single crystal with respect to the magnetic field, this coupling can be determined to be approximately 0.4 - 0.5 mT. Since the unit cell angle β is very close to 90° the three crystallographic axes were used as ESR reference axes. A complete single-crystal analysis of **1a** was obtained from rotation of the crystal in the ab, ac, and bc planes. It was found that the principal hyperfine tensor and the **g** tensor share the same principal axes, and also coincide with the crystallographic axes (Table I).

Table I. **g** And hyperfine coupling (MHz) tensors for **1a** and **1b**.

Radical	Temperature (K)	Total tensor		Direction cosines		
				a	b	c
1a	105	g	2.003	1	0	0
			2.010	0	1	0
			2.004	0	0	1
		[31]P	2021	1	0	0
			1647	0	1	0
			1660	0	0	1
		[1]H	~13		nearly isotropic	
1b	240	g	2.018	1	0	0
			2.012	0	1	0
			2.010	0	0	1
		[31]P	771	1	0	0
			979	0	1	0
			1001	0	0	1
		[1]H	~13		nearly isotropic	

Upon raising the temperature, the intensity of the signals assigned to **1a** decreases and the radical is irreversibly lost at 180 K. Concurrently with the loss of **1a** a new phosphorus doublet **1b** with a smaller ^{31}P coupling is detected (Fig. 2b). This new formed radical remains in the single crystal for several hours, even at room temperature. The principal hyperfine couplings and g values of **1b** are directed along the three crystallographic axes (Table I), as for **1a**. Their magnitudes show, however, a very anomalous behaviour because $A_\perp$ (= 990 MHz) > $A_{//}$ (= 772 MHz) indicating an opposite sign for A^{iso} and B. Furthermore, all three g values deviate from the free-electron value. The powder spectrum of **1b** (Fig. 2c) is in accordance with the single-crystal analysis and shows the expected pattern for a radical exhibiting $A_{//} < A_\perp$ and $g_{//} > g_\perp$. Radical **1b** exhibits additional ^{1}H splitting of approximately 0.5 mT.

The fact that the same axes system diagonalizes both the ^{31}P hyperfine tensor and the g tensor for **1a** as well as **1b**, and the observation that the ^{31}P hyperfine tensors are essentially axially symmetric, indicates an overall C_{3v} symmetry for the two radicals. Since the directions of the parallel hyperfine couplings also coincide with the a axis, the a axis must be the direction of PS bond of the undamaged molecule. This result is in
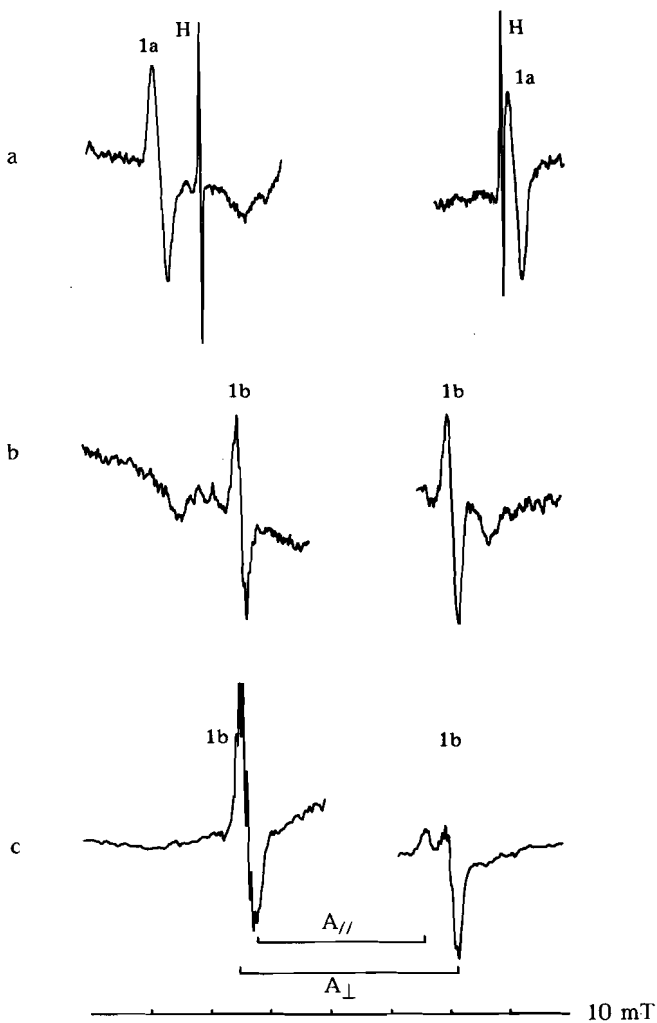
93

Figure 2. ESR spectra of x-irradiated Me₃PS (1): (a) Single-crystal ESR spectrum of **1a** at 105 K, magnetic field parallel to the *c* axis. Lines marked H result from trapped hydrogen atoms; (b) Single-crystal spectrum of **1b** at 240 K, magnetic field parallel to the *c* axis; (c) Powder spectrum of **1b** at 200 K.

accordance with the crystal structure analysis of trimethylphosphine selenide (section 3.4) which is isomorphous with that of the present compound.[13] The g tensor of 1a does not possess a C_{3v} symmetry. The principal value in the b direction is clearly different from those in the ac plane.

3.2. Triethylphosphine sulphide (2)

Triethylphosphine sulphide (2) crystallizes as long needles in the hexagonal space group P6$_3$mc. The cell dimensions are $a = 8.98$ Å and $c = 6.32$ Å.[14] The PS bond of the molecules is aligned along the c axis which is parallel to the needle axis. The molecules possess a staggered conformation of the ethyl groups. One of the CH$_2$ hydrogen atoms is in a *trans* location with respect to the PS bond. The methyl groups and the remaining hydrogen atom are in the *gauche* positions. The molecules possess a C_3 symmetry.
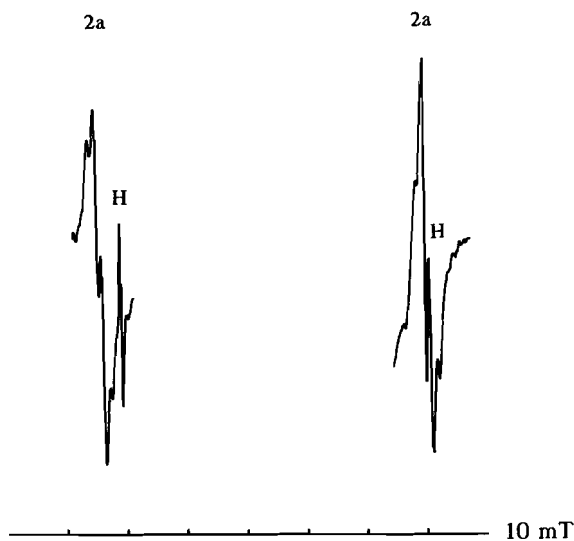

Figure 3. Single-crystal ESR spectrum of radical 2a at 105 K. Lines marked H result from hydrogen atoms. Magnetic field parallel to c axis.

x Irradiation of a single crystal of 2 at 77 K generates an electron capture phosphoranyl radical 2a. The ESR spectrum of 2a (Fig. 3) clearly shows a large ^{31}P doublet with an additional splitting due to three equivalent ^{1}H nuclei. This splitting of 1.2 mT is essentially isotropic.

For all orientations of the crystal with the c axis perpendicular to the magnetic field identical spectra, giving $A_\perp$ and $g_\perp$, are observed. Rotation of the single crystal in the ac plane reveals the parallel values of the g and ^{31}P hyperfine coupling tensors (Table II). Both tensors are completely axially symmetric. From this observation it can be concluded that the irradiation process does not lead to any detectable distortion from C_3 symmetry for **2a**. The extra hyperfine splitting arises most likely from the three *trans* oriented ^{1}H nuclei. Radical **2a** is irreversibly lost from the ESR spectrum at 170 K. No new species could be detected.

Table II. **g** And hyperfine coupling (MHz) tensors for **2a**.

Radical	Temperature (K)	Total tensor		Direction cosines		
				a	a	c
2a	105	g	2.006	1	0	0
			2.006	0	1	0
			2.002	0	0	1
		^{31}P	1517	1	0	0
			1517	0	1	0
			1943	0	0	1
		^{1}H	~34		nearly isotropic	

3.3. Tricyclohexylphosphine sulphide (3)

Crystals of tricyclohexylphosphine sulphide (**3**) are orthorhombic with $a = 10.906$ Å, $b = 15.836$ Å, and $c = 10.362$ Å.[15] The reported crystal structure parameters refer to the centrosymmetric space group Pnma. The four molecules in the unit cell lie on a mirror plane which is parallel to the ac plane. The PS bond directions are pairwise aligned, resulting in two different orientations, which are inclined by an angle of 15.8°. Recrystallization gives plate like crystals (b axis perpendicular to the plate-face).

The ESR spectrum of a x-irradiated single crystal of **3**, recorded at 105 K (Fig. 4), exhibits a weak phosphorus doublet which can be attributed to the cyclohexylphosphine sulphide radical anion (**3a**). The low and high field transitions are broadened due to additional ^{1}H splitting. Upon rotation of a single crystal in the ac plane, two different sites are observed. The spectra of the two sites coalesce for all orientations in which the magnetic field direction is parallel or perpendicular to the a or c axis. The principal ESR parameters were determined by rotating the crystal in the ac, ab, and bc planes (Table III). The principal hyperfine couplings and g values of the two sites are identical within experimental error. The two hyperfine coupling tensors are inclined by an angle of 19.5°, which is close to the crystallographic angle of 15.8° between the two

PS bonds. The directions of the ESR parameters of **3a** correspond with the C_s symmetry of the parent molecule.

The signals of **3a** are irreversibly lost from the ESR spectrum at temperatures above 160 K.
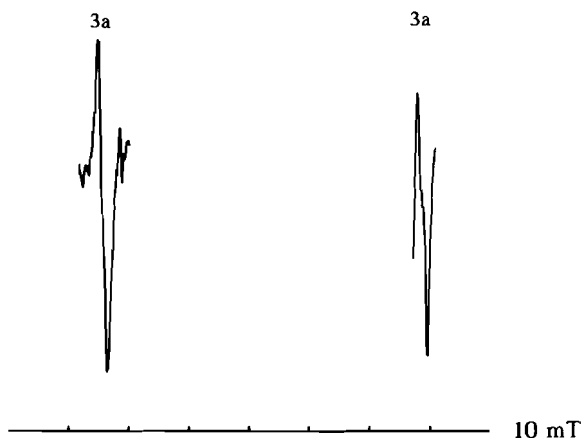

Figure 4. Single-crystal ESR spectrum of radical **3a** at 105 K. Magnetic field parallel to c axis.

Table III. g And hyperfine coupling (MHz) tensors for **3a**.

Radical	Temperature (K)	Total tensor		Direction cosines		
				a	b	c
3a	105	g	2.004	0.986	0	± 0.169
			2.006	0	1	0
			2.008	-0.169	0	± 0.986
		^{31}P	1902	0.986	0	± 0.169
			1481	0	1	0
			1474	-0.169	0	± 0.986
		^{1}H	<17	nearly isotropic		

3.4. Trimethylphosphine selenide (4)

The crystal structure of trimethylphosphine selenide (4) is very similar to that of the corresponding sulphide. The compound crystallizes in the monoclinic space group $P2_1/m$ with unit cell parameters $a = 6.453$ Å, $b = 7.806$ Å, $c = 6.586$ Å, and $\beta = 90.46°$.[13] The two molecules in the unit cell lie on a mirror plane with a staggered conformation of the methyl groups. The PSe bond directions of the two molecules are parallel and nearly directed along the crystallographic a axis. The deviation is only 1°. Furthermore the crystallographic angle β is close to 90°. This justifies the use of the a, b, and c axes as orthogonal axes for the ESR experiments.

x Irradiation of a single crystal of 4, and analysis of the ESR spectrum at 105 K, reveals the formation of two different phosphorus-centred radicals (Fig. 5). The first species, 4a, exhibits a ^{31}P doublet broadened by ^{1}H splitting. The signals of the second radical product, 4b, are much weaker and consist of a ^{31}P doublet with an additional splitting of 1.38 mT. Raising the temperature shows a decrease of signal intensity for both radicals. At 140 K the small extra coupling of 4b coalesces into a normal ^{31}P doublet. A further increase of the temperature results in the irreversible loss of 4b at 180 K and of 4a at approximately 220 K.
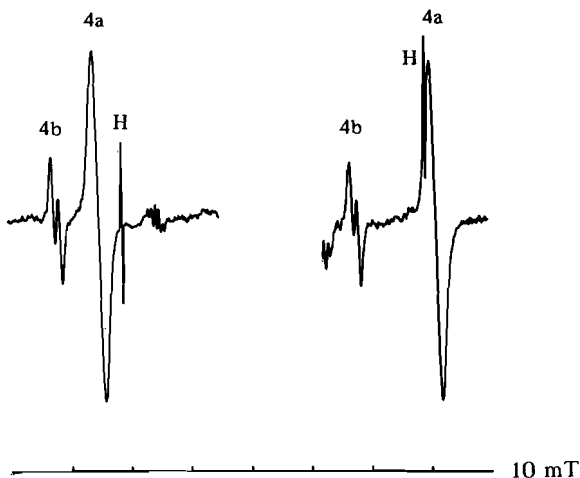

Figure 5. Single-crystal ESR spectrum of 4a and 4b at 105 K. Magnetic field parallel to the c axis. The positions of the Se satellites are marked.

The presence of the ^{77}Se isotope ($I = \frac{1}{2}$, natural abandance 7.58%) in 4 offers a possibility for the determination of the Se hyperfine interaction in the radicals 4a and 4b. The intensity of a single ^{77}Se satellite transition amounts only 3.79% of the corresponding ^{31}P transition. This weak intensity precluded the analysis of the ^{77}Se satellites for 4b. For 4a, however, the ^{77}Se satellites could be clearly identified for most

orientations of the single crystal with respect to the magnetic field. The anisotropic ESR spectra reveal that the parallel ^{31}P and ^{77}Se couplings coincide. For perpendicular orientations the ^{77}Se coupling is small and the satellite absorptions lie under the broad ^{31}P transitions. The determination of the perpendicular ^{77}Se couplings was achieved by a regression analysis of A_{se}^2 versus $\cos^2\theta$.

Rotation of a single crystal of **4** in the crystallographic *ab*, *ac*, and *bc* planes revealed the principal ESR parameters of **4a** and **4b**, and their relative directions (Table IV). For **4a**, the g tensor and both ^{31}P and ^{77}Se hyperfine tensors are aligned and directed along the *a* axis and thus along the PSe bond. The two hyperfine tensors possess a near axial symmetry. These results lead to the conclusion that **4a** has retained the original near C_{3v} symmetry. The g and ^{31}P hyperfine tensors do not share the same principal axes in for **4b**. The type of symmetry is now C_s, because in the direction of the *b* axis, perpendicular to the *ac* mirror plane, the g and ^{31}P tensor have a mutual principal axis. The direction of the maximum anisotropy of **4b** forms an angle of 31° with the PSe bond. The C_s symmetry leads to the suggestion that in **4b** one of the methyl groups contributes more to the SOMO than the other two. The distorted structure can be considered as an intermediate between a C_{3v} σ^* and a TBP-e configuration. The extra splitting of 1.25 mT could then be the result of the *trans* located CH$_3$ hydrogen atom in the mirror plane.

Table IV. g And hyperfine coupling (MHz) tensors for **4a** and **4b**.

Radical	Temperature (K)	Total tensor		Direction cosines		
				a	*b*	*c*
4a	105	g	1.998	1	0	0
			2.003	0	1	0
			2.041	0	0	1
		^{31}P	1937	1	0	0
			1561	0	1	0
			1561	0	0	1
		^{77}Se	783	1	0	0
			193	0	1	0
			200	0	0	1
		^{1}H		not resolved		
4b	105	g	2.001	0.875	0	0.483
			2.072	0	1	0
			2.059	-0.483	0	0.875
		^{31}P	1624	0.854	0	-0.520
			1439	0	1	0
			1408	0.520	0	0.854
		^{1}H	35-40			

3.5. Triethylphosphine selenide (5)

The crystal structure of triethylphosphine selenide (5) is isomorphous with that of the corresponding sulphide (2). Triethylphosphine selenide crystallizes in the hexagonal space group P6₃mc with unit cell dimensions $a = 9.06$ Å and $c = 6.54$ Å.[16] All PSe bonds of the molecules in the unit cell are directed along the c axis, which is the elongation axis of the needle shaped crystal.

After x irradiation at 77 K, the ESR spectrum of 5 at 105 K shows the features of two different phosphoranyl radicals 5a and 5b (Fig. 6). The intensity of the lines attributed to 5b is appreciably larger than for 5a. Both radicals exhibit a large ^{31}P hyperfine coupling with an additional splitting from three equivalent ^{1}H nuclei. This extra coupling is somewhat larger for 5a, and better resolved, than for 5b. The ^{77}Se satellites are well defined for both species.

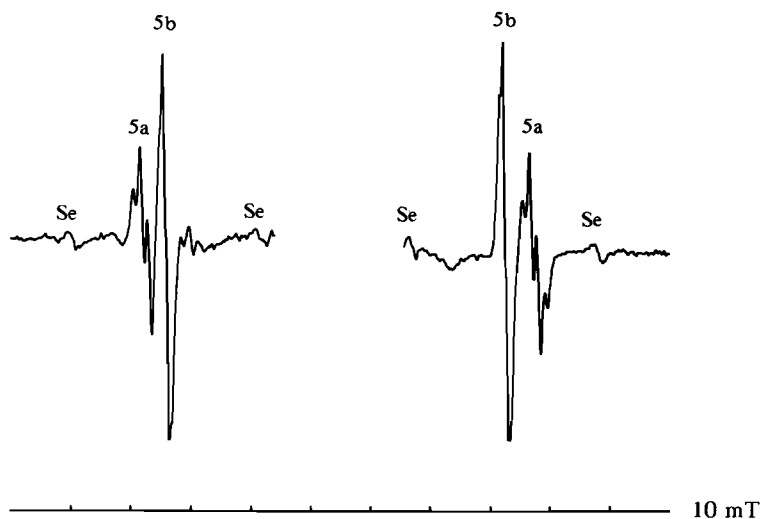**Figure 6.** Single-crystal ESR spectrum of 5a and 5b at 105 K. Magnetic field parallel to c axis.

As for the corresponding sulphide 2a, a single-crystal ESR analysis of 5a and 5b reveals that both radicals possess axially symmetric g and hyperfine tensors (Table V). This must be the consequence of their C_3 symmetry. The parallel features coincide with the PSe bond. The ESR parameters of 5a and 5b indicate that their structures are rather similar. Two substantial differences, however, can be noted. First, the value of $\Delta g_\perp$ ($= g_\perp - g_e$) is much larger for 5b than for 5a. Second, the difference $A_{//} - A_\perp$ (3B) is for 5b (156 MHz) significantly smaller than for 5a (414 MHz). As for 2a the ^{1}H splitting of 5a and 5b results from the *trans* located CH_2 hydrogen atoms.

Table V. g And hyperfine coupling (MHz) tensors for **5a** and **5b**.

Radical	Temperature (K)	Total tensor		Direction cosines		
				a	b	c
5a	105	g	2.014	1	0	0
			2.014	0	1	0
			1.998	0	0	1
		^{31}P	1399	1	0	0
			1399	0	1	0
			1813	0	0	1
		^{77}Se	268	1	0	0
			268	0	1	0
			862	0	0	1
		^{1}H	33		nearly isotropic	
5b	105	g	2.047	1	0	0
			2.047	0	1	0
			2.003	0	0	1
		^{31}P	1423	1	0	0
			1423	0	1	0
			1579	0	0	1
		^{77}Se	319	1	0	0
			319	0	1	0
			865	0	0	1
		^{1}H	15		nearly isotropic	

The signal intensity of **5b** decreases rapidly upon warming, and the radical is irreversibly lost at 205 K. Further warming results in the loss of **5a** at approximately 270 K.

3.6. Tricyclohexylphosphine selenide (6)

Single crystals of tricyclohexylphosphine selenide (6) are colourless well defined plates. No x-ray crystal structure analysis of this compound has been reported.

The ESR spectrum of an x-irradiated single crystal of **6** (Fig. 7) shows the features of an electron capture phosphoranyl radical (**6a**) together with a much weaker spectrum of a second radical product (**6b**). The spectrum of **6a** exhibits additional hyperfine splitting from three ^{1}H nuclei with somewhat different coupling constants. The ^{77}Se satellites of **6a** are well defined for most orientations.
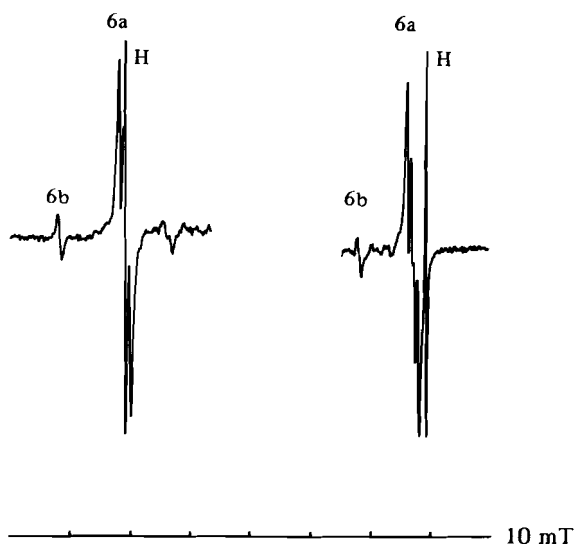
Figure 7. Single-crystal ESR spectrum of **6a** and **6b** at 105 K. Magnetic field parallel to z axis.

The ESR reference y axis was chosen perpendicular to the plate-face and the x and z axes were chosen, with the use of a polarization microscope, coincident with the extinction directions of the crystal perpendicular to y. When the single crystal is mounted with the y axis parallel to the goniometer axis a site splitting for **6a** and **6b** is observed. Coalescence of the differently oriented radicals occurs when the magnetic field direction is parallel to x or z. The results of the single-crystal analysis of **6a** and **6b** are compiled in Table VI. The directions of the largest ^{31}P hyperfine coupling for the two orientations of **6a** are inclined by an angle of 18.0°. This result and the fact that the xz plane appears to be a mirror plane leads to the conclusion that the crystals of **6** are isomorphous with tricyclohexylphosphine sulphide (**3**).[15] The [77]Se coupling of **6a** was found to be nearly parallel to the ^{31}P coupling. Due to the low intensity of the satellites and the small angle between the two orientations an accurate determination of the direction cosines was not possible (Table VI).

The analysis of **6b** reveals that its **g** and ^{31}P hyperfine tensors form an angle of 25.9°. The angle between the two ^{31}P tensors of the two orientations is 33.6°, and they are therefore not directed along the PSe bonds. The assignment of the relation between the two orientations of **6a** and **6b** is not without ambiguity. However, based on the C_s symmetry of the parent molecule, the x-ray analysis of the related sulphide **3** and the results of **4a** and **4b**, it seems likely that the assignment is as shown in Fig. 8. From this it follows that from a single molecule of **6** two phosphorus centred radicals can result with an angle of 25.8° between their principal ^{31}P hyperfine directions.

Table VI. g And hyperfine coupling (MHz) tensors for **6a** and **6b**.

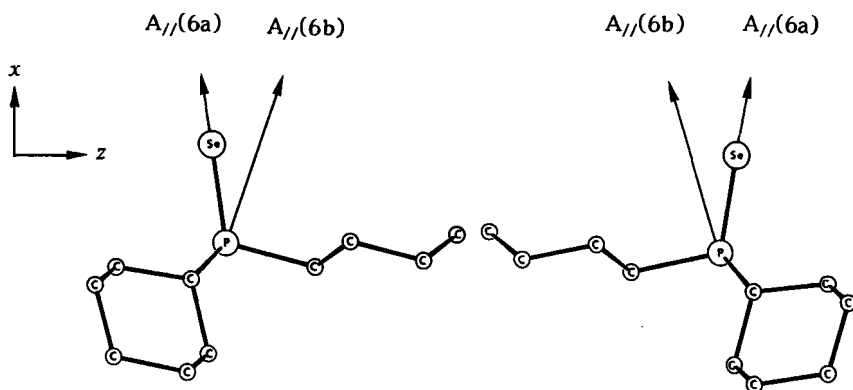| Radical	Temperature (K)	Total tensor		a	b	c
6a	105	g	1.999	0.988	0	± 0.156
			2.031	0	1	0
			2.008	-0.156	0	± 0.988
		^{31}P	1747	0.988	0	± 0.156
			1344	0	1	0
			1332	-0.156	0	± 0.988
		^{77}Se	853	∼ 1	0	0
			199	0	1	0
			225	0	0	∼ 1
		^{1}H	28	nearly isotropic		
6b	105	g	2.006	0.987	0	± 0.158
			2.072	0	1	0
			2.047	-0.158	0	± 0.987
		^{31}P	1562	0.957	0	∓ 0.289
			1424	0	1	0
			1435	-0.289	0	∓ 0.957
		^{1}H		not resolved		

Figure 8. Directions of the principal ^{31}P hyperfine couplings of **6a** and **6b** relative to the x and z axes.

Annealing of the crystal leads to the irreversible loss of **6b** at 140 K and of **6a** at 200 K.

3.7. Triphenylphosphine sulphide (7) and triphenylphoshine selenide (8)

σ* Type radicals of triphenylphosphine sulphide (7) and triphenylphosphine selenide (8) have been reported to be formed in frozen methanolic (7)[2] and sulphuric acid (7, 8)[17] solutions. In sulphuric acid the parent phosphine sulphide and selenide are very likely to be protonated, and the radicals formed are probably Ph$_3\dot{P}$SH and Ph$_3\dot{P}$SeH.

Exposure of powdered samples or single crystals of 7 and 8 to x rays at 77 K does not result in the formation of electron capture phosphoranyl radicals. The same negative result, regarding phosphoranyl radical formation, was reported by Evans et al. for γ irradiation of pure Ph$_3$PS.[2]

4. QUANTUM CHEMICAL CALCULATIONS

In the previous sections it was demonstrated that x irradiation of trialkylphosphine sulphides and selenides at low temperature invariably yields a phosphoranyl radical anion with (approximately) C_3 symmetry. These anions are rather unstable and at temperatures above 200 K their signals irreversibly disappear from the ESR spectra.

Quantum chemical calculations can, in principle, give additional information on the structure of these radicals. It must be born in mind that, in general, these calculations are performed on a single isolated radical and that effects of surrounding molecules in the single–crystal matrix are neglected. Clark has shown, however, that ab initio calculations with a restricted basis set on radical anions can give a good simulation of condensed phase behaviour.[18,19]

4.1. Computational details

The 4-31G(*) open shell calculations were performed as described in chapters 3 and 4. Additionally, hyperfine interactions were computed from the SOMO, neglecting all lower lying α and β MOs.
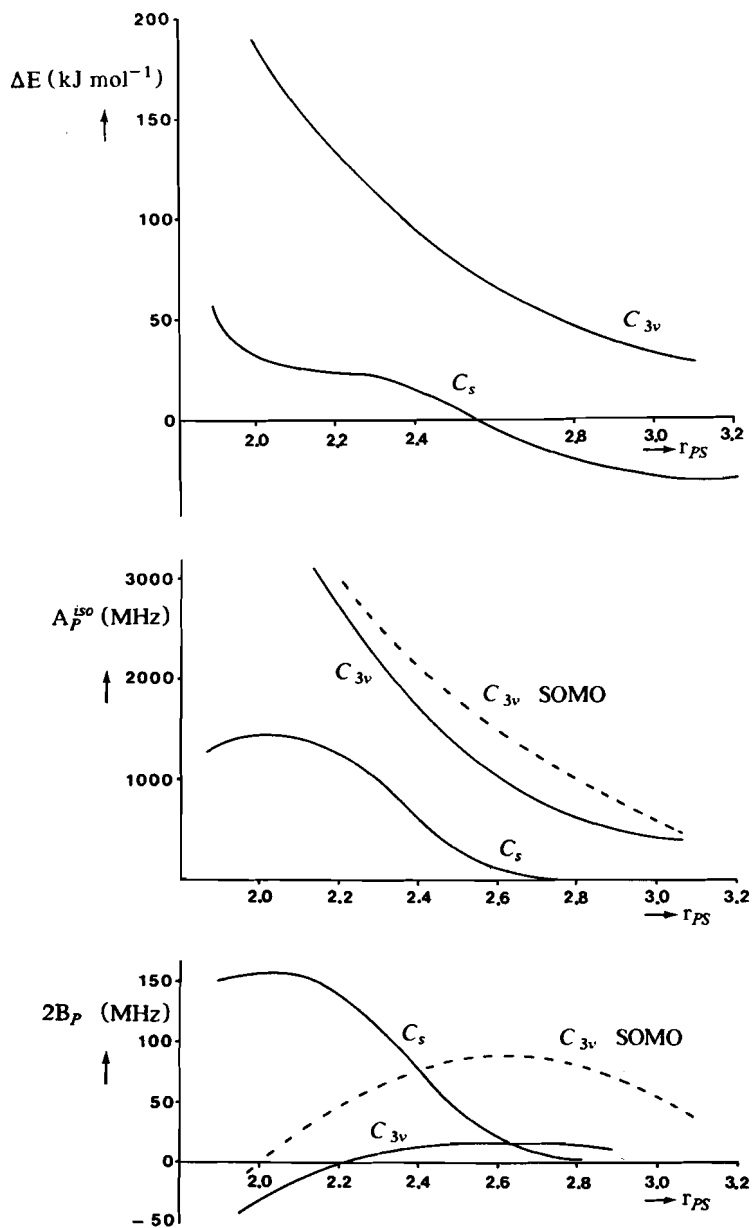
Figure 9. H$_3$ṖS$^-$ radical within C_{3v} and C_s symmetry, 4-31G(*) basis: (a) UHF energy relative to isolated PH$_3$ and S$^-$ in kJ mol^{-1}; (b) Isotropic hyperfine interaction (MHz); (c) Dipolar hyperfine interaction (MHz). Solid lines refer to results after annihilation of the wave function, dashed lines represent results of the SOMO.

4.2. Results of the calculations

Geometry optimization for $H_3\dot{P}S^-$ within C_{3v} symmetry, as a model for the observed radical anions, leads to the dissociation of the three-electron PS bond and results in a neutral PH_3 molecule and S^- radical. Figure 9a shows the potential energy curve of H_3PS^- within C_{3v} and C_s symmetry constraint as a function of the PS distance (r_{PS}). In these calculations all geometric parameters, except r_{PS}, were optimized. The C_s structures are predicted to be significantly lower in energy than the C_{3v} arrangements. After annihilation of the largest spin contaminant all expectation values of the S^2 operator are less than 0.7505.
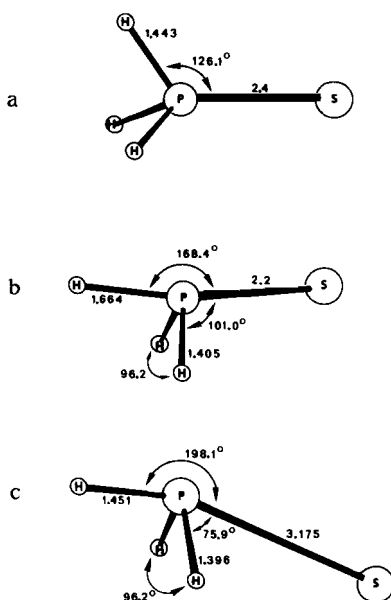

Figure 10. Optimized structures of $H_3\dot{P}S^-$: (a) C_{3v} at $r_{PS} = 2.45$ Å; (b) C_s at $r_{PS} = 2.2$ Å; (c) C_s fully optimized.

The calculated SOMO of the C_{3v} $H_3\dot{P}S^-$ radical anion consists essentially of the phosphorus $3s$ and sulphur $3p_z$ orbitals. Upon elongation of the PS bond, the contribution of the sulphur $3p_z$ orbital increases. Simultaneously a decrease of the spin density in the phosphorus $3s$ orbital, and thus of A_P^{iso} (Fig. 9b) is found. For r_{PS} between 2.4 and 2.5 Å the calculated isotropic coupling (1800-1300 MHz) agrees with the experimental values. The spin density in the phosphorus $3p_z$ orbital is very small, in contrast with the experimental results (Table VII). The small phosphorus $3p_z$ spin density is

reflected in the calculated values of the dipolar hyperfine interaction (Fig. 9c). For the structure with $r_{PS} = 2.45$ Å (Fig. 10a) the calculated value of $2B_P$ (14 MHz) is only a fraction of the experimental values (100-300 MHz). A schematic description of the SOMO for $r_{PS} = 2.4$ Å is shown in Fig. 11a. When the hyperfine couplings are computed from the SOMO alone, and not from the spin-annihilated wave function, increased values of A_P^{iso} and $2B_P$ are predicted. At $r_{PS} = 2.6$ Å the SOMO reveals $A_P^{iso} = 1615$ MHz and $2B_P = 87$ MHz.
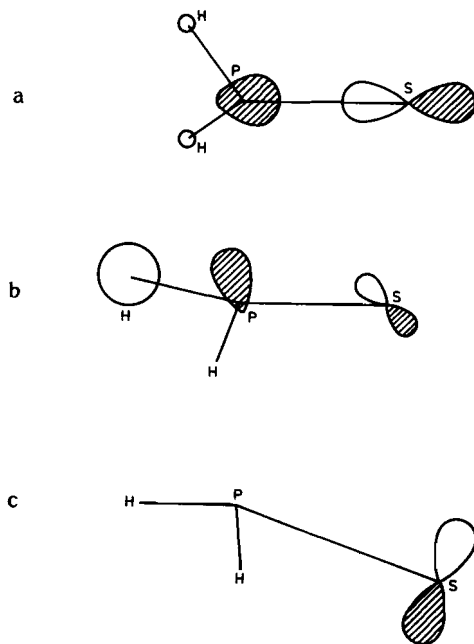

Figure 11. Schematic representation of the SOMOs of the structures in Fig. 10.

Within C_s symmetry two special structures can be noted. At $r_{PS} = 2.2$ Å the potential energy curve reveals a point of inflection and for $r_{PS} = 3.175$ Å a geometry of minimal energy is found. The first structure (Fig. 10b) corresponds to a TBP-e like configuration with large contributions of the central phosphorus nucleus ($A_P^{iso} = 1270$ MHz; $2B_P = 142$ MHz) and the apical sulphur and hydrogen atom. The isotropic and dipolar hyperfine interactions of the second structure (Fig. 10c) indicate that the SOMO is largely confined to a sulphur $3p$ orbital with a small delocalization on the adjacent phosphorus atom. The SOMOs of the two structures are shown in Fig. 11.

The energy of the fully optimized C_s structure of H_3PS^- ($E = -739.15444$ a.u.) lies 30 kJ mol^{-1} below the sum of the energies of isolated PH_3 (C_{3v} optimized:

PH= 1.406 Å, HPH= 94.1°, E= −342.08983 a.u.) and S⁻ (E= −397.05280 a.u.). The total energy of isolated $\dot{P}H_3^+$ (C_{3v} optimized: PH= 1.384 Å, HPH= 112.6 Å, E= −341.77548 a.u.) and S²⁻ (E= −396.70959 a.u.) is very high (1757 kJ mol⁻¹ above C_s H₃$\dot{P}$S⁻), and makes this dissociation route very unfavourable.

The crystal structures of Me₃PS, Et₃PS, Me₃PSe and Et₃PSe reveal that the molecules are oriented with a mutual C_3 axis. The relative orientation of the molecules may prevent a complete dissociation of the trialkylphosphine sulphide and selenide radical anions. In order to test the effect of the crystal matrix on the stability and spin density distribution of these radical anions a STO-3G* calculation on two Me₃PS molecules, of which one is the radical centre, was performed. The molecular parameters were partly set on the experimental values from the crystal structure analysis of Me₃PS.¹² The P-P distance between the two molecules was fixed at the length of the a axis (6.27 Å). This value is close to the corresponding distance in Et₃PS (6.32 Å). The extra electron was assigned to the molecule on the left in Fig. 12. Optimization of the PS and PC bond lengths together with the SPC bond angle of the radical anion in this simulated C_{3v} crystal cavity leads to a stable arrangement (Fig. 12). The optimized values are PS= 2.929 Å, PC= 1.845 Å, and SPC= 120.6°. The unpaired electron in this structure is again largely confined to the sulphur $3p_z$ orbital with a small contribution of the phosphorus $3s$ orbital. A subsequent 4-31G(*) calculation of the magnetic hyperfine interactions of this structure from the wave function reveals A_P^{iso}= 592 MHz and $2B_P$= 25 MHz. The SOMO calculation again results in higher values: A_P^{iso}= 920 MHz and $2B_P$= 112 MHz.
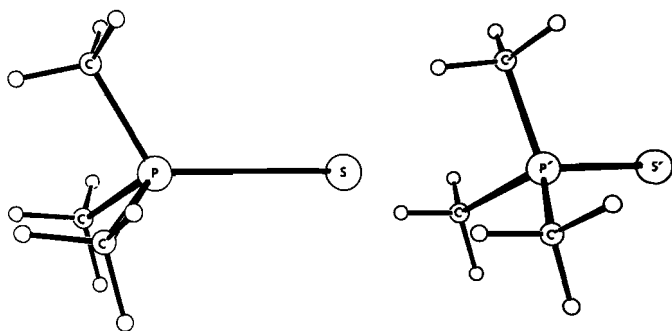

Figure 12. STO-3G* optimized structure for Me₃$\dot{P}$S⁻···Me₃PS. Fixed parameters PP'= 6.27 Å, P'S'= 1.96 Å, P'C'= 1.86 Å, S'P'C'= 113.2°, C'H'= 1.1 Å. Optimized parameters PS= 2.929 Å, PC= 1.845 Å, SPC= 120.6°. E(UHF)= −1695.05959 a.u.

5. DISCUSSION

The ESR experiments show that x irradiation of trialkylphosphine sulphides and selenides at low temperature leads to the formation of the corresponding electron capture radical anions. Table VII comprises the isotropic and anisotropic hyperfine couplings for the studied radicals together with the approximate orbital spin densities.[20] Radicals **1a**, **2a**, **3a**, **4a**, **5a** and **6a** clearly possess a similar spin density distribution. The phosphorus $3s$ contribution lies in the range of 11 to 14%, and 33 to 41% is located in the $3p$ orbital. The unpaired electron density on selenium is approximately 40%, mainly confined to the $4p$ orbital. All radicals show a small spin delocalization on the α hydrogen nuclei of the alkyl groups. The isotropic ^{31}P hyperfine coupling decreases in the series methyl > ethyl > cyclohexyl, and is consequently larger for the sulphide than for the corresponding selenide. The dipolar hyperfine coupling for the methyl derivatives (**1a**, **4a**) is smaller than those of the ethyl and cyclohexyl substituted compounds (**2a**, **3a**, **5a**, **6a**). The ^{31}P and ^{77}Se anisotropic hyperfine couplings are directed along the PS or PSe bonds of the undamaged molecules. The p/s ratio for ^{31}P varies from 2.5 to 3.7.

Table VII. Isotropic and dipolar hyperfine couplings (MHz) and approximate orbital spin densities (%).

Radical	^{31}P				^{77}Se				^{1}H	
	A^{iso}	2B	ρ_s	ρ_p	A^{iso}	2B	ρ_s	ρ_p	A^{iso}	ρ_s
1a	1776	245	13.3	33.3					13	0.9
1b	± 917	∓ 145	± 6.9^a	∓ 19.8^a					13	0.9
2a	1659	284	12.5	38.7					34	2.4
3a	1619	283	12.2	38.6					< 17	1.2
4a	1686	251	12.7	34.2	392	391	1.9	39.8		
4b	1490	134	11.2	18.3					35	2.5
5a	1537	276	11.6	37.6	466	396	2.3	40.2	38	2.7
5b	1475	104	11.1	14.2	501	364	2.5	37.0	15	1.1
6a	1474	300	11.1	40.9	426	427	2.1	43.4	28	2.0
6b	1474	88	11.1	12.0						

^{a} Calculated for valence orbital couplings (see text).

All these structural data lead to the conclusion that the radicals possess a three-electron PS or PSe bond in which the unpaired electron is located in an axial symmetric antibonding σ^* orbital.
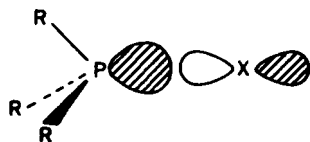
Since the spin densities are not very sensitive to the nature of the irradiated compound, it can be concluded that a matrix effect is not an important factor for the structure of these radicals. Nevertheless, the principal hyperfine couplings and g values reflect, in an elegant way, the symmetry properties of the precursor crystal structures. The complete axial symmetry of the A and g tensors of the radicals 2a and 5a is a result of the hexagonal space group of the crystals of 2 and 5. The radicals 1a, 3a, 4a and 6a originate from the molecules of C_s symmetry. Although the deviation of the geometry of 4 from C_{3v} towards C_s symmetry is very small and the corresponding phosphoranyl radical 4a possesses a principal axis along the PSe bond (near C_3 axis), a very large difference is found for the two perpendicular g values. This must be the result of steric and electronic constraints imposed upon the radical by the surrounding crystal matrix. Similar effects are found for the radicals 1a, 3a and 6a.

Until now no satisfying assignment can be made to the nature of radical 1b. This radical seems to be formed from 1a upon warming and is relatively stable. The single-crystal analysis and powder spectrum of 1b (Fig. 2c) clearly indicate an opposite sign for A^{iso} and B. Because of the relatively large value of the hyperfine coupling, 1b must be a phosphorus centred radical. Furthermore, the presence of additional ^1H splitting and the fact that the principal axis of the A and g tensor are parallel to the PS bond of the precursor molecule lead to the suggestion that the three methyl groups remain covalently bond to the central phosphorus atom. It is unlikely that 1b is a trimethylphosphonium radical cation, since these $R_3\dot{P}^+$ type radicals are known to possess approximately 10% $3s$ and over 90% $3p$ character.[21,22]

The absolute values of A_P^{iso} and B_P of 1b are too large to be the result of spin polarization. Inner-shell polarization could be an explanation, but there is no obvious reason why this should be a dominant effect for 1b. Another possibility is that a negative value of the dipolar hyperfine coupling is the result of $3d$ orbital spin density. The C_{3v} symmetry of 1b restricts the contribution of d-type orbitals to d_{z^2} or to a $d_{x^2}+d_{y^2}$ combination. The first of these two seems most probable, but only a $d_{x^2}+d_{y^2}$ combination can yield a negative value for B_{zz}.[23] Again, there seems to be no compelling reason to justify extensive d orbital participation.

Irradiation of trialkylphosphine selenides generates, besides a σ^* radical (4a, 5a, 6a), a second species (4b, 5b, 6b). The thermal stability of these second radicals is much less than for the σ^* structures and they are quickly lost upon slight annealing. The isotropic hyperfine coupling is somewhat smaller for these structures than for the σ^* radicals. The most striking difference is, however, the low value of the anisotropic hyperfine coupling (2B, Table VII) and the large deviation of $g_\perp$ from the free-electron value. As mentioned before (Section 3.4 and 3.6), radicals 4b and 6b possess an intermediate structure between a σ^* and TBP-e configuration. The formation of only one orientation of radical 4a in a crystal of 4, of at least three possibilities, again emphasizes the subtle effects of matrix interactions.

In contrast to 4b and 6b, 5b possesses an exact C_{3v} symmetry and can therefore not be attributed to a TBP-e structure. In principle 5b could be a TBP-a radical, but the large spin density on selenium (Table VII) argues against this assignment.

Radicals 4b, 5b and 6b are tentatively assigned to σ^*-like structures, although it is not yet fully understood why these structures exhibit a small anisotropic phosphorus

hyperfine coupling.

It is possible to analyse the large difference in $\Delta g_\perp$ for **5a** and **5b** in some detail. The g shifts of these C_{3v} radicals arise from the admixture of excited states with the ground state of the radicals. The positive value of $\Delta g_\perp$ indicates that the induced mixing of the ground state $|0>$ with an excited state $|n>$ involves a transfer of one of the paired electrons of a filled e orbital into a half-filled a_1 orbital. If only the valence orbitals of phosphorus and selenium are considered, the orbitals involved in a calculation of the g tensor are

$$|a_1> = c_{3s}(P)\phi_{3s}^P + c_{3p_z}(P)\phi_{3p_z}^P + c_{4s}(Se)\phi_{4s}^{Se} + c_{4p_z}(Se)\phi_{4p_z}^{Se} \qquad 7.1$$

$$|e> = \begin{vmatrix} c_{3p_x}(P)\phi_{3p_x}^P + c_{4p_x}(Se)\phi_{4p_x}^{Se} \\ c_{3p_y}(P)\phi_{3p_y}^P + c_{4p_y}(Se)\phi_{4p_y}^{Se} \end{vmatrix} \qquad 7.2$$

By first order perturbation theory the $\Delta g_\perp$ $(=\Delta g_{xx} = \Delta g_{yy})$ and $\Delta g_{//}$ $(=\Delta g_{zz})$ values are easily obtained.[24]

$$\Delta g_\perp = \frac{2[c_{3p_z}(P)c_{3p_y}(P) + c_{4p_z}(Se)c_{4p_y}(Se)][c_{3p_z}(P)c_{3p_y}(P)\zeta_P + c_{4p_z}(Se)c_{4p_y}(Se)\zeta_{Se}]}{E_n - E_0} \qquad 7.3$$

$$\Delta g_{//} = 0 \qquad 7.4$$

where $E_n - E_0$ is the (positive) energy difference between the two states and ζ_P $(=299$ cm$^{-1})$ and ζ_{Se} $(=1688$ cm$^{-1})$ are the spin-orbit coupling constants. The orbital populations of the SOMO of **5a** and **5b** indicate that $c_{4p_z}(Se)$ is approximately equal for both radicals and that $c_{3p_z}(P)$ is smaller for **5b** than for **5a**. The large value of $\Delta g_\perp$ for **5b** must therefore originate from an increase of $c_{4p_x}(Se)$ and $c_{4p_y}(Se)$ or a decrease of $E_n - E_0$.

In general the quantum chemical calculations do not reproduce the experimental hyperfine couplings. The computed couplings from the SOMO show a better agreement with the experimental values than those from the spin-annihilated wave function. The calculations reveal that, within C_{3v} symmetry, the three-electron PS bond is not stable. Clark has pointed out that the stability of a three-electron bond is closely related to the energy for the transfer of a single electron between the two species forming the bond.[25] The calculated single-electron transfer energy ΔE_{SET} at HF/4-31G* level reveals that the combination $PH_3 + S^-$ is favoured over $\dot{P}H_3^+ + S^{2-}$ by 1727 kJ mol^{-1}.[26] It is clear that this large value of ΔE_{SET} results in a low value of the three-electron bond dissociation energy.

Although the calculated and experimental value of ΔE_{SET} clearly favours a $[H_3P \cdots \dot{S}]^-$ arrangement with the unpaired electron density mainly on sulphur, the experimental spin density distribution indicates a large delocalization on the phosphorus nucleus and thus a $[R_3P \therefore S]^-$ structure. It is somewhat strange, however, that

upon annealing no dissociation from $R_3\dot{P}S^-$ σ^* radicals into $R_3\dot{P}^+$ radicals is observed, since rupture of a three-electron bond has been established for other σ^* radicals.[27]

A possible way by which $R_3\dot{P}S^-$ σ^* radicals could be stabilized is the presence of a nearby radical cation, shielding the negative charge on sulphur. Recent calculations by Gonbeau et al. nevertheless predict that a tetrahedral configuration of $H_3\dot{P}SH$ is unstable and results in an immediate elongation of the bond, leading to rupture.[28] In case a second proton is added to the sulphur atom ($H_3PSH_2^+$), a stable three-electron bond has been calculated.[25]

REFERENCES

1. A. Begum and M.C.R. Symons, J. Chem. Soc., Faraday Trans. 2, 69, 43 (1973).

2. J.C. Evans, S.P. Mishra and C.C. Rowlands, Chem. Phys. Lett., 72, 168 (1980).

3. M. Geoffroy, A. Llinares and E. Krzywanska, J. Magn. Reson., 58, 389 (1984).

4. T.A. Albright, W.J. Freeman and E.E. Schweizer, J. Org. Chem., 40, 3437 (1975).

5. R.R. Carlson and D.W. Meek, Inorg. Chem., 13, 1741 (1973).

6. M.W. Schmidt and M.S. Gordon, J. Am. Chem. Soc., 107, 1922 (1985).

7. J.E. Huhee, Inorganic Chemistry: Principles of Structure and Reactivity (Harper and Row, New York, 1978) p. 839-851.

8. E.N. Tsvetkov, T.A. Chepaikina and M.I. Kabachnik, Izv. Akad. Nauk SSSR, Ser. Khim., 426 (1979).

9. K. Issleib and A. Brach, Z. Anorg. Allg. Chem., 277, 258 (1954).

10. R.R. Renshaw and K.F. Bell, J. Am. Chem. Soc., 43, 916 (1921).

11. R.A. Zingara and R.E. McGlothlin, J. Org. Chem., 26, 5205 (1961).

12. P.G. Eller and P.W.R. Corfield, Chem. Commun., 105 (1971).

13. A. Cogne, A. Grand, J. Laugier, J.B. Robert and L. Wiesenfeld, J. Am. Chem. Soc., 102, 2238 (1980).

14. M. van Meersche and A. Léonard, Bull. Soc. Chim. Belg., 68, 683 (1959).

15. K.A. Kerr, P.M. Boorman, B.S. Misner and J.G.H. van Roode, Can. J. Chem., 55, 3081 (1977).

16. M. van Meersche and A. Léonard, Acta Cryst., 12, 1053 (1959).

17. G.W. Eastland and M.C.R. Symons, J. Chem. Soc., Faraday Trans. 2, 73, 833 (1977).

18. T. Clark, J. Chem. Soc., Chem. Commun., 93 (1984).

19. T. Clark, Faraday Discuss. Chem. Soc., 78, 203 (1984).

20. J.R. Morton and K.F. Preston, J. Magn. Reson., **30**, 577 (1978).

21. A. Hasegawa, G.D.G. McConnachie and M.C.R. Symons, J. Chem. Soc., Faraday Trans. 1, **80**, 1005 (1984).

22. M.C.R. Symons and G.D.G. McConnachie, J. Chem. Soc., Chem. Commun., 851 (1982).

23. W. Weltner, *Magnetic Atoms and Molecules* (Scientific and Academic Editions, New York, 1983).

24. P.W. Atkins and M.C.R. Symons, *The Structure of Inorganic Radicals* (Elsevier, Amsterdam, 1967).

25. T. Clark, J. Comput. Chem., **4**, 404 (1983).

26. An experimental estimate of ΔE_{SET} (1360 kJ mol^{-1}) can be obtained from the ionization potential of PMe$_3$ (828 kJ mol^{-1}, 8.60 eV, Disc. Faraday Soc., **35**, 232 (1963)) and the electron affinity of S$^-$ (532 kJ mol^{-1}, C. Chambers and A.K. Holliday, *Inorganic Chemistry* (Butterworth Scientific, London, 1982)).

27. R.A.J. Janssen, M.H.W. Sonnemans and H.M. Buck, J. Am. Chem. Soc., **108**, 6145 (1986). Chapter 5.

28. D. Gonbeau, M.-F. Guimon, J. Ollivier and G. Pfister-Guillouzo, J. Am. Chem. Soc., **108**, 4760 (1986).

CHAPTER 8

General Discussion

1. INTRODUCTION

The preceeding chapters have shown that electron capture of four-coordinated phosphorus compounds can result in a number of different radical structures. From a hypothetical compound $A_3P=B$ two different TBP-e and two different σ^* structures can result after electron addition (Fig. 1).
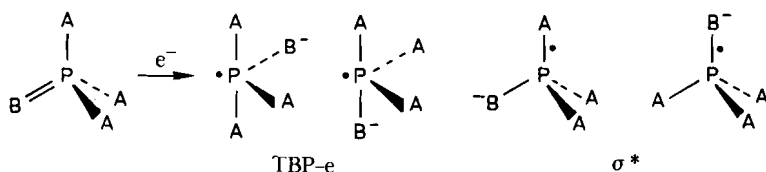
Figure 1. Possible TBP-e and σ^* structures for $A_3\overset{.}{P}B^-$ radicals.

The formation and spin density distribution of all four configurations has been established in chapters 4 to 7. The analysis of these structures reveals that they are more or less intermediate between pure TBP-e and pure σ^*. From this it can be concluded that likely a continuum of configurations between the TBP-e and σ^* extremes exists. Before the factors that rule the specific formation of a TBP-e or a σ^* structure can be discussed, it is instructive to get a more detailled understanding of a σ^* configuration.

2. σ^* CONFIGURATIONS

It has been argued by various authors that a three-electron two-centre bond, which contains two bonding σ electrons and one antibonding σ^* electron, is significantly stabilized when the energy levels of the two species forming the bond are (nearly) degenerate (Fig. 2a).[1-3] This is reflected in the relatively large amount of symmetrical three-

electron bond radicals which are known experimentally. The formation of a stable three–electron bond is not restricted to higher row atoms with possible d orbital participation, e.g. various $R_3N\dot{\cdot}NR_3^+$ radicals have spectroscopically been identified.[4,5] Ab initio quantum chemical calculations on symmetrical σ^* configurations invariably predict a stable three–electron bond.[6-8] The energy match requirement appears also in a valence bond (VB) description of a three–electron bond between atoms A and B. A large contribution to resonance stabilization will occur if the the structures $A\dot{:}$ $\cdot B$ and $A\cdot$ $\dot{:}B$ are of (almost) equal energy.

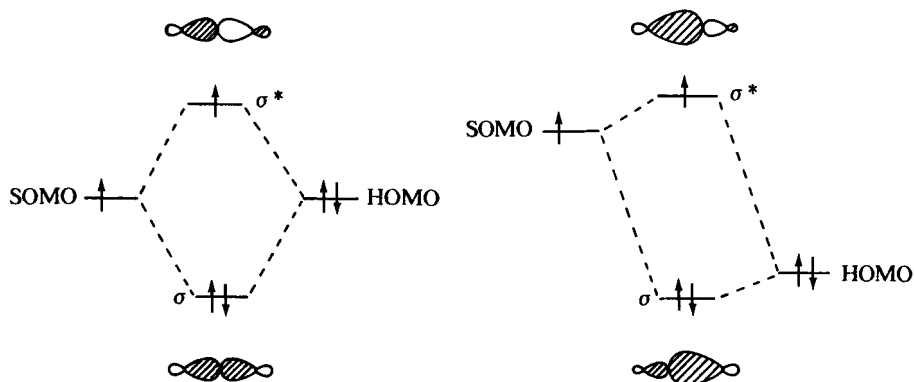Figure 2. σ^* Bonds in symmetric (a) and asymmetric (b) radicals.

Asymmetric three–electron bonds are less familiar in free radical chemistry. The asymmetry of the radical is likely to yield different energy levels for the overlapping singly occupied molecular orbital (SOMO) and highest occupied molecular orbital (HOMO) of the two constituents (Fig. 2b). Since the stabilization due to three–electron (HOMO-SOMO) interactions falls off rapidly with increasing energy gap,[8] an asymmetric σ^* configuration is expected to be less stable.

Nevertheless, three–electron bond phosphoranyl radicals between a phosphorus moiety R_3P and a substituent group X are identified for a variety of substituents X. In chapters 4, 5 and 7, single–crystal ESR evidence has been provided for the formation of $R_2P(S)\dot{\cdot}P(S)R_2^-$, $(R_2N)_2P(S)\dot{\cdot}Cl^-$, $R_3P\dot{\cdot}S^-$ and $R_3P\dot{\cdot}Se^-$ three–electron bond configurations. Additional σ^* structures have been described in literature for $R_3P\dot{\cdot}PR_3^+$,[9] $(RO)_3P\dot{\cdot}P(OR)_3^+$,[10] $(MeO)_2P(S)\dot{\cdot}Br^-$,[11] $R_3P\dot{\cdot}Cl$,[12,13] and $Me_3P\dot{\cdot}SMe$[14] on basis of single–crystal, polyoriented or liquid phase ESR. It is noteworthy that no examples of a σ^* structure between phosphorus and a first row element are known.

Quantum chemical methods subjected to σ^* phosphoranyl radicals only reveal stable three–electron bonds and reproduce the experimental spin density distribution for symmetric radicals as $H_3P\dot{\cdot}PH_3^+$ and $H_2P(S)\dot{\cdot}P(S)H_2^-$.[8,15] On the other hand these calculations are releatively unsuccessful when asymmetric σ^* configurations are considered. The only asymmetric phosphoranyl radical predicted by ab initio quantum chemical

calculations to possess a stable three-electron bond is $H_3P \dot{\cdot} SH_2^{\dot{+}}$.[8] Unfortunately no experimental analogue of this radical has been reported. In contrast, for the radicals $Me_3P \dot{\cdot} SMe$, $Me_3P \dot{\cdot} SH$ and $R_3P \dot{\cdot} S^-$, which have been detected by ESR spectroscopy, calculations conducted by Gonbeau et al.[16] on the model $H_3P \dot{\cdot} SH$ and those presented in chapter 7 on $H_3P \dot{\cdot} S^-$ reveal an immediate rupture of the PS bond. Furthermore, the calculated dipolar hyperfine coupling is not well reproduced, even for a range of PS distances. Another example where theory and experiment diverge is found for the $R_3P \dot{\cdot} Cl$ phosphoranyl radicals. The well known Ph_3P-Cl radical possesses a near perfect σ^* structure and ESR studies on polyoriented systems have shown that e.g. $Me_3P \dot{\cdot} Cl$ radicals can be formed in $Me_3PCl^+Cl^-$ salts.[12,13] The calculations presented in chapter 2 on $H_3P \dot{\cdot} Cl$ reveal only a shallow minimum (8.6 kJ mol^{-1}) at a PCl distance of 3.21 Å, which essentially represents a chlorine atom and a neutral PH_3 molecule, and not the experimentally observed σ^* P$\dot{\cdot}$Cl configuration.

Summarizing, it appears that that UHF calculations overemphasize the energy match requirement of HOMO and SOMO discussed above. The deviations from the experimental spin density distribution and stability cannot be completely contributed to matrix interactions or solvation, which are neglected in the calculations. Clark, who encountered the same problem for $H_2S \dot{\cdot} X$ radicals (X= Cl, SH), suggested that the spin density distribution may be considerably changed if the $\sigma^1 \sigma^{*2}$ state contributes significantly to the correlated wave function.[7,8] However, no quantitative accessment to its importance was made. A satisfactorily theoretical analysis is probably only possible with a full configuration interaction and an appropriate description of the crystal matrix.

In VB terms the stabilization of an asymmetric three-electron bond can be understood if the interaction element between the A$\dot{\cdot}$ ·B and A· :B resonance structures is large. In such a case the resulting structure can be intermediate even when there is a considerable energy difference between the two limiting configurations.

3. TBP-e VERSUS σ^*

The formation of a specific structure, TBP-e or σ^*, is determined by the nature of the substituents around phosphorus, the geometry of the precursor, and, although less quantitatively described, the presence and symmetry of the single-crystal matrix. In chapters 5 and 6 it has been argued that the P-substituent bond energy and the substituent electron affinity are key factors in the formation of σ^* or TBP-e structures. Hypervalent-bonding MO concepts place the extra electron in a molecular orbital which possesses substantial antibonding character. This antibonding orbital extends for a TBP-e radical over phosphorus and the two apical ligands. A σ^* phosphoranyl radical possesses a SOMO with a single nodal plane between phosphorus and the unique substituent. The introduction of an antibonding component results in a weakening and elongation of the the bond. In VB terms important stabilization can be acquired from the contribution of the following structure:

R
\
P• :X
R /
R
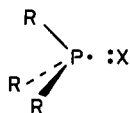
Hence, it can be expected that the preferred structure adopted by a phosphoranyl radical will depend on the relative ease of dissociation of the P-ligand bonds (PX) and on the energy required for the redistribution of charge. Parameters involved in this process are the homolytic bond dissociation energy, the electron affinity of the ligand and the ionization potential of the phosphorus moiety. The impact of these parameters, for all four substituents, results in a structure of minimal energy. Particularly, a σ^* structure can be expected if one P-ligand bond accommodates the extra electron appreciably better than the remaining three bonds. Alternatively, if two ligands with equal delocalizing properties are present, a TBP-e structure will be formed.

The experiments described in chapter 4 on tetraethyldiphosphine disulphide reveal that three different phosphoranyl radical configurations (2a, 2b, and 2c) are formed simultaneously. This indicates that the energy differences between these structures are small. It can be expected that subtle steric and electronic effects in the crystal matrix modulate the relative energies of the different configurations. Moreover, stabilization of an electron capture phosphoranyl radical will occur only if relaxation of the molecular geometry of the precursor to a structure of minimum energy is possible. Hence, the formation will depend on steric properties of the molecules and of the surrounding matrix. This is confirmed by the experiments described in chapter 4 and 7.

REFERENCES

1. N.T. Anh and C. Minot, J. Am. Chem. Soc., **102**, 103 (1980).
2. N.C. Baird, J. Chem. Educ., **54**, 291 (1977).
3. M. Göbl, M. Bonifačić and K.-D. Asmus, J. Am. Chem. Soc., **106**, 5984 (1984).
4. N. Ganghi, J.L. Wyatt and M.C.R. Symons, J. Chem. Soc., Chem. Commun., 1424 (1986).
5. B. Kirste, R.W. Alder, R.B. Sessions, M. Bock, H. Kurreck and S.F. Nelsen, J. Am. Chem. Soc., **107**, 2635 (1985).
6. W.J. Bouma and L. Radom, J. Am. Chem. Soc., **107**, 345 (1985).
7. T. Clark, J. Comput. Chem., **3**, 112 (1982).
8. T. Clark, J. Comput. Chem., **4**, 404 (1983).
9. A.R. Lyons and M.C.R. Symons, J. Chem. Soc., Faraday Trans. 2, **68**, 1589 (1972).
10. T. Gillbro, C.M.L. Kerr and F. Williams, Mol. Phys., **28**, 1225 (1974).

11. M.C.R. Symons, Chem. Phys. Lett., **40**, 226 (1976).

12. T. Berclaz, M. Geoffroy and E.A.C. Lucken, Chem. Phys. Lett., **36**, 677 (1975).

13. M.C.R. Symons and R.L. Petersen, J. Chem. Soc., Faraday Trans. 2, **75**, 210 (1979).

14. J.R.M. Giles ánd B.P. Roberts, J. Chem. Soc., Perkin Trans. 2, 1211 (1981).

15. R.A.J. Janssen. M.H.W. Sonnemans and H.M. Buck, J. Chem. Phys., **84**, 3694 (1986). Chapter 4.

16. D. Gonbeau, M.-F. Guimon, J. Ollivier and G. Pfister-Guillouzo, J. Am. Chem. Soc., **108**, 4760 (1986).

SUMMARY

This thesis describes an experimental single-crystal ESR and a quantum chemical study of phosphoranyl radicals ($\dot{P}R_4$). Phosphoranyl radicals can be generated by x-ray induced electron capture of four-coordinated phosphorus compounds. These radicals can adopt a variety of configurations depending on the distribution of the unpaired electron and the geometry of the radical. After electron capture of the precursor the radical can adopt a trigonal bipyramidal (TBP) structure with the unpaired electron in an equatorial location (TBP-e) or in an apical position (TBP-a). Alternatively, the orginal tetrahedral geometry can be preserved leading to a $\sigma*$ configuration in which the unpaired electron is part of a two-centre three-electron bond.

In chapter 2, the electronic structure of C_{3v} phosphoranyl ($\dot{P}R_4$) and C_{4v} phosphorane anion ($\dot{P}R_5^-$) radicals is described by quantum chemical methods. From the calculations it is concluded that the angle between the unique substituent in the C_3 or C_4 axis and the three or four remaining substituents is decisive for the choice between TBP-a and C_{3v} $\sigma*$ or between octahedral (O_h) and C_{4v} $\sigma*$. In case this angle is less than $100°$ a TBP-a or O_h structure is expected, for angles larger than $100°$ a C_{3v} or C_{4v} $\sigma*$ configuration prevails.

Ab initio calculations of isotropic and anisotropic hyperfine interactions are given in chapter 3. The results of the calculations are in good agreement with experimental values. A new aspect of the structure of phosphoranyl radicals is established, i.e. the dipolar hyperfine coupling of the ligands does not coincide with the phosphorus–ligand linkage. This precludes an exact determination of the geometry of a radical from the experimental couplings.

Chapter 4 describes the ESR study of electron capture phosphoranyl radicals in single crystals of substituted diphosphine disulphides [$R_2P(S)$-$P(S)R_2$, R= Me, Et, Ph]. It is shown that in all three compounds a three-electron P-P bond is formed. The unpaired electron is found to be symmetrically distributed over the two phosphorus atoms. The alkyl substituted diphosphine disulphides reveal furthermore a radical in which the unpaired electron is asymmetrically distributed over the two phosphorus atoms in a TBP-e configuration with apical locations for the second phosphorus nucleus and sulphur. Irradiation yields for R= Et and Ph also a three-electron P-S bond radical and a number of dissociation products. Quantum chemical calculations of the isotropic and anisotropic hyperfine couplings are in good agreement with the experimental values and clearly show the antibonding nature of the singly occupied molecular orbital (SOMO).

An example of the strong dependence of the radical structure on the nature of the ligands is presented in chapter 5. A low-temperature single-crystal ESR study on $(R_2N)_2\dot{P}(S)Cl^-$ and $(R_2N)_2\dot{P}(S)F^-$ radicals reveals the formation of a $\sigma*$ and a TBP-e configuration, respectively. The explanation for this striking difference lies in the antibonding nature of the SOMO, which favours electron delocalization on relatively weakly bound ligands with a high electron affinity. The experiments reveal that on

119

warming, the P-Cl $\sigma *$ bond dissociates in the single-crystal matrix via an in-line mode.

Experiments and calculations on the $\dot{S}PCl_2F^-$ radical, described in Chapter 6, lead to a deformed TBP-e structure in which two chlorine nuclei occupy the apical site and fluorine is in an equatorial position. The reversed apicophilicity of fluorine and chlorine with respect to five-coordinated phosphoranes is a direct result of the anti-bonding nature of the SOMO of this TBP-e radical.

Chapter 7 describes a single-crystal ESR study on various trialkylphosphine sulphide and selenide electron addition radicals. The unpaired electron resides in a $\sigma *$ P$\doteq$S or $\sigma *$ P$\doteq$Se bond. The ^{77}Se isotope gives access to the spin density on selenium. The experiments reveal the subtle effects of the symmetry of the single-crystal matrix on the ESR parameters. Quantum chemical calculations on $H_3\dot{P}S^-$ do not reproduce the experimental couplings accurately and predict an immediate rupture of the three-electron P-S bond in H_3P and S^-.

In chapter 8, the experimental and theoretical results of the preceeding chapters are discussed. It is argued that a continuum of configurations between the TBP-e, TBP-a and $\sigma *$ structures exists. The nature of the ligands, and to some extend the single-crystal matrix, determines the structure of a phosphoranyl radical. If the tendency of one substituent to contribute to the electron delocalization of the extra electron is appreciably larger than for the other three, a $\sigma *$ bond can be expected. If, however, two substituents with equal delocalizing properties are present a TBP-e structure is expected.

SAMENVATTING

Dit proefschrift beschrijft een experimentele éénkristal ESR en een kwantum-chemische studie aan fosforanylradikalen ($\dot{P}R_4$). Fosforanylradikalen kunnen gegenereerd worden onder invloed van Röntgenstraling door electron-capture van viergekoordineerde fosforverbindingen. Deze radikalen kunnen verschillende konfiguraties aannemen afhankelijk van de verdeling van het ongepaarde elektron en de geometrie van het radikaal. Na electron-capture van de precursor kan het radikaal een trigonale bipyramidale struktuur (TBP) aannemen waarin het ongepaarde elektron in een equatoriale positie (TBP-e) of in een apikale positie (TBP-a) gelokaliseerd is. Daarnaast is het mogelijk dat de tetraedrische geometrie behouden blijft en een $\sigma *$ konfiguratie gevormd wordt, waarin het ongepaarde elektron deel uitmaakt van een twee-center drie-elektron binding.

In hoofdstuk 2 wordt de elektronische struktuur van C_{3v} fosforanyl- ($\dot{P}R_4$) en C_{4v} fosforaananionradikalen ($\dot{P}R_5^-$) beschreven met behulp van kwantumchemische methodieken. Uit de berekeningen wordt gekonkludeerd dat de hoek tussen de substituent in de C_3- of C_4-as en de drie of vier resterende substituenten bepalend is voor de keuze tussen TBP-a en C_{3v} $\sigma *$ of tussen octaedrisch (O_h) en C_{4v} $\sigma *$. Als deze hoek kleiner dan 100° is, wordt een TBP-a of O_h struktuur verwacht, voor hoeken groter dan 100° is een C_{3v} of C_{4v} $\sigma *$ konfiguratie gunstiger.

Ab initio berekeningen van isotrope en anisotrope hyperfijninterakties worden beschreven in hoofdstuk 3. De resultaten van de berekeningen stemmen goed overeen met experimentele waarden. Een nieuw aspect van de struktuur van fosforanylradikalen wordt vastgesteld, namelijk, de dipolaire hyperfijnkoppeling van de liganden valt niet samen met de fosfor-ligand binding. Dit verhindert een exacte bepaling van de geometrie van een radikaal met behulp van de experimentele koppelingen.

Hoofdstuk 4 beschrijft de ESR studie van electron-capture fosforanylradikalen in éénkristallen van gesubstitueerde difosfinedisulfides [$R_2P(S)-P(S)R_2$, R= Me, Et, Ph]. Het blijkt dat in deze verbindingen steeds een radikaal met een drie-elektron P-P binding gevormd wordt. Het ongepaarde elektron blijkt symmetrisch verdeeld te zijn over de twee fosforatomen. De alkyl-gesubstitueerde difosfinedisulfides geven bovendien een radikaal waarin het ongepaarde elektron asymmetrisch verdeeld is over de twee fosforatomen in een TBP-e konfiguratie met een apikale positie voor de tweede fosforkern en zwavel. Bestraling leidt voor R= Et en Ph ook tot een drie-elektron P-S binding en een aantal dissociatieprodukten. Een kwantumchemische berekening van de isotrope en anisotrope hyperfijnkoppelingen stemt goed overeen met de experimentele waarden en bevestigt het antibindend karakter van de enkelbezette moleculaire orbitaal (SOMO).

Een voorbeeld van de sterke invloed van de aard van de liganden op de radikaal-struktuur wordt gegeven in hoofdstuk 5. Een lage-temperatuur éénkristal ESR studie aan $(R_2N)_2\dot{P}(S)Cl^-$ en $(R_2N)_2\dot{P}(S)F^-$ radikalen toont de vorming van respektievelijk een $\sigma *$ en een TBP-e konfiguratie. De verklaring voor dit opvallende verschil ligt in het antibindende karakter van de SOMO, die elektrondelokalisatie op relatief zwak gebonden

liganden met een hoge elektronenaffiniteit bevoordeeld. De experimenten laten zien dat bij het verhogen van de temperatuur de P-Cl σ* binding in de éénkristalmatrix dissocieert via een in-line proces.

Experimenten en berekeningen aan het $\overset{.}{S}PCl_2F^-$ radikaal, beschreven in hoofdstuk 6, tonen een gedeformeerde TBP-e struktuur waarin twee chloorkernen de apikale positie innemen en fluor een equatoriale positie. De veranderde voorkeur voor de apikale positie van fluor en chloor ten opzichte van vijfgekoordineerde fosforanen is het gevolg van het antibindend karakter van de SOMO van dit TBP-e radikaal.

Hoofdstuk 7 beschrijft een éénkristal ESR studie aan verschillende trialkylfosfine-sulfide en -selenide elektronadditie-radikalen. Het ongepaarde elektron bevindt zich in een σ* P$\overset{.}{-}$S of een σ* P$\overset{.}{-}$Se binding. De ^{77}Se isotoop geeft de mogelijkheid om de spin-dichtheid op seleen te bepalen. Het blijkt dat ongeveer gelijke ongepaarde elektronen-dichtheid op fosfor en seleen aanwezig is. De experimenten tonen de subtiele effekten van de symmetrie van de éénkristalmatrix op de ESR-parameters. Kwantumchemische berekeningen aan $H_3\overset{.}{P}S^-$ geven geen nauwkeurige beschrijving van de experimentele koppelingen en voorspellen een verbreking van de drie-elektron P-S binding in H_3P en $S^{\overset{.}{-}}$.

In hoofdstuk 8 worden de experimentele en theoretische resultaten van de voorafgaande hoofdstukken besproken. Het blijkt dat een reeks van konfiguraties tussen TBP-e, TBP-a en σ* strukturen bestaat. De aard van de liganden, en tot op een bepaalde hoogte de éénkristalmatrix, bepaalt de struktuur van een fosforanylradikaal. Als één ligand duidelijk beter bijdraagt aan de delokalisatie van het ongepaarde elektron dan de overige drie kan een σ* struktuur verwacht worden. Als twee substituenten met gelijke delokalisatiemogelijkheden aanwezig zijn, wordt een TBP-e struktuur verwacht.

CURRICULUM VITAE

van René Janssen, geboren op 25 juni 1959

Na het behalen van het atheneum-B diploma aan het Bisschoppelijk College Broekhin te Roermond in 1977, begon ik in datzelfde jaar met de studie voor scheikundig ingenieur aan de Technische Hogeschool Eindhoven. In november 1981 werd mij de Unilever chemieprijs toegekend. Het afstudeerwerk werd verricht bij de vakgroep Organische Chemie. In januari 1983 werd het ingenieursexamen met lof afgelegd.

Het onderzoek, zoals dat in dit proefschrift beschreven is, werd gestart in februari 1983 en stond onder leiding van prof. dr. H.M. Buck. Van 1 februari 1983 tot 1 oktober 1984 was ik in dienst van de Nederlandse Organisatie voor Zuiver Wetenschappelijk Onderzoek. Sinds 1 oktober 1984 ben ik als universitair docent in dienst van de Technische Universiteit Eindhoven en werkzaam bij de vakgroep Organische Chemie.

NAWOORD

Aan het totstandkomen van dit proefschrift hebben velen een bijdrage geleverd. Voor alle adviezen en assistentie op theoretisch, synthetisch en technisch gebied ben ik zeer erkentelijk.

Bijzonder veel dank ben ik verschuldigd aan mijn afstudeerders ir. Max Sonnemans en ir. Joost Kingma voor hun inzet en inzicht bij het uitvoeren van de experimenten en berekeningen. De vele discussies met hen zijn steeds een bron van nieuwe ideeën en inzichten geweest. Daarnaast wil ik de prettige samenwerking noemen met de kollega's van de vakgroep, in het bijzonder dr. ir. Leo Koole, ir. Marcel van Genderen en ir. Do Dormans. Hun belangstelling voor het promotieonderzoek is steeds een belangrijke steun voor mij geweest.

De vele tekeningen in dit proefschrift en de lay-out werden verzorgd door Henk Eding.

Stellingen

1. De vaststelling van Symons dat in het radikaalkation van tetramethylureum een geringe delokalisatie van het ongepaarde elektron op de carbonylgroep aanwezig is, lijkt een bevestiging voor de door hem onwaarschijnlijk geachte parallelle orientatie van de carbonylgroep en de enkelbezette orbitaal op stikstof.

   M.C.R. Symons, J. Chem. Soc., Chem. Commun., 11 (1986).

2. De conclusies die door Hess et al. worden getrokken met betrekking tot de theoretische voorspelling van het kinetisch isotoopeffekt in thermische [1,5]H-shifts in pentadieen worden in belangrijke mate bepaald door de beperkingen van het gehanteerde model.

   B.A. Hess, Jr., L.J. Schaad en J. Pancir̆, J. Am. Chem. Soc., **107**, 149 (1985).

3. Bij de studie naar de stereochemie van thiofosforyloverdrachtsreakties door Cullis en Iagrossi dient opgemerkt te worden dat een mechanistische beschrijving op basis van een kortlevende vijfgekoördineerde fosforstruktuur waarin pseudorotatie plaatsvindt, een goed alternatief is voor het voorgestelde mechanisme waarin het thiometafosfaatanion als intermediair optreedt.

   P.M. Cullis en A. Iagrossi, J. Am. Chem. Soc., **108**, 7870 (1986).

4. De conclusie van Niecke et al. dat de vier fosforatomen in het radikaalkation van tetrakis(diisopropylamino)cyclotetrafosfine sterk gepyramidaliseerd zijn, kan niet in overeenstemming zijn met een fosforkoppeling van slechts 5 Gauss in het ESR spektrum van dit radikaal.

   H.-G. Schäfer, W.W. Schoeller, J. Niemann, W. Haug, T. Dabisch en E. Niecke, J. Am. Chem. Soc., **108**, 7481 (1986).

5. De bewering van Glidewell dat bij een kwantumchemische berekening van isotrope hyperfijnkoppelingskonstanten geen matrixeffekten worden verrekend is geen afdoende verklaring voor de discrepantie van zijn berekeningen en experimentele gegevens.

   C. Glidewell, J. Chem. Soc., Perkin Trans. 2, 229 (1985).

6. Helaas wordt, zelfs in moderne leerboeken, bij de verklaring van de chemische binding van vijf- en zesgekoördineerde niet-overgangsmetaalverbindingen weinig of geen aandacht besteed aan een molecular-orbital beschrijving waarin d-funkties geen essentiële rol spelen.

C.E. Mortimer, *Chemistry* (Wadsworth Publishing Company, Belmont California, 1986).
A.G. Sharpe, *Inorganic Chemistry* (Longman, London, 1986).
P.W. Atkins, *Physical Chemistry* (Oxford University Press, Oxford, 1986).

7. De bewering van Gordy dat in ESR spektra de koppelingskonstante nauwkeurig bepaald kan worden uit het verschil tussen de m_I en $-m_I$ posities, zonder daarbij tweede-orde korrekties toe te passen, blijft een onnauwkeurige weergave van de werkelijkheid.

W. Gordy, *Theory and Applications of Electron Spin Resonance* (Wiley Interscience, New York, 1980).

8. Het ontstaan van een dubbele ketenbreuk in DNA door γ-straling onder kondities waarbij met behulp van ESR alleen guanine kationradikalen en thymine anionradikalen waarneembaar zijn, is op zich geen aanwijzing voor een direkt causaal verband.

P.M. Cullis, M.C.R. Symons, M.C. Sweeney, G.D.D. Jones en J.D. McClymont, J. Chem. Soc., Perkin Trans. 2, 1671 (1986).

9. Het verdient aanbeveling aandacht te besteden aan de mogelijkheid dat de natuurlijke aardolie- en aardgasbronnen niet noodzakelijkerwijs hun oorsprong vinden in biologisch materiaal maar ook gevormd kunnen zijn uit de aanwezige koolstof in de aardmantel.

T. Gold, New Scientist, **1514**, 42 (1986).
P.J. Hooker, R.K. O'Nions en E.R. Oxburgh, Nature, **318**, 273 (1985).

10. Het inmiddels klassieke ^{19}F NMR experiment aan PF_5 waarmee Berry het pseudorotatieproces in vijfgekoördineerde fosforverbindingen introduceerde, is aan twijfel onderhevig.

R.S. Berry, J. Chem. Phys., **32**, 933 (1960).
P. Lazeretti en J.A. Tossell, J. Magn. Reson., **70**, 461 (1986).

11. Ten onrechte wordt door Gorenstein et al. bij de konformatie-analyse van zesringfosforinanen op basis van ^{31}P chemical shifts geen rekening gehouden met de invloed van het oplosmiddel op het verschil in chemical shift tussen chair en twist-boat konformaties.

D. Gorenstein, R. Rowell en J. Findlay, J. Am. Chem. Soc. **102**, 5077 (1980).
K. Taira, K. Lai en D.G. Gorenstein, Tetrahedron, **42**, 229 (1986).

12. Mede gelet op de relatieve snelheid van fietsers en gemotoriseerde voertuigen in het huidige drukke stadsverkeer verdient het aanbeveling de voorrangsregels, voor wat betreft zogenaamd langzaam- en snelverkeer, te veranderen ten gunste van de lichtste der beide potentiële botsingspartners.

R.A.J. Janssen   Eindhoven, 6 maart 1987